INVESTIGATION OF SYSTEMS AND TECHNIQUES
FOR MULTI-COMPONENT MICRO-FORCE MEASUREMENTS
ON WIND TUNNEL MODELS

Semiannual Status Report

on

NASA Grant NGR 47-005-026

Submitted by Co-principal Investigators:

Dr. James W. Moore
Associate Professor of Mechanical Engineering

Dr. Eugene S. McVey
Associate Professor of Electrical Engineering

Research Laboratories for the Engineering Sciences

University of Virginia

Charlottesville

Report No. EME-4029-101-65U

August 1965

INVESTIGATION OF SYSTEMS AND TECHNIQUES
FOR MULTI-COMPONENT MICRO-FORCE MEASUREMENTS
ON WIND TUNNEL MODELS

Semiannual Status Report

on

NASA Grant NGR 47-005-026

Submitted by Co-principal Investigators:

Dr. James W. Moore
Associate Professor of Mechanical Engineering

Dr. Eugene S. McVey
Associate Professor of Electrical Engineering

RESEARCH LABORATORIES FOR THE ENGINEERING SCIENCES
SCHOOL OF ENGINEERING AND APPLIED SCIENCE
UNIVERSITY OF VIRGINIA
CHARLOTTESVILLE, VIRGINIA

Report No. EME-4029-101-65U
August 1965

Copy No. /5

FOREWORD

This semi-annual report covers the period from January 15 to July 15, 1965. This is the first report for this research grant. The original grant was funded for one year and a supplemental one year grant was started June 15 to study skin friction measurement problems.

The introduction contains a condensed theoretical description of the over-all system which is being developed for the measurement of multi-component micro-forces.

The section on air bearing development is intended to be the final report on this particular part of the research effort. Additional air bearing developments, data, etc. will, of course, be reported on by future reports when the need arises. The air bearing section was used as a mechanical engineering masters thesis by Major David. A. Hicks.

The servo system work will be considered in detail in a latter report. The information reported here is intended to indicate just the state of progress rather than to provide a source of technical details.

SECTION I

INTRODUCTION

This section contains a condensed theoretical description of the system being developed to measure multi-component micro-forces. This material was originally written as a paper which has been submitted for publication by the International Federation of Automatic Control Congress to be held in 1966 at London, England.

The paper has been accepted by the American review board. The international review board decision will not be announced until early 1966. If the paper is not accepted it will probably be published as a society transaction paper, either ASME or IEEE.

When some form of final acceptance is given, publication permission will be formally requested from NASA in accordance with applicable procedures. In the meantime, this report will provide the sponsor with the information contained in the paper.

The text of the paper and the figures are presented below in almost exactly the form that the material will have in the published paper.

Introduction

A system of force measurement is described here which permits the force being measured to be a very small fraction of the weight of the force producing object. A combination of closed loop control and air bearing technology makes possible the solution of this difficult measurement problem. An air bearing can support large weights and provide a virtually frictionless platform for static conditions. The platform is servoed to obtain force components. A practical example of a situation requiring this new force measuring technique is an ion engine. An experimental ion engine weighing fifty pounds (22.7 Kg) may produce a thrust vector of only a few milli-pounds. Even though the thrust to be measured can be at a 90° angle with respect to the engine weight component, it is still very difficult to resolve the desired force because the scale must support the engine. Problems such as

1

hysteresis, nonlinear friction and deadband limit the available force measuring schemes when the weight to force ratio is large.

Another practical example of the application of the new system concerns the measurement of forces on wind tunnel models. Relatively large test models are used in subsonic wind tunnel work. The forces such as lift and drag and pitch moment are relatively large for the model weight. In hypersonic tunnels the test models produce relatively small forces for their weight because they are small and may be of solid metal, such as copper, due to temperature problems (velocities in the range of Mach 8-12 are of concern here). The large vibration fields which are often a part of the wind tunnel measurement problem should not harm either the air bearing or servo system because there are no mechanical bearings or contacts.

Force measurements are presently made in several ways. For relatively large forces conventional wind tunnel balances are used. Recent work has been done with magnetic support systems for use in the same manner as the conventional balance. In general, these are not adequate for force measurements in the very low ranges. Successful measurement systems embodying flexures and strain gages have been used for forces an order of magnitude greater than those considered here. These have measured three components of force and three moment components. Their small size permits mounting within the model. Their configuration tends to hold deflections to miniscule amounts. However, when their use is attempted for measuring forces an order of magnitude lower, several limitations become apparent. The flexure system is required to support the weight of the model. As the applied forces become very small the ratio of support stiffness to force measurement stiffness becomes very unfavorable. As deflections become small hysteresis in the flexure material becomes a significant factor. As models become smaller the flexures are more difficult to machine and it is more difficult to mount strain gages. All these factors combine to indicate that a new approach is required.

2

As indicated earlier, the system consists of two major parts: 1) the control system which produces motor control currents proportional to applied forces, 2) the air bearing which supports the model under test. Force components are determined by measuring the associated servo motor armature currents. Proper motor design should minimize cross-coupling of force components in the servo system and, hence, in the readout system to a degree which will make this system superior to other systems it is hoped. However, proof of this point must await final calibration data. Data manipulation will be simplified by the cross-coupling improvement if it is achieved.

The Control System

The control system consists of three independent servoes which control the rotation angle θ of the platform and the x-y positions of the platform in a plane parallel to the surface of the air bearing. The tare forces due to model and instrument weight are effectively eliminated by working in the horizontal plane. A simplified schematic of the control system is shown in Figure 1. The servo motor only is shown for the x-axis control system in order to keep the diagram simple.

Consider the action of the x-axis servo: if a force is applied to the platform in the x direction the platform is displaced along the x-axis. The linear variable differential transformer (LVDT) sensor generates a voltage proportional to the displacement. The a-c output from the LVDT is demodulated and applied to the amplifier. The amplifier output drives the x-axis servo motor which generates a restoring force on the platform.

The motor force is proportional to armature current. Thus, the x-axis force to be measured can be determined by metering the servo-motor current. Current levels of 0.1 to 1.0 amperes have been found to be practical. The y-axis force measuring servo is identical to the x-axis servo.

The torque measuring control loop is identical to the x and y axis control loops except that the servo motor force acts at a moment arm of length "d" to null and measures applied torques.
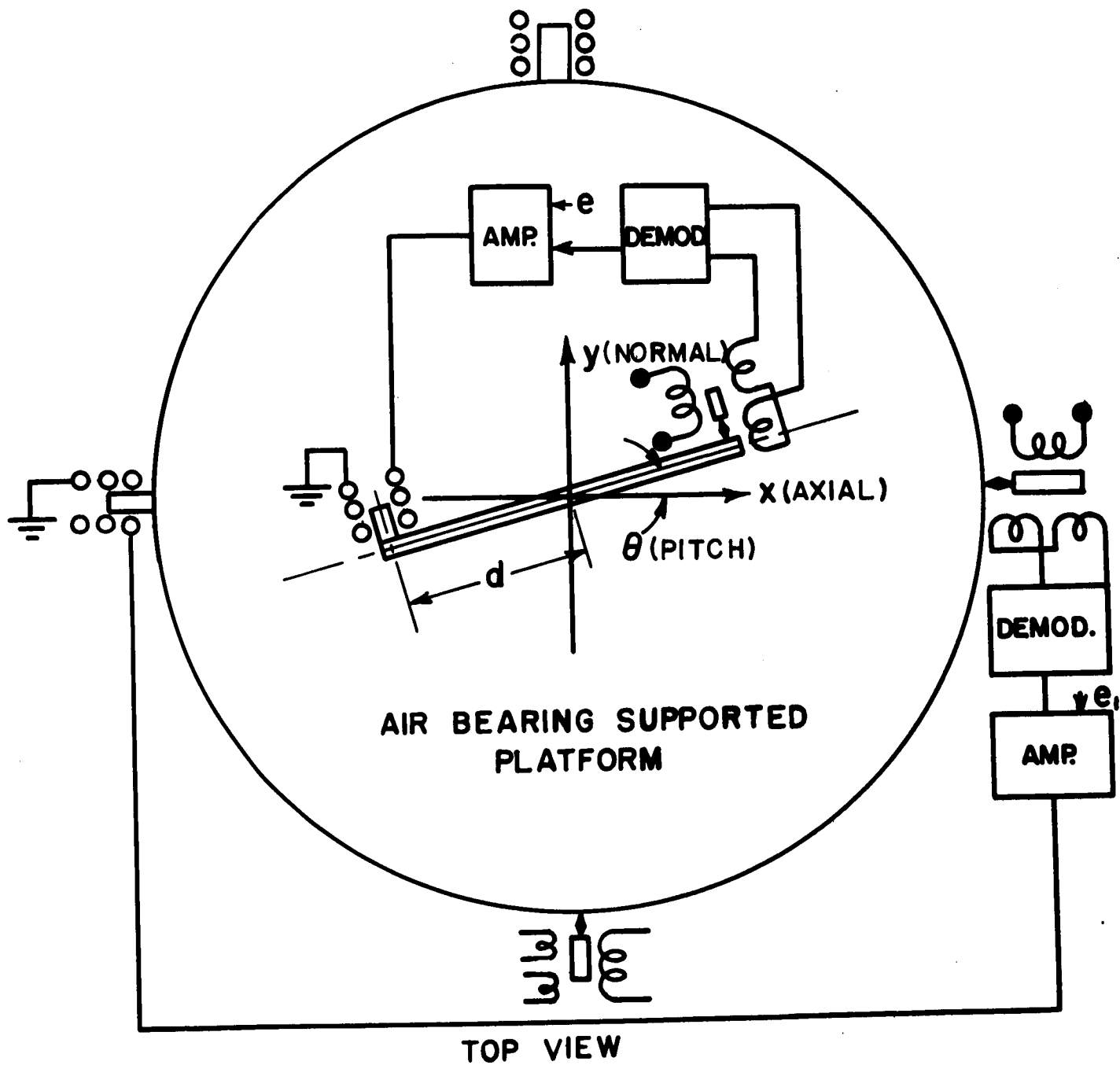
3

FIGURE-I

SCHEMATIC OF BALANCE SERVOES

4

The forces or torques to be measured appear as load disturbances to the servoes, as indicated in the x-axis servo block diagram of Figure 2. If the system is built to contain an integration with respect to applied load disturbances, the steady state position error of the platform would be zero during test. Otherwise a position error will be present which is dependent on the force to be measured and on the loop gain constant. Platform position changes along an axis cause the sensor and motor constants along other axes to change. These changes are, in effect, cross-coupling terms.

Cross-coupling terms can be made theoretically equal to zero with proper design. However, the required integrators introduce practical problems, notably drift, which necessitates caging of the system just prior to test, and also other well known problems. With proper motor and sensor design the cross-coupling effects are negligible. For example, LVDT's with 20,000 cps carrier currents and having a radial clearance of 20 mils are relatively independent of radial displacements of a few hundred micro-inches.

The motors have been designed with air core coils for the armature and with a permanent magnet field. The gap between the field and the armature is on the order of an inch (2.54 cm). These factors make the motor cross-coupling negligible, according to calculations.

The control system can be analyzed by considering each loop separately because the cross-coupling is negligible. The analysis of only one loop will be sufficient because the x and y axis servoes are identical and the θ servo is similar to the x and y servoes.

Considering the x-axis servo, the force balance equation for the platform is

$$F + F_m - f\dot{x} = M\ddot{x} \qquad (1)$$

where F is the applied force to be measured, F_m is the x-axis motor force, f is the viscous friction of the air bearing and M is the system mass
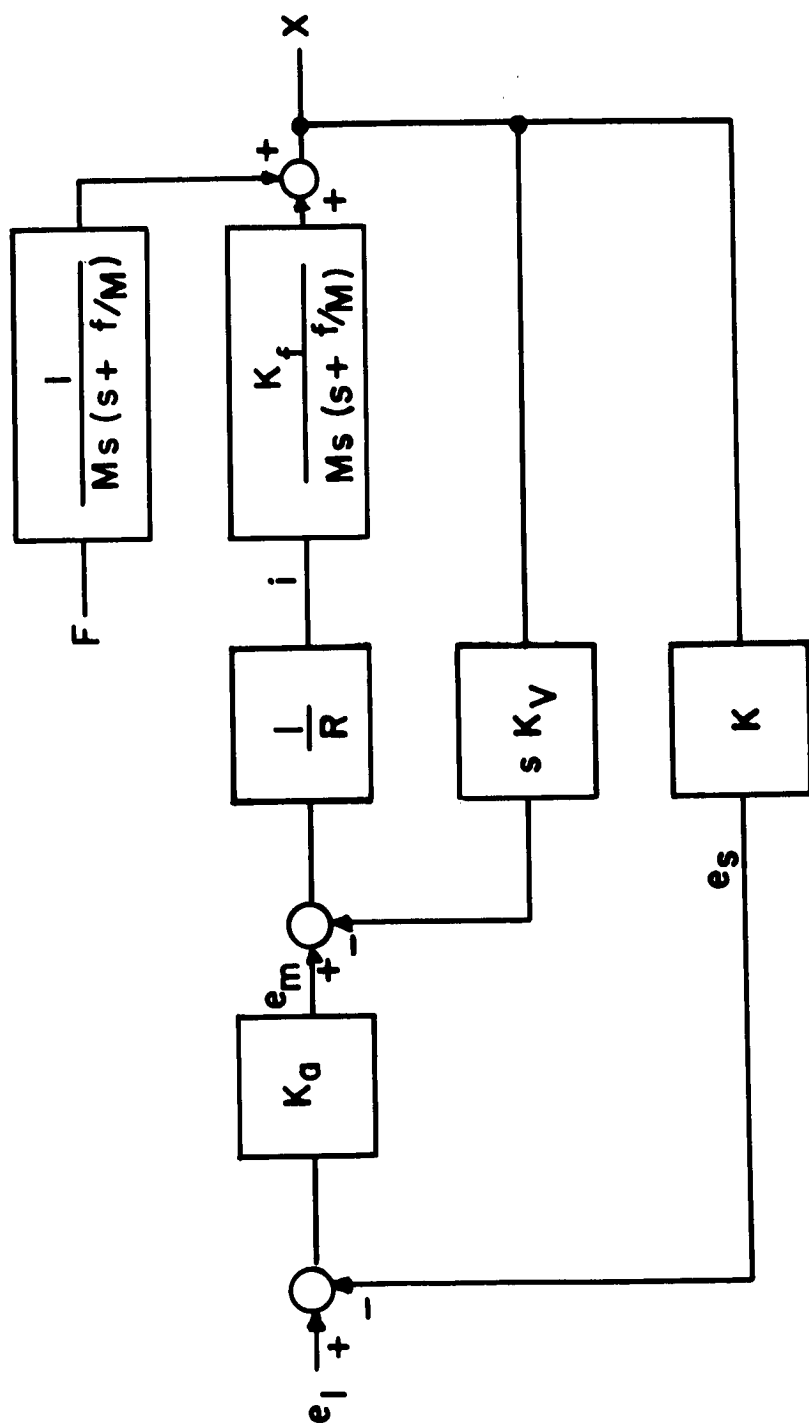
5

FIGURE-2

X - AXIS SERVO BLOCK DIAGRAM

including the movable part of the air bearing. The static friction of the air bearing is zero but there is, of course, a viscous friction force $f\dot{x}$.

The motor force is proportional to its armature current, i.e.,

$$F_m = K_f i \tag{2}$$

Equations (1) and (2) yield

$$F(s) + K_f i(s) = Ms (s + f/M) x(s) \tag{3}$$

The armature inductance of the motor and the servo amplifier output impedance are assumed to be negligible (this is usually a good assumption). The output voltage to the motor is

$$e_m = iR + K_v \dot{x} \tag{4}$$

where K_v is the motor back e.m.f. constant. Then

$$i(s) = \frac{e_m(s) - sK_v x(s)}{R} \tag{5}$$

The motor input voltage, e_m, is

$$e_m(s) = [e_1(s) - e_s(s)] K_a \tag{6}$$

where e_1 is the position reference signal which would normally be referred to as the system input, K_a is the amplifier constant and e_s is the signal from the sensor demodulator. For the sensor,

$$e_s(s) = K x(s) \tag{7}$$

where K is defined by the equation.

The analysis equations may be used to draw the block diagram of Figure 2. As noted earlier, e_1 is used to establish the zero position of the platform and does not enter into the analysis in any other way. In the absence of a force input, F, the steady state position error will be zero theoretically because the open loop transfer function contains an integration with respect to position.

Let the platform position be chosen so that e_1 is zero. The equation relating motor current and the applied force is determined by observing that

$$i(s) = \frac{e_m(s) - s K_v x(s)}{R} \tag{8}$$

$$e_m(s) = -K_a K x(s) \tag{9}$$

$$x(s) = \frac{i(s) K_f + F(s)}{Ms(s + f/M)} \tag{10}$$

These equations yield

$$i(s) = -\frac{K_v}{RM} \frac{\left(s + \frac{KK_a}{K_v}\right) F(s)}{\left[s^2 + \left(\frac{f}{M} + \frac{K_f K_v}{RM}\right) s + \frac{K_f K_a K}{RM}\right]} \tag{11}$$

It is assumed that the system is fast compared to the rate at which test conditions change and that final values are of primary interest. For a step value of force having a magnitude F as previously defined,

$$i_{ss} = -\frac{F}{K_f} \tag{12}$$

8

from the final value theorem. The form of this relationship is the same as Equation (2) where the current can be replaced by i_{ss} from Equation (12) for steady state conditions. Thus

$$F_m = -F \tag{13}$$

or in words, the motor force is equal and opposite to the force applied to the platform, as asserted from physical reasoning.

The force can be monitored by measuring i as indicated by Equation (2).

The magnitude of displacement from zero position is of interest because it must be small in order to make cross-coupling terms negligible. The displacement calculation requires the transfer function from a force input to a position output, i.e.,

$$\frac{x(s)}{F(s)} = \frac{1/M}{s^2 + \left(\dfrac{f}{M} + \dfrac{K_f K_v}{RM}\right) s + \dfrac{K_a K_f K}{RM}} \tag{14}$$

The steady state position error is found by applying the final value theorem to Equation (14). It is

$$x_{ss} = \frac{R}{K K_a K_f} F \tag{15}$$

The steady state displacement error depends on the systems gain constant and applied force, as one would expect. Amplification is easy to obtain so the factor which keeps displacement from being arbitrarily small is system stability. For example, from Equation (14) it can be seen that the natural frequency of the system is

$$\omega_n^2 = \frac{K K_a K_f}{RM} \tag{16}$$

9

and from Equation (15) the loop gain constant is seen to be

$$\text{Gain} = \frac{KK_aK_f}{R} \tag{17}$$

From the two relationships it is apparent that

$$\text{Gain} = M\omega_n^2 \tag{18}$$

The weight of a practical system is on the order of 8 pounds (3.62 Kg). If the natural frequency can be made equal to 30 cps (high, but not unreasonable for this system), the gain will be

$$
\begin{aligned}
\text{Gain} &= 0.25 \ (2\pi30)^2 \\
&= 8800 \ \#/\text{ft} \\
&= 740 \ \#/\text{in} = 13,900 \ \text{Kg/m}
\end{aligned}
\tag{19}
$$

From Equation (15), a model force of 0.5 pounds will result in a displacement of

$$
\begin{aligned}
x_{ss} &= \frac{0.5}{740} \\
x_{ss} &= 0.000677 \ \text{in} = 0.00172 \ \text{cm}
\end{aligned}
\tag{20}
$$

This displacement is well within the resolution of the sensors used and is also small enough to make the cross-coupling terms negligible.

The Air Bearing

An air bearing has been selected to support the model and sting because of its very high stiffness in the direction of support and because air bearings have no static friction. A schematic diagram of the air bearing support system is shown in Figure 3. The lower bearing pad supports the weight of the model and sting (support arm). The wind tunnel

FIGURE-3
SCHEMATIC OF AIR BEARING

AIR
SUPPLY

BEARING   ARMATURE

TO VAC.

TUNNEL WALL

HEAT AND
WIND SHIELD

11
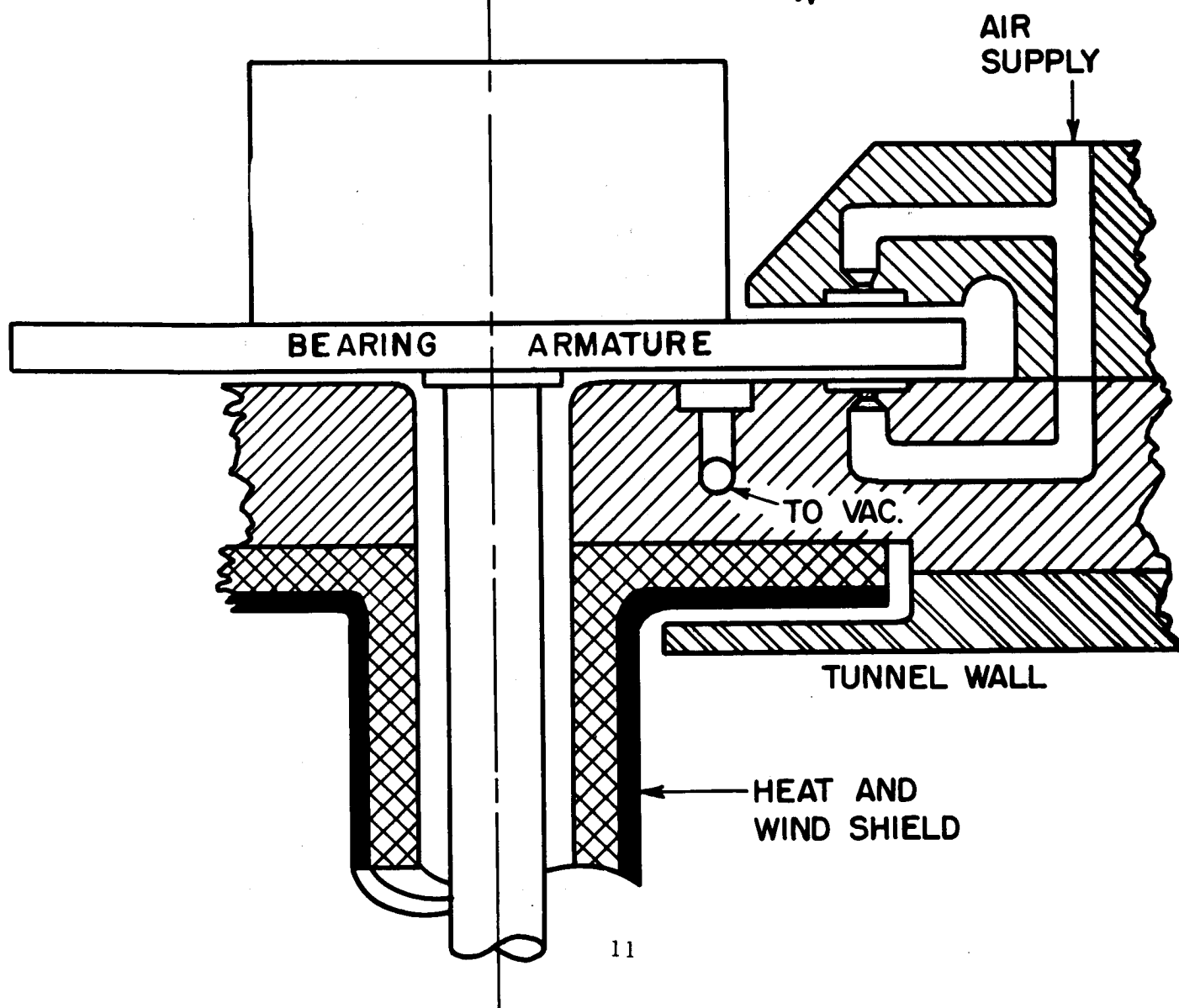
in which this system will be used will be operated at very low pressures so the air bearing must also support atmospheric pressure. This accounts for the major vertical load if the bearing chamber is not also evacuated.

The bearing pad is divided into four segments. Flow of air to each segment is controlled by a separate capillary tube of about 0.010 inch. (.0254 cm) diameter. The separation into segments permits operation as four separate bearings. This is necessary to give rotational stability in all vertical planes and to resist forces tending to rotate the bearing in these vertical planes.

Four separate upper air bearings act as hold down bearings. These are necessary to help resist over-turning moments. In addition, they permit higher air pressures in the lower bearings. This, in turn, gives higher bearing spring constants. Thus, by adjusting the pressures between the upper and lower bearings, the total spring constant can be adjusted.

The hold down bearings have another function. Air bearings normally are subject to unbalanced torques, called turbine torques, due to uneven flow of air from the bearing. Thus, the bearing armature may rotate or slide to the side. Each hold down bearing in this design is mounted with three bolts as shown in Figure 3. By tightening or loosening these bolts selectively the hold down bearing can be tilted slightly. Since the bolts work against the solid metal the change is only a few millionths of an inch, but this amount is sufficient. If one or more of the hold down bearings are tilted in the same direction the bearing armature can be made to rotate or a rotation can be stopped. If opposite bearings are adjusted the armature can be made to translate or a translation can be stopped. Thus this arrangement can be used to balance out extraneous forces and can also be used to adjust for the base pad of the bearing being slightly out of level.

The forces to be measured on the model are the drag, the lift and the pitching moment. These are diagrammed in Figure 4. The lift force is perpendicular to the paper and the pitching moment is about the vertical axis of the bearing. The drag and lift forces cause moments,
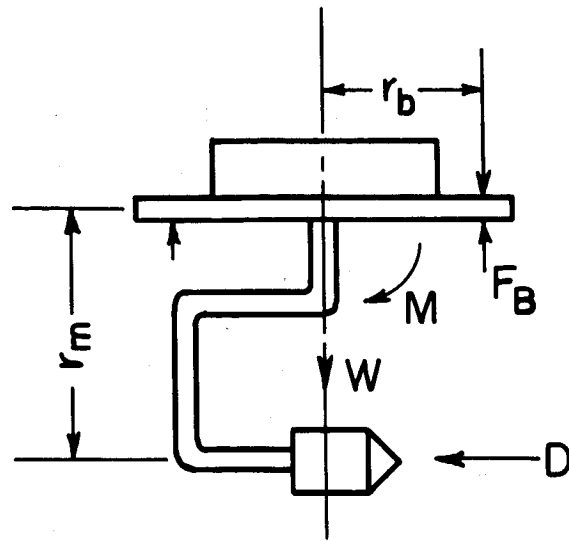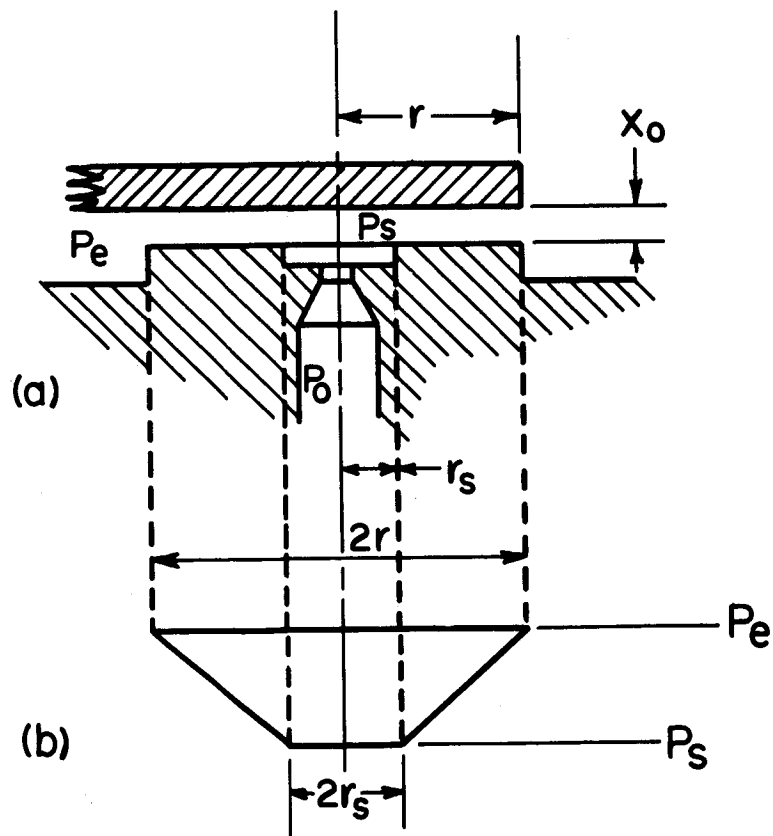
FIGURE-4
MODEL AND BEARING FORCES

FIGURE-5
BEARING PAD SCHEMATIC

M, which must be resisted by air bearing forces, F_B. Steady state horizontal forces and the pitching moment are resisted by the servo motors only.

Air bearings tend to have two types of spring constants which may be thought of as a high frequency constant and a low frequency or static constant. At intermediate frequencies both exist to some extent. The low frequency constant is due to a change in the pressure, P_s, Figure 5 as the gap x_o is changed.

Experiments on this bearing indicate that this spring constant is on the order of 100,000 to 400,000 lb/in (1.8×10^6 to 7.2×10^6 Kg per meter) depending on the initial gap and on the supply pressure P_o.

At high pressures the air trapped in the bearing does not have time to flow so that the system acts as a piston in a cylinder. Assuming this process to be isentropic, we have

$$\frac{dp}{dv} = -k \frac{P}{V} \tag{21}$$

The bearing has a constant area and the pressure P is fixed by the steady state load, F_o, so the spring constant can be written as

$$\frac{dF}{dx} = \frac{-k(F_o + 15A)}{x_o} \tag{22}$$

where A is the bearing area and x_o is the steady state bearing gap. Assuming A = 1 sq in (6.7 sq cm), x_o = 0.0005 in (0.00127 cm) and k = 1.4 for air, we have

$$\frac{dF}{dx} = 126,000 \text{ lb/in} \ (2.24 \times 10^6 \text{ Kg/meter}) \tag{23}$$

Thus the total dynamic spring constant for four pads is 504,000 lb/in (9×10^6 Kg/meter). This may be raised by increasing the supply pressure or the area or by decreasing the gap.

The initial bearing armature is a 1-in (2.54 cm) thick by 5-in (12.70 cm) diameter opitical glass flat. Since the bearing base is a polished surface this permits the use of a monochromatic light to study motion and deflections of the armature. The bearing is stable at all pressures that have been used. These have ranged from zero to 40 psi (28,120 Kg/sq meter).

Conclusions

The principles of operation of a new technique for measuring multiple force components of small value relative to the weight of the force producing object have been presented. Analysis and design considerations have been presented in sufficient detail to allow other workers in the field to build models. Extensive date are not yet available at the time this is written but sufficient experimental work has been done to verify the main ideas and assumptions.

Overall accuracies are expected to be better than one percent. The main sources of error appear to be:

1. Calibration
2. Motor current measurement
3. Cross-coupling in the control loops
4. Motor constant variations
5. Platform becoming out of level

The order of importance of these errors is not yet known.

The calibration problem is no different than that experienced with other techniques for the degree of accuracy considered here. It is believed that calibration may ultimately be a limiting factor, however, when the full potential of this new technique is utilized. The current measurement problem should be of minor importance in obtaining 0.1% accuracy when making steady state measurements. Cross-coupling data are as yet incomplete but preliminary measurements indicate that these errors will be below 1%. It should be noted that cross-coupling effects are not really fundamental errors because these effects may be

15

removed by proper calibration. The greatest unknown is the problem
associated with the force constant K_f of the motors. Changes in K_f
will introduce errors directly into the measurements. This is primarily
a dimensional stability problem. Control of the ambient temperature
and careful attention to heat transfer in the motor coils will be important.

The problem of leveling the system may well be a major one.
Level sensors are available which will indicate 0.01 second of arc. This
is more than the accuracy required for obtaining the necessary overall
system accuracy. A closed loop servo system is being studied as a
means of solving the leveling problem.

SECTION II

AIR BEARING

Presented in this section is the complete reproduction of a Masters Thesis presented to the School of Engineering and Applied Science by David Allan Hicks, August 1965.

ABSTRACT

Design considerations and fabrication techniques for a gas

thrust bearing to be used as a frictionless support for a wind-tunnel

balance, capable of measuring model forces from 0.005 to 0.5 pounds,

are presented. The bearing is externally-pressurized, has flat,

parallel surfaces, and is suspended between two gas lubricating

films each 0.0007 inch thick. Theory of gas flow between two

parallel planes is reviewed and consolidated. Relationships between

pressure, gap height, and lift for longitudinal flow are developed.

Static and dynamic equations of motion for the bearing are stated.

Experimental results indicate a static spring constant of the

order of 300,000 pounds per inch and gas flow rates less than 0.002

pounds per second for various supply pressures and bearing loads.

Sensitivity of the bearing to vibratory fields indicates a natural

frequency in the neighborhood of 30 cycles per second, depending

on the lubricating film spring constant. Results indicate further that

a negative pressure region exists in the lubricating film that is not

predicted by theory.

The bearing is suitable for use as a support for a wind-tunnel

balance.

ACKNOWLEDGMENT

TABLE OF CONTENTS

CHAPTER PAGE

LIST OF TABLES

LIST OF FIGURES

FIGURE   PAGE

FIGURE   PAGE

FIGURE   PAGE

LIST OF SYMBOLS

A   Area, square inches

b   Width of bearing, inches

C, D   Constants of integration

d   Depth of groove, inches

F   Force, pounds

g   Acceleration due to gravity, 386 in/sec^2

h   Gap height, inches

J   Polar moment of inertia

l   length of restrictor, inches

m   exponent, type of gas flow

M   Mass flow, lbs per second

P   Distributed pressure, p. s. i. a.

Q   Volume flow, cubic inches per second

r   Radial flow: radial distance in direction of flow, in.

            Tubular flow: radius of tube, inches

R   Universal gas constant

Re   Reynolds number

T   Absolute temperature, °R.

u   Distributed velocity, in/ sec

U   Maximum velocity, in/ sec

V   Average velocity, in/ sec

x   Incremental length in direction of flow, inches

y   Incremental height, inches

z   Incremental height, tubular flow, inches

ν Ratio of specific heats

δ Deflection

υ Kinematic viscosity, or Poisson ratio

λ Flow resistance coefficient

μ Dynamic viscosity

π 3. 1417

ρ Mass density

τ Skin friction coefficient

Subscripts:

c   Conditions at restrictor

e   Exhaust, ambient conditions

g   Groove conditions

o   Conditions at end of entrance tube

s   Supply conditions

1   Conditions at entrance to lands, or upstream conditions

2   Downstream conditions

CHAPTER I

INTRODUCTION

General. An air-bearing support for a wind-tunnel balance is desirable because of the very low friction forces in an air-bearing. The forces on a hypersonic wind-tunnel model are from 0.005 to 0.5 pounds--making a virtually frictionless support a necessity. Figure 1 indicates the way the air-bearing support will be mounted on the wind-tunnel and the conditions under which it will operate.

Cross-coupling effects of a conventional strain-gage force-measuring device are reduced to second or third order by an air-bearing support with a vertical equivalent spring constant of 80,000 pounds per inch. The equivalent spring is acting against model forces of from 0.005 to 0.5 pounds at the end of a twenty-four inch sting, as indicated in Figure 1.

The major considerations in the design are

a. Material requirements--must be capable of retaining a smooth finish and be scratch and corrosion resistant.

b. Geometry requirements--to give maximum stiffness.

c. Mass flow requirements--since the wind-tunnel is activated by a vacuum sphere, the mass flow contributed by the bearing must be kept to about 1/100 of the total mass flow--on the order of 0.01 pound per second--to have little effect on the available run time.

d. Supply pressure requirements--to support a given load

1

Gas Inlets

Hold-down Pads

Glass **Bearing**

Spacers

Bearing Pad

Gas Inlets

Sting

0.005 to 0.5 Pound

Model

Arc Heater

To Vacuum Sphere

Air Speed   Mach 13⁺
Air Temp.   8000° F.⁺
Mass Flow   I Lb/sec.
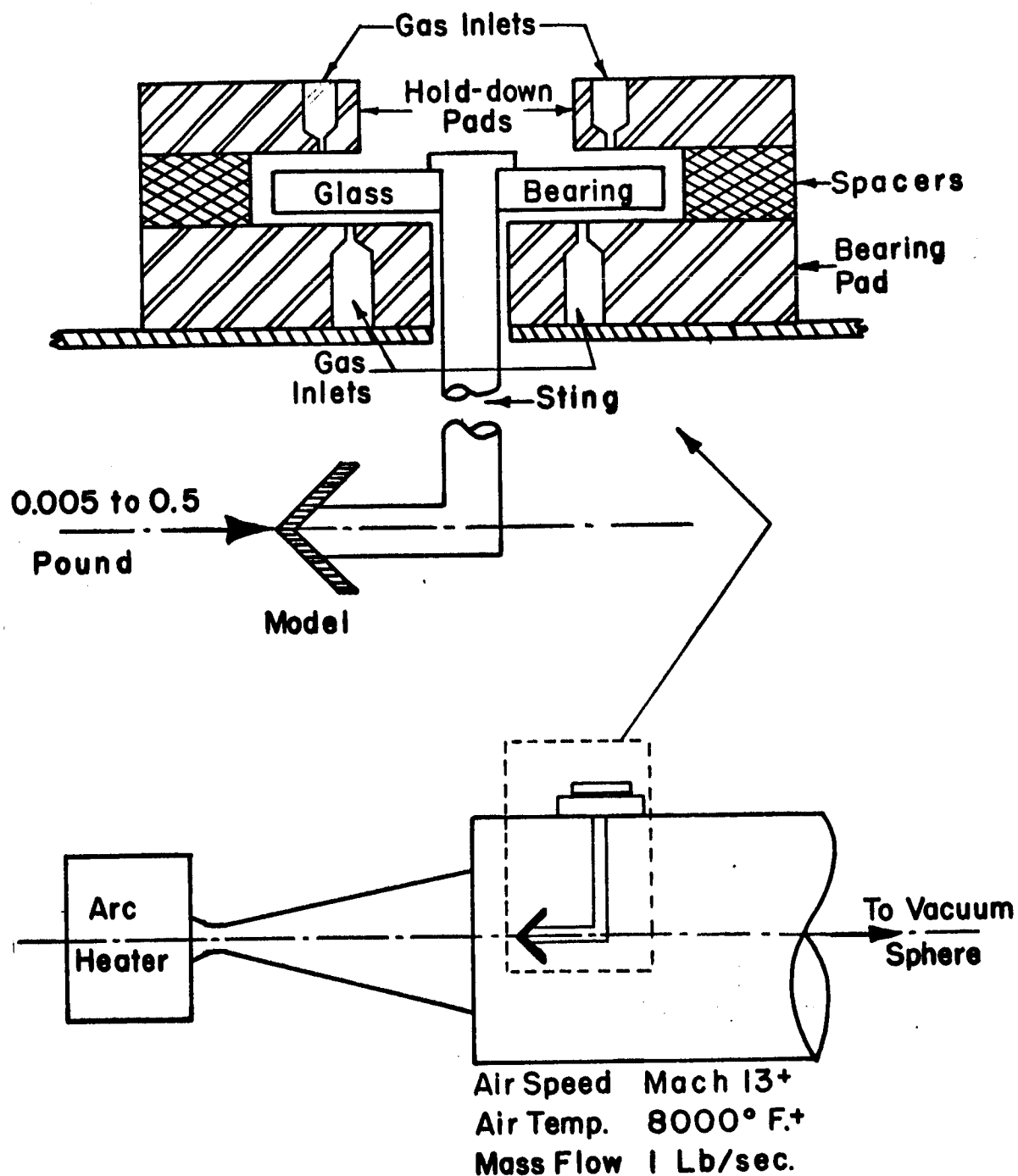
Figure 1. Schematic of Wind-Tunnel and Air Bearing Support for a

Wind-Tunnel Balance.

and provide required stiffness.

e. Stability requirements--the natural frequencies of the system must be well removed from the background vibratory fields present at the site.

It is difficult to specify which of the above considerations is most important. All items (except a) are interdependent and all are necessary for the proper operation of the bearing. Mere satisfaction of one requirement will not insure that the others are satisfied; therefore there is no set procedure to follow in the formulation and design stage. Each characteristic must be developed in terms of the others as the design progresses.

Depending on their application, gas bearings are designated as thrust, journal, or spherical bearings. The two general types of gas bearings are the self-acting type and the externally-pressurized type. The self-acting type has both surfaces in contact when it is at rest, but as the speed of the moving part increases, gas is dragged between the surfaces and is compressed until the surfaces are eventually separated by a film of gas. This type of bearing must be moving to be lubricated, therefore it is also called a hydrodynamic gas bearing.

The externally-pressurized, or hydrostatic, gas bearing has a lubricating film developed by pressure applied to the gas externally-- therefore the surfaces are always separated by a film of gas. When this bearing is rotated, it may be designed to perform as a self-acting bearing and the external pressure may be removed. This thesis considers a gas-lubricated, hydrostatic thrust bearing with no rotation.

A general view of the prototype bearing designed and discussed in this thesis is photographed in Figure 2.

Scope. A brief review of the large number of papers written about gas bearings with emphasis on the publications of particular interest and aid in the preparation of this thesis is presented. Theory of the operation of a parallel-surface, gas-lubricated thrust bearing is developed and relationships are derived for velocities and pressures in the lubricating film, mass flow, and the load-carrying capacity of the bearing. Equivalent spring constants and the equations of motion of the bearing are stated.

Experimental work, including the design, fabrication, and performance testing of a full-size bearing is presented. The report includes graphs of the equivalent spring constant and mass flow as functions of supply pressure, load, and film thickness. Instrument set-up and measurement techniques are discussed. A description of each instrument and the methods followed in its calibration are included as appendices to this thesis. Background vibratory fields are determined and the effect of these fields on the bearing is stated.

Finally, an analysis and comparison of the experimental results with the theory developed indicates the work remaining to make an optimum bearing for use as a wind-tunnel balance support.

Review of the literature. A review of the literature reveals many papers concerning the theory of gas flow and the effects of changing various parameters for all types of gas bearings. Very few
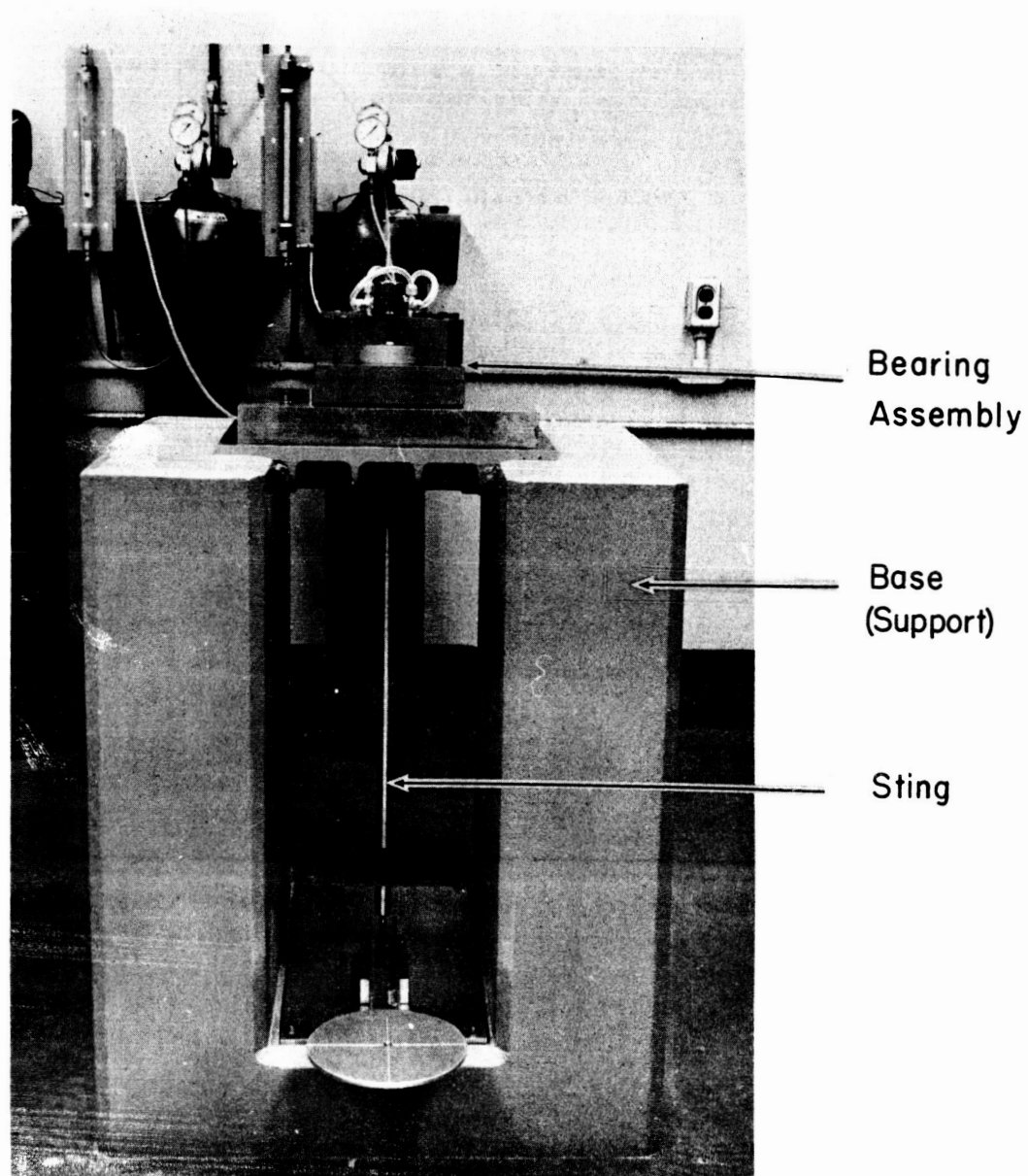
Figure 2   Prototype Bearing Designed for use as a Wind-Tunnel Balance Support

deal with the actual design of a gas bearing for a particular application. Stark's paper[1] is the most useful from a design standpoint--design of a particular bearing is specified and a simplified theoretical analysis is presented.

Publications supported by experimental results are scarce. A notable exception is the exhaustive theoretical and experimental treatment of gas flow between two parallel planes under normal temperatures and pressures by Comolet.[2] Unfortunately the paper is in French and a translation is not available through Batelle Memorial Institute, although a translation has been made by J. Cherubim and Y. Gagne for the Stratos Division of Fairchild Corporation.[3] Much of the theoretical portion of this thesis was taken from Comolet's paper, translation accomplished with the assistance of the French Department of the University of Virginia.

---

[1]Kenneth W. Stark, "The Design of Various Types of Air Bearings for Simulating Frictionless Environments," NASA TN D-1100, National Aeronautics and Space Administration, Washington, D. C., May 1962.

[2]Raymond Comolet, "Ecoulement d'un Fluide Entre Deux Plans Paralleles, Contribution a l'Etude des Butees d'Air," Publications Scientifiques et Techniques du Ministere de l'Air, No. 334, 1957.

[3]Proceedings of the First International Symposium on Gas Lubricated Bearings, Office of Naval Research, ACR-49, 1958.

Another set of papers, well supported and verified by experimental results, is the series by Laub[4], which cover all types of gas bearings, from simple single-orifice thrust bearings to multi-orifice spherical bearings.

A book by Gross[5] presents a thorough theoretical and analytical treatment of both types of gas bearings--self-acting and externally-pressurized--and is the only book dealing exclusively with gas bearings.

Columbia University has prepared a survey of all gas bearing literature through 1958.[6] This survey includes a critical comparison of the treatment of gas bearing theory by various authors and is an excellent resume and evaluation of the work done to that date in the field of gas bearings. The survey also includes a complete

---

[4]J. H. Laub, "Hydrostatic Gas Bearings," ASME Trans. June 1960, pp. 276-286.

-----, "Externally Pressurized Journal Gas Bearings," ASLE Trans., Vol. 4, 1961, pp. 156-171.

-----, and R. H. Norton, "Externally Pressurized Spherical Gas Bearings," ASLE Trans., Vol. 4, 1961, pp. 172-180.

-----, "Gas Lubrication in Instruments and Control Devices," ISA Trans., October 1962, pp. 305-314.

-----, and H. D. McGinness, "Gas Floated Spinning Spheres," ASME-ASLE Paper No. 60, LC-16, 1961.

[5]W. A. Gross, Gas Film Lubrication, (New York: John Wiley and Sons, Inc., 1962)

[6]G. F. Boeker, D. D. Fuller, and C. F. Kayan, "Gas Lubricated Bearings--A Critical Survey," Columbia University, Wright Air Development Division, USAF, WADC Tech. Rpt. 58-495.

bibliography of literature pertaining to gas bearing theory through 1958.

CHAPTER II

DEVELOPMENT OF THEORY

I. GENERAL

Two flat plates, separated by a film of air which is supplied
under pressure are able to support a load and may be used as an air-
lubricated thrust bearing. The force exerted on the bearing plate by
the air jet depends on the external supply pressure and the film thick-
ness, or gap height, between the plates.
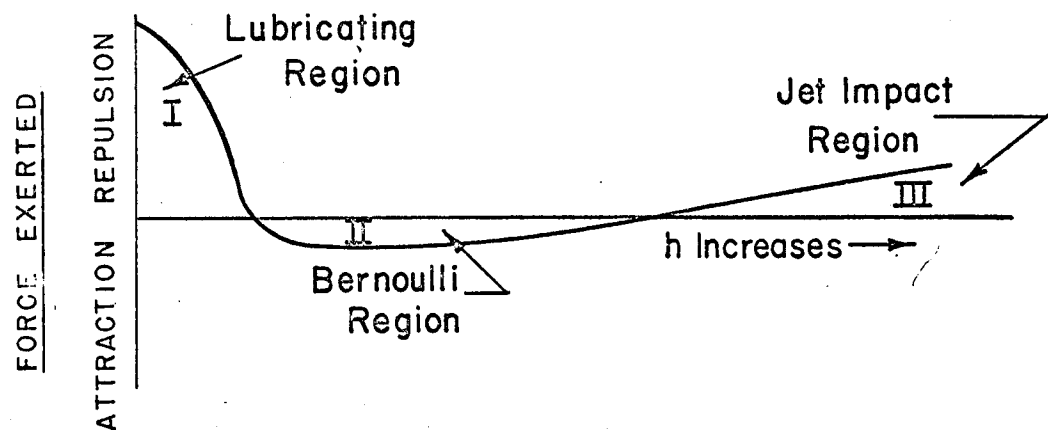
Figure 3. Force exerted on a flat plate in relation to distance from air jet.

As the movable plate (the bearing) is brought near the plate
containing the air jet (the bearing pad), the first force observed is
repulsion--in the jet impact region (III, above). The total force ex-
erted on the bearing in this region is not large and the bearing has
very little load carrying capacity. As the bearing is brought closer
to the pad into the Bernoulli region, an attractive force is felt and

the bearing must be pulled away to maintain a constant gap height. This effect is demonstrated by placing a round piece of cardboard on the end of a soda straw and attempting to blow it away--the harder one blows, the more the cardboard is attracted to the end of the straw. Fluid inertia forces dominate in region II and the bearing has a negative load-carrying capacity.

As the gap is reduced still further, the lubricating region (I, in figure 3) is reached. Viscous forces dominate in this region and the bearing is capable of carrying great loads. Air bearings are designed to operate only in region I, but the gap height depends on the supply pressure, geometry of the bearing pad, load on the bearing, and the type of air flow through the gap separating the bearing from the pad.
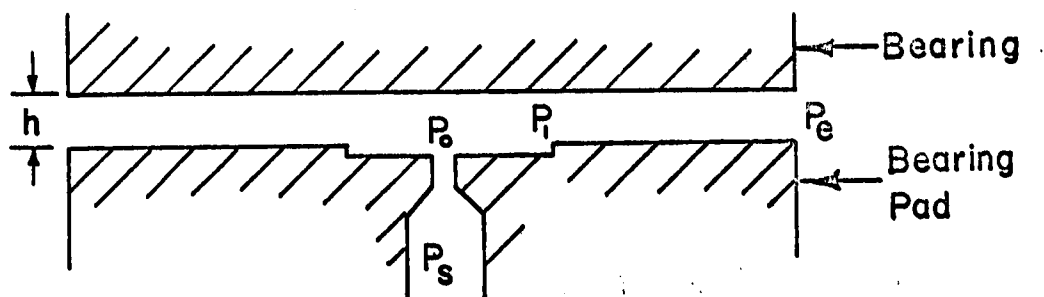
Figure 4. Schematic bearing and bearing pad.

Gas flows from a plenum at constant pressure $P = P_s$, through a restrictor where it is reduced to $P = P_0$. The gas then enters a recess (sometimes not present) and flows through the recess to the lubricating film inlet. The pressure at the inlet, $P = P_1$, will be equal to or less than P_0, depending on whether the annular area presented to flow at the exit of the restrictor is greater or less than the cross sectional area of the restrictor. If the annular area is greater, then $P_1 = P_0$ and the bearing is externally compensated. If the annular area is less than the area of the restrictor, then $P_1 < P_0$ and the bearing is inherently compensated. The gas passes through the lubricating film (with thickness h) and exhausts at $P = P_e$.

The load carrying capacity of the bearing is:

$$\text{Lift} = \int P \cdot dA \qquad (2.1)$$

where P is the distributed pressure acting on the bearing surface normal to an element of area, dA.

The hydrostatic bearing is self-regulating; it will vary the pressure acting on the bearing to compensate for an increased (or decreased) load. Referring to figure 4, if the load is increased, the gap height will be decreased and there will be more resistance to flow over the bearing pad. Therefore the pressure P_0 will increase automatically to balance the increased load. If the load is decreased, the process is reversed. The load which causes P_0 to equal P_s also causes the bearing to touch the pad and is called the closure load.

The maximum allowable load depends on the bearing geometry (the area over which P acts), the supply pressure, P_s, and the distributed pressure P.

There are many factors which govern the gas flow from pressure $P = P_s$ to $P = P_e$; and each factor affects the load-carrying capacity:

    a. The geometry of the pad determines whether the flow is longitudinal, radial, or a combination of both.

    b. The gap height and pressure drops between sections determine whether the flow is laminar or turbulent and whether viscous or inertia forces dominate.

    c. Velocities of the gas may exceed the speed of sound (especially in radial flow) and shockwaves may develop in the lubricating film.

The bearing under study has the following types of flow:

    a. Flow through a tube (through the restrictor),

    b. Radial flow between two parallel walls (at exit of the restrictor),

    c. Flow through a rectangular duct in combination with radial flow (across the pad), and

    d. Longitudinal flow between two parallel walls (at the exit).

II: LONGITUDINAL FLOW

Laminar longitudinal flow. The following assumptions are made:

a. Flow is fully developed (streamlines are parallel).

b. Flow is steady, conservative, and one-dimensional.

c. Coefficient of dynamic viscosity is independent of the pressure.
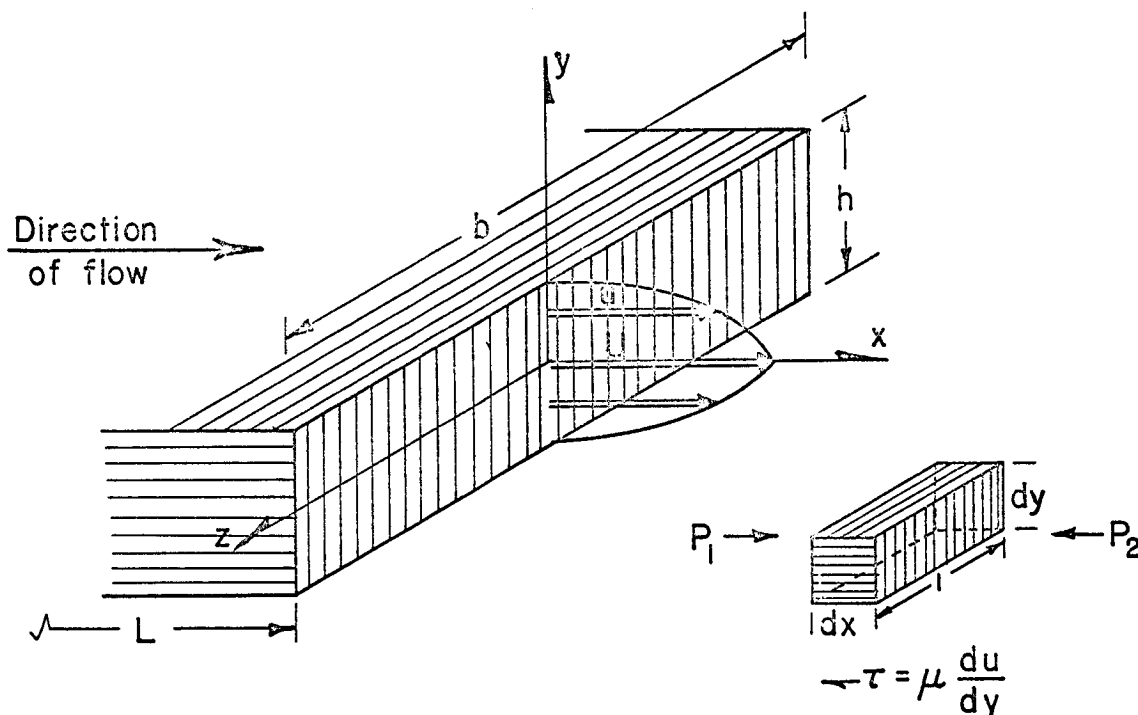
Figure 5. Laminar longitudinal flow.

Consider a parallelepiped of fluid length dx (in the direction of flow), height dy, and unit width; acted on by forces of pressure and viscosity. Neglecting the body forces of weight and inertia, the Navier-Stokes equations reduce to:[7]

---

[7]Salamon Eskinazi, Principles of Fluid Mechanics, (Boston: Allyn and Bacon, 1962). p. 362.

$$-\frac{dP}{dx} + \mu\frac{d^2u}{dy^2} = 0$$

$$\frac{dP}{dx} = \mu\frac{d^2u}{dy^2} , \qquad\qquad (2.2)$$

written as a total derivative since all other partials are zero under the assumptions made. The pressure, P, depends only on x over the entire length, L. The velocity, u, depends only on y. Therefore both sides of equation (2.2) must be equal to a constant, since one side cannot be a function of x alone and the other a function of y alone. Also, since the pressure decreases as the distance x increases, dP/dx must be a negative constant.

Holding dP/dx constant and integrating,

$$\frac{dP}{dx} y = \mu\frac{du}{dy} + C \qquad\qquad (2.3)$$

At the center of the channel, $(y = 0)$, there is no change in velocity; therefore du/dy = 0 and C = 0.

Again holding dp/dx constant and integrating,

$$\frac{dP}{dx} \frac{y^2}{2} = \mu u + D \qquad\qquad (2.4)$$

Since the flow is steady and conservative, the mass flow is constant. Therefore (2.9) is

$$\rho \left(\frac{dP}{dx}\right) = \frac{-12\mu M}{h^3} = \text{Constant}$$

and using (2.10)

$$\rho_1 \left(\frac{P}{P_1}\right)^{1/m} \left(\frac{dP}{dx}\right) = \frac{-12\mu M}{h^3} \quad . \tag{2.11}$$

Now, integrating from section 1 where the pressure is P_1 to another section a distance x from section 1:

$$\rho_1 \int_{P_1}^{P} \frac{P^{1/m}}{P_1^{1/m}} dP = \frac{-12\mu M}{h^3} \int_0^x dx \quad ;$$

$$\tag{2.12}$$

$$\frac{m}{m+1} \frac{\rho_1}{P_1^{1/m}} \left[P_1^{(m+1)/m} - P^{(m+1)/m} \right] = \frac{12\mu M}{h^3} x$$

which expresses $P^{(m+1)/m}$ as a linear function of x.

At a distance $x = L$ where the pressure is $P = P_2$, equation (2.12) is:

$$\tag{2.13}$$

$$\frac{m}{m+1} \frac{\rho_1}{P_1^{1/m}} \left[P_1^{(m+1)/m} - P_2^{(m+1)/m} \right] = \frac{12\mu M}{h^3} L$$

By dividing (2.12) by (2.13), the ratio

$$\frac{P_1^{(m+1)/m} - P^{(m+1)/m}}{P_1^{(m+1)/m} - P_2^{(m+1)/m}} = \frac{x}{L} \tag{2.14}$$

is formed, from which the distributed pressure, P, may be expressed in a form independent of the gap height, h:

(2.15)

$$P = \left[P_1^{(m+1)/m} - \frac{x}{L} \left(P_1^{(m+1)/m} - P_2^{(m+1)/m} \right) \right]^{m/(m+1)}$$

Solving (2.13) for the mass flow, M:

$$M = \frac{h^3}{12\mu L} \cdot \frac{m}{m+1} \frac{\rho_1}{P_1^{1/m}} \left[P_1^{(m+1)/m} - P_2^{(m+1)/m} \right] \quad (2.16)$$

For isothermal flow, m = 1, and the viscosity, μ, is constant for constant temperature (previously assumed unchanging with pressure). Equations (2.15) and (2.16):

$$P = \left[P_1^2 - \frac{x}{L} \left(\frac{\rho_1}{P_1} \right) \left(P_1^2 - P_2^2 \right) \right]^{1/2} \quad (2.17)$$

and

$$M = \frac{h^3}{24\mu L} \left(\frac{\rho_1}{P_1} \right) \left(P_1^2 - P_2^2 \right) \quad (2.18)$$

or, in terms of volume flow, $Q_1 = M / \rho_1$:

$$Q_1 = \frac{h^3}{24\mu L} \frac{\left(P_1^2 - P_2^2 \right)}{P_1} \quad (2.19)$$

The above equations are for a unit width and for the simplified theory where the body forces of weight and inertia have been neglected.

Considering the forces of inertia, Euler's theorem is applied to the surfaces of a control volume ABCD with thickness dx and unit width:
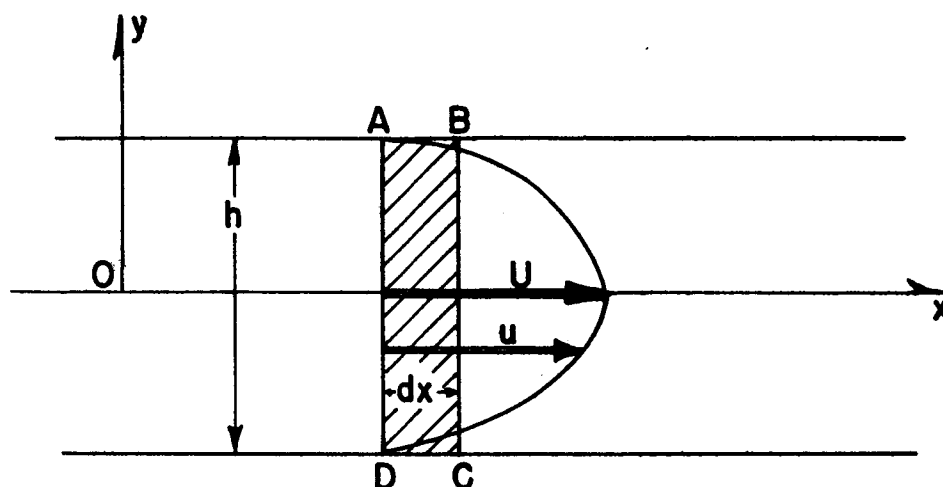
Figure 6. Laminar longitudinal flow considering the forces of inertia.

The following assumptions are made:

a. The pressure, P, temperature, T, and specific mass, ρ, are functions of x alone--constant in the same cross section.

b. The change is polytropic:

$$\frac{P}{\rho^m} = \frac{P_1}{\rho_1^m} \tag{2.20}$$

c. The velocity distribution is symmetric in relation to OX and is of the form:

$$\frac{u}{U} = f\left(\frac{2y}{h}\right) \sim y, \tag{2.21}$$

for the moment unknown, and U is the maximum velocity in the center of the channel, $f(0) = 1$, a function of x alone.

    d. The total mass flow is constant, given by:

$$M = \int_{-h/2}^{+h/2} \rho u\, dy$$

but $u = U \cdot f(2y/h)$, from equation (2.21). Setting $\alpha = 2y/h$,

$$dy = \frac{h}{2}\, d\alpha; \quad \text{when } y = +\frac{h}{2}, \ \alpha = 1; \ y = -\frac{h}{2}, \ \alpha = -1$$

Now

$$M = \rho U \frac{h}{2} \int_{-1}^{1} f(\alpha)\, d\alpha = \rho U h \int_{0}^{1} f(\alpha)\, d\alpha = \rho U h a \tag{2.22}$$

The mass entering the control volume through face AD:

$$I_1 = \int_{-h/2}^{h/2} \rho u\, dy\, u = \rho U^2 h \int_{0}^{1} f^2(\alpha)\, d\alpha = \rho U^2 h b$$

where

$$\int_{0}^{1} f^2(\alpha)\, d\alpha = b, \text{ and } \int_{0}^{1} f(\alpha)\, d\alpha = a,$$

constants depending on the velocity distribution.

The mass leaving the control volume through face BC:

$$I_2 = hb\rho U^2 + hb \frac{d}{dx} (\rho U^2) dx$$

where the second term is due to a change in inertia forces in the thickness dx.

Neglecting the forces of gravity and calling T the skin friction for a unit surface between faces AB and CD, Euler's theorem is written:

$$I_2 - I_1 = hP - h(P + \frac{dP}{dx} dx) + 2dx \cdot T = - h \frac{dP}{dx} dx + 2 T dx$$

therefore:

$$hb \frac{d}{dx} (\rho U^2) = - h \frac{dP}{dx} + 2 T \tag{2.23}$$

Using equation (2.22), $M = \rho U h a$, the LHS of (2.23):

$$\frac{d}{dx} (\rho U^2) = \frac{d}{dx} (\frac{M}{ha} U) = \frac{M}{ha} \cdot \frac{dU}{dx}$$

and (2.23) may now be written:

$$\frac{b}{a} M \frac{dU}{dx} = - h \frac{dP}{dx} + 2 T$$

or

$$\frac{b}{a} \cdot \frac{M}{h} \cdot \frac{dU}{dx} = - \frac{dP}{dx} + \frac{2T}{h} \qquad (2.24)$$

To evaluate the constants a and b, consider the velocity distribution as parabolic:

$$\frac{u}{U} = 1 - \left(\frac{2y}{h}\right)^2$$

from which

$$a = \int_0^1 (1 - \alpha^2) \, d\alpha = \frac{2}{3}$$

and

$$b = \int_0^1 (1 - \alpha^2)^2 \, d\alpha = \frac{8}{15} \quad .$$

For laminar flow, the skin friction, T, on a unit surface, is

$$T = \mu \left(\frac{du}{dy}\right)_{y = \frac{h}{2}} = - \frac{4\mu U}{h} \qquad (2.25)$$

Using this expression for T and the numerical values of the constants a and b, equation (2.24) is

$$\frac{4}{5} \cdot \frac{M}{h} \cdot \frac{dU}{dx} = - \frac{dP}{dx} - \frac{12\mu V}{h^2}$$

or, with the average velocity $V = 2/3\ U$,

$$\frac{6}{5} \cdot \frac{M}{h} \cdot \frac{dV}{dx} = - \frac{dP}{dx} - \frac{12\mu V}{h^2} \ ;$$

$$\frac{6}{5} \frac{M}{h} dV + dP = - \frac{12\mu V}{h^2} dx \ . \tag{2.26}$$

Eliminate V from this equation by using the equation of state (2.20) and the equation of continuity:

$$\rho V = \rho_1 V_1 = \text{Constant} \tag{2.27}$$

$$V = \frac{\rho_1 V_1}{\rho} = V_1 \left(\frac{P_1}{P}\right)^{1/m}.$$

Using this relationship for V, equation (2.26) may be written:

$$\left[\frac{6}{5} \cdot \frac{M}{h} \cdot \frac{m}{m+1} \cdot \frac{V_1}{P} - \left(\frac{P}{P_1}\right)^{1/m}\right] dP = \frac{12\mu V_1}{h^2} dx \tag{2.28}$$

and after integrating

$$\frac{6}{5} \cdot \frac{M}{h} \frac{m}{m+1} V_1 \text{Ln} P - \frac{m}{m+1} \frac{P^{(m+1)/m}}{P_1^{1/m}} = \frac{12\mu V_1}{h^2} + C \ , \tag{2.29}$$

or

$$\frac{6}{5} \cdot \frac{M^2}{h^2} \cdot \frac{m}{m+1} \text{Ln} P - \frac{m}{m+1} \frac{\rho_1}{P_1^{1/m}} P^{(m+1)/m} = \frac{12\mu M}{h^3} x + C \ .$$

At $x = 0$, $P = P_1$. Evaluating the constant and inserting it back into equation (2.29):

$$\frac{m}{m+1} \frac{\rho_1}{P_1^{1/m}} (P_1^{(m+1)/m} - P^{(m+1)/m}) - \frac{6}{5} \frac{m}{m+1} \frac{M^2}{h^2} \ln \frac{P_1}{P} =$$

$$\frac{12 \mu M}{h^3} x. \tag{2.30}$$

This equation, which may be written for a section 2, distance L from section 1, is comparable to equation (2.12), derived without considering the forces of inertia. The term $\ln P_1/P$ denotes the change in momentum in the direction of flow.

Turbulent longitudinal flow. The Reynolds number, based on the hydraulic mean depth, is defined by

$$Re \triangleq \frac{2hV}{\nu} \tag{2.31}$$

where h is gap height, V is the average velocity in the gap, and ν is the kinematic viscosity = μ/ρ. The Reynolds number is a dimensionless ratio of inertial forces to viscous forces and is an indication of whether the flow is turbulent. Laminar flow generally exists for Reynolds numbers less than 2,000. At greater Reynolds numbers, turbulent flow may exist, but under extremely well controlled conditions, laminar flow has been observed at Reynolds numbers up to 24,000.[a]

---

[a]Hermann Schlichting, Boundary Layer Theory, (New York: McGraw-Hill Book Co. Inc., 1955) p. 309.

A resistance coefficient, λ, is defined by setting the pressure gradient proportional to the dynamic head, i. e. to the square of the average velocity of flow:[9]

$$- \frac{dP}{dx} = \frac{\lambda}{d} \frac{\rho}{2} V^2 \qquad (2.32)$$

For longitudinal flow between parallel walls: [10]

$$- \frac{dP}{dx} = \frac{\lambda}{h} \rho V^2 \qquad (2.33)$$

The resistance coefficient is related to the Reynolds number-- for turbulent flow between two parallel walls, Blasius found experimentally[11]

$$\lambda = \frac{0.079}{Re^{1/4}} , \qquad (2.34)$$

where Re is based on the hydraulic mean depth.

Substituting this value in equation (2.33):

$$- \frac{dP}{dx} = \frac{0.079}{h\,Re^{1/4}} \rho V^2. \qquad (2.35)$$

---

[9] Ibid., p. 63.

[10] Oscar Pinkus and Beno Sternlicht, Theory of Hydrodynamic Lubrication, (New York: McGraw-Hill Book Co., 1961), p. 26.

[11] Ibid., p. 24.

Now, from equation (2.31)

$$Re = \frac{2hV}{\nu} = \frac{2\rho hV}{\mu}$$

and

$$Re^{1/4} = \frac{1.18\rho^{1/4}h^{1/4}V^{1/4}}{\mu^{1/4}} \quad .$$

Substituting in equation (2.35):

$$-\frac{dP}{dx} = \frac{0.079\rho V^2 \mu^{1/4}}{1.18h\rho^{1/4}h^{1/4}V^{1/4}}$$

and using the relationship $M = g\rho Q = g\rho b h V$,

$V^2 = M^2 / g^2 \rho^2 b^2 h^2$; and $M^{1/4} = g^{1/4} \rho^{1/4} b^{1/4} h^{1/4} V^{1/4}$;

$$-\frac{dP}{dx} = \frac{0.067 M^2 \mu^{1/4}}{M^{1/4} g^{7/4} b^{7/4} \rho h^3} = \frac{0.067 M^{7/4} \mu^{1/4}}{g^{7/4} b^{7/4} \rho h^3} \quad (2.36)$$

Multiplying both sides by $P = g\rho R T$ and separating variables:

$$-P dP = \frac{0.067 M^{7/4} \mu^{1/4} R T}{g^{3/4} b^{7/4} h^3} dx.$$

Integrating from the point $x = 0$ where the pressure is P_1 to a point x where the pressure is P:

$$P_1^2 - P^2 = \frac{.133 M^{7/4} \mu^{1/4} R T}{g^{3/4} b^{7/4} h^3} x \quad (2.37)$$

and at $x = L$, $P = P_e$:

$$P_1^2 - P_e^2 = \frac{.133\, M^{7/4} \mu^{1/4} RT}{g^{3/4} b^{7/4} h^3} L \quad . \tag{2.38}$$

Dividing (2.37) by (2.38) results in the same form of pressure distribution as in laminar flow, equation (2.14).

Solving (2.38) for M, mass flow,

$$M = \left[\frac{g^{3/4} b^{7/4} h^3}{.133 \mu^{1/4} L} \quad \frac{(P_1^2 - Pe^2)}{RT} \right]^{4/7} \tag{2.39}$$

an equation for mass flow under turbulent conditions analogous to equation (2.18), derived for laminar flow.

Lift. The lift provided by longitudinal flow in the bearing is the integral of the distributed pressure, P, over an element of area, dA:

$$\text{Lift} = \int P \cdot d A \tag{2.1}$$

For longitudinal flow:

$$P = P_1 \left\{ 1 - \frac{x}{L} \left[1 - \left(\frac{Pe}{P_1} \right)^2 \right] \right\}^{1/2} \quad .$$

$$d A = b\, dx \tag{2.17}$$

where b is the width of the longitudinal gap.

The pressures are absolute, therefore the force exerted by the ambient pressure on the top of the bearing above the longitudinal gap must be subtracted to obtain the net lift. With this consideration,

equations (2.1) and (2.17) combine to form

$$\text{Lift} = \int_0^L P_1 \left\{ 1 - \frac{x}{L} \left[1 - \left(\frac{Pe}{P_1}\right)^2 \right] \right\}^{1/2} b\,dx - bLPe \ .$$

Evaluating the integral:

$$P_1 b \int_0^L (1 - Ax)^{1/2} \, dx$$

where

$$A = \frac{1}{L} \left[1 - \left(\frac{Pe}{P_1}\right)^2 \right] \text{ is constant for a given load.}$$

$$\int = P_1 b \left(- \frac{2}{3A}\right)(1 - Ax)^{3/2} \bigg|_0^L = - \frac{2}{3} \cdot \frac{P_1 b}{A} (1 - AL)^{3/2}$$

$$+ \frac{2P_1 b}{3A}$$

$$= \frac{2}{3} \cdot \frac{P_1 b}{A} \left[1 - \left(\frac{Pe}{P_1}\right)^3 \right] \ .$$

$$\text{Lift} = \frac{2}{3} P_1 b L \frac{\left[1 - \left(\frac{Pe}{P_1}\right)^3 \right]}{\left[1 - \left(\frac{Pe}{P_1}\right)^2 \right]} - bLPe$$

$$\text{Lift} = bLP_1 \left\{ \frac{2\left[1 - \left(\frac{Pe}{P_1}\right)^3 \right]}{3\left[1 - \left(\frac{Pe}{P_1}\right)^2 \right]} - \frac{Pe}{P_1} \right\} \tag{2.40}$$

an expression for lift provided by flow through a gap of width b and

length L.

III. RADIAL FLOW

Laminar radial flow. Using the same procedure as in developing the theory for longitudinal flow between two parallel planes, the flow rate

$$Q = \frac{M}{\rho} = - \frac{h^3}{12\mu} \frac{dP}{dx} \qquad (2.9)$$

for a unit width. In radial flow, the width is

$$2 \pi r$$

and the length in the direction of flow, dr, varies from r_c to R_3 (using the notation in the geometry analysis, Chapter III, Figure 15). The flow rate in radial flow:

$$Q = - \frac{2\pi r h^3}{12\mu} \frac{dP}{dr} . \qquad (2.41)$$

For compressible flow, with polytropic expansion,

$$Q = Q_0 \left(\frac{P_0}{P} \right)^{1/m} ,$$

therefore equation (2.41) becomes

$$Q_0 \left(\frac{P_0}{P} \right)^{1/m} = - \frac{\pi h^3 r}{6\mu} \frac{dP}{dr} .$$

Separating variables,

$$Q_0 P_0^{1/m} \frac{dr}{r} = \frac{-\pi h^3}{6\mu} \cdot P^{1/m} dP,$$

and integrating

$$Q_0 P_0^{1/m} \ln r = -\frac{\pi h^3}{6\mu} \cdot \frac{m}{m+1} P^{(m+1)/m} + C.$$

At $r = r_c$, $P = P_0$. Therefore the constant C is

$$C = Q_0 P_0^{1/m} \ln r_c + \frac{\pi h^3}{6\mu} \frac{m}{m+1} \cdot P_0^{(m+1)/m}$$

and substituting this value into equation (2.42):

$$Q_0 P_0^{1/m} \ln \frac{r}{r_c} = \frac{\pi h^3}{6\mu} \cdot \frac{m}{m+1} (P_0^{(m+1)/m} - P^{(m+1)/m}). \tag{2.43}$$

At $r = R_3$, $P = P_1$. Equation (2.43) becomes

$$Q_0 P_0^{1/m} \ln \frac{R_3}{r_c} = \frac{\pi h^3}{6\mu} \frac{m}{m+1} (P_0^{(m+1)/m} - P_1^{(m+1)/m}). \tag{2.44}$$

For isothermal flow, $m = 1$. Equations (2.43 and 2.44) are now

$$Q_0 P_0 \ln \frac{r}{r_c} = \frac{\pi h^3}{12\mu} (P_0^2 - P^2) \tag{2.45}$$

and

$$Q_0 P_0 \ln \frac{R_3}{r_c} = \frac{\pi h^3}{12\mu} (P_0^2 - P_1^2) \tag{2.46}$$

Dividing (2.45) by (2.46), form the ratio

$$\frac{\ln \frac{r}{rc}}{\ln \frac{R_3}{rc}} = \frac{P_0{}^2 - P^2}{P_0{}^2 - P_1{}^2}$$

from which the pressure distribution for radial flow is

$$P = \left[P_0{}^2 - \frac{\ln \frac{r}{rc}}{\ln \frac{R_3}{rc}} (P_0{}^2 - P_1{}^2) \right]^{1/2} \qquad (2.47)$$

The volume flow, from equation (2.46), is

$$Q_0 = \frac{\pi h^3}{12 \mu \ln \frac{R_3}{rc}} \cdot \frac{(P_0{}^2 - P_1{}^2)}{P_0} \qquad (2.48)$$

and the mass flow, using the relationship $M = \rho_0 Q_0$:

$$M = \frac{\pi h^3}{12 \mu \ln \frac{R_3}{rc}} \frac{\rho_0}{P_0} (P_0{}^2 - P_1{}^2) \qquad (2.49)$$

Turbulent radial flow. In developing the relationships for

turbulent longitudinal flow, it was pointed out that the friction

factor is a function of the Reynolds number. The Reynolds number,

in turn, is a function of the average velocity of flow. In radial flow,

the gas behaves in a manner much different than in longitudinal flow.

The velocity profile tends to a constant value as r tends to infinity.

Therefore the flow never becomes fully developed and the velocity

is changing at all times. This phenomenon is known as radial

diffusion--there is no simple substitution as in fully developed

turbulent longitudinal flow.

Comolet[12] discusses turbulent flow and points out work accomplished by other authors. He states that none of the theory is completely satisfactory--except for small gap heights and very low Reynolds numbers. He observed turbulent flow for Reynolds numbers as low as 550. Analytical treatment and even a good empirical formula for turbulent radial flow remain problems to be solved.

Lift. The total lift provided by radial flow in the bearing includes the lift by the pressure P_0 acting over the radius of the entrance tube, r_c. Integrating the distributed pressure from equation (2.47) over the area as for longitudinal flow,

$$\text{Lift} = \pi r_c^2 P_0 + \int_{rc}^{R_3} 2\pi r P \, dr - \pi R_3^2 P_1 \, . \qquad (2.50)$$

In this expression, $P = P_0 \left\{ 1 - \dfrac{\ln \frac{r}{re}}{\ln \frac{R_3}{re}} \left[1 - (\frac{P_1}{P_0})^2 \right] \right\}^{1/2} .$

$$2A^2 = \frac{1}{\ln \frac{R_3}{rc}} \left[1 - (\frac{P_1}{P_0})^2 \right]$$

is constant for a given load. Therefore

$$P = P_0 \left[1 - 2A^2 \ln \frac{r}{rc} \right]^{1/2}$$

Now

$$\text{Lift} = \pi(r_c^2 P_0 - R_3^2 P_1) + 2\pi P_0 \int_{r_c}^{R_3} \left[1 - 2A^2 \ln \frac{r}{r_c} \right]^{1/2} r \, dr \, . \qquad (2.51)$$

---

[12]Raymond Camolet, op. cit., pp. 38, 39.

Let $r/r_c = x$; $dr = r_c\, dx$; $r = rx_c$ and when $r = R_3$, $x = R_3/r_c$; when $r = r_c$, $x = 1$.

The integral becomes:

$$\int = 2\pi P_0 r_c^2 \int_1^{R_3/r_c} [1 - 2A^2 \ln x]^{1/2} x\, dx\ .$$

Make the substitution

$$1 - 2A^2 \ln x = A^2 t^2$$

$$\ln x = \frac{1}{2A^2} - \frac{t^2}{2}\ ; \quad x = e^{\frac{1}{2A^2} - \frac{t^2}{2}}\ ; \quad x\, dx = -e^{\frac{1}{A^2} - t^2} t\, dt\ .$$

Evaluating the limits: at $x = 1$, $t = 1/A$; at $x = R_3/r_c$,

$$t = \sqrt{\frac{1}{A^2} - 2\ln \frac{R_3}{r_c}} = \frac{1}{A}\left(\frac{P_1}{P_0}\right)$$

The integral is now

$$\int = 2\pi P_0 r_c^2 \int_{1/A}^{1/A(P_1/P_0)} At\,(-e^{1/A^2 - t^2}) t\, dt = -2\pi P_0 r_c^2 A e^{1/A^2} \int_{1/A}^{1/A(P_1/P_0)} t^2 e^{-t^2}\, dt\ .$$

Integrating by parts:

$$\int = \pi P_0 r_c^2 A e^{1/A^2} \left[t e^{-t^2} \Big|_{1/A}^{1/A(P_1/P_0)} - \int_{1/A}^{1/A(P_1/P_0)} e^{-t^2}\, dt \right.$$

$$\int = \pi P_0 r_c{}^2 A e^{1/A^2} \left[\frac{1}{A} \left(\frac{P_1}{P_0}\right) e^{-1/A^2 (P_1/P_0)^2} - \frac{1}{A} e^{-1/A^2} + \int_{1/A(P_1/P_0)}^{1/A} e^{-t^2} dt \right]$$

with the limits of integration reversed since $P_1/P_0 < 1$.

$$\int = \pi P_0 r_c{}^2 e^{1/A^2} \left(\frac{P_1}{P_0} e^{-1/A^2 (P_1/P_0)^2} - e^{-1/A^2}\right)$$

$$+ \pi P_0 r_c{}^2 e^{1/A^2} \left[\int_0^{1/A} e^{-t^2} dt - \int_0^{1/A(P_1/P_0)} e^{-t^2} dt \right]$$

Now, using the error function:[13]

$$\text{erf } x = \frac{2}{\sqrt{\pi}} \int_0^x e^{-t^2} dt,$$

$$\int = \pi P_1 r_c{}^2 e^{[1 - (P_1/P_0)^2]/A^2} - \pi P_0 r_c{}^2 + \frac{\pi^{3/2} P_0 r_c A e^{1/A^2}}{2}$$

$$\left\{ \text{erf}\left(\frac{1}{A}\right) - \text{erf}\left[\frac{1}{A}\left(\frac{P_1}{P_0}\right)\right] \right\}$$

and combining with equation (2.51):

---

[13] Granino A. Korn and Theresa M. Korn, Mathematical Handbook for Scientists and Engineers, (New York: McGraw-Hill Book Company, 1961) Table F-13, p. 899.

$$\text{Lift} = \pi(r_c{}^2 P_0 - R_3{}^2 P_1) + \pi P_1 r_c{}^2 e^{[1 - (P_1/P_0)^2]/A^2} - \pi P_0 r_c{}^2$$

$$+ \frac{\pi^{3/2} P_0 r_c{}^2 A e^{1/A^2}}{2} \left\{ \text{erf}\left(\frac{1}{A}\right) - \text{erf}\left[\frac{1}{A}\left(\frac{P_1}{P_0}\right)\right] \right\}$$

Now

$$e^{[1 - (P_1/P_0)^2]/A^2} = e^{2 \ln(R_3/r_c)} = \frac{R_3{}^2}{r_c{}^2}$$

and after canceling like terms,

$$\text{Lift} = \frac{1}{2} \pi^{3/2} A P_0 r_c{}^2 e^{1/A^2} \left\{ \text{erf}\left(\frac{1}{A}\right) - \text{erf}\left[\frac{1}{A}\left(\frac{P_1}{P_0}\right)\right] \right\} \qquad (2.52)$$

where $A = \left[\dfrac{1 - \left(\dfrac{P_1}{P_0}\right)^2}{2\ln\dfrac{R_3}{r_c}} \right]^{1/2}$, constant for a given load.

IV. FLOW THROUGH TUBES

Laminar tubular flow. With the same assumptions as proposed for longitudinal flow and considering a cylinder of fluid-- length dx, radius $r^2 = y^2 + z^2$, it is best to use cylindrical coordinates.
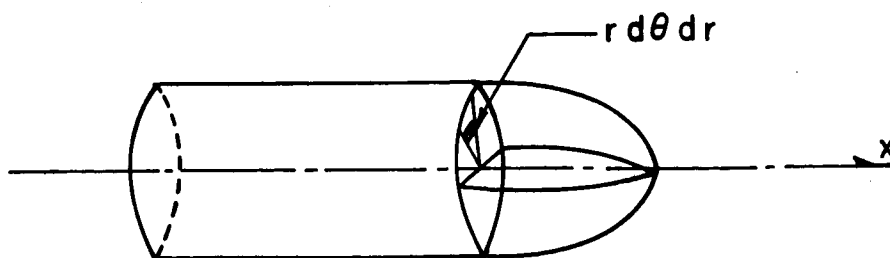
Figure 7. Laminar fully developed flow through a tube.

The required transformations are:

$$\frac{\partial^2 u}{\partial y^2} \quad \text{and} \quad \frac{\partial^2 u}{\partial z^2} \,.$$

u is the axial component of the velocity and is the only component in steady laminar flow. Therefore u is a function of r alone, and there are no acceleration terms since the velocity is constant.

$$\frac{\partial r}{\partial y} = \frac{y}{r} \; ; \; \frac{\partial r}{dz} = \frac{z}{r}$$

$$\frac{\partial u}{\partial y} = \frac{\partial u}{\partial r} \frac{\partial r}{\partial y} = \frac{y}{r} \frac{\partial u}{\partial r}$$

$$\frac{\partial u}{\partial z} = \frac{\partial u}{\partial r} \frac{\partial r}{\partial z} = \frac{z}{r} \frac{\partial u}{\partial r}$$

and differentiating again,

$$\frac{\partial^2 u}{\partial y^2} = \frac{y^2}{r^2} \frac{\partial^2 u}{\partial r^2} + \left(\frac{1}{r} - \frac{y^2}{r^2} \right) \frac{\partial u}{\partial r}$$

$$\frac{\partial^2 u}{\partial z^2} = \frac{z^2}{r^2} \frac{\partial^2 u}{\partial r^2} + \left(\frac{1}{r} - \frac{z^2}{r^2} \right) \frac{\partial u}{\partial r}$$

The viscous terms in the Euler equation become:

$$\mu \left(\frac{\partial^2 u}{\partial y^2} + \frac{\partial^2 u}{\partial z^2} \right) = \mu \left(\frac{\partial^2 u}{\partial r^2} + \frac{1}{r} \frac{\partial u}{\partial r} \right)$$

and the equation of motion is

$$\frac{dP}{dx} = \mu \left(\frac{\partial^2 u}{\partial r^2} + \frac{1}{r} \frac{\partial u}{\partial r} \right) = \mu \frac{1}{r} \cdot \frac{d}{dr} \left(r \frac{du}{dr} \right) \qquad (2.53)$$

where total derivatives are used since all other partials vanish. The pressure is a function of x alone and the velocity is a function of r alone. Since one side of an equation cannot be a function of x and the other a function of r, both must be equal to the same constant and the equation may be integrated. Integration of (2.53) with dP/dx constant in that cross section yields:

$$r \frac{du}{dr} = \frac{r^2}{2\mu} \frac{dP}{dx} + C$$

or

$$\frac{du}{dr} = \frac{r}{2\mu} \frac{dP}{dx} + \frac{C}{r}$$

and integrating again,

$$u = \frac{r^2}{4\mu} \cdot \frac{dP}{dx} + C \ln r + D \qquad (2.54)$$

At r = 0 (the center of the tube) du/dr is zero, and at $r = r_c$ (the sides of the tube) u is zero. With these boundary conditions, the constants C and D are evaluated:

$$C = 0, \quad D = -\frac{r_c^2}{4\mu} \frac{dP}{dx} .$$

Equation (2.54) becomes:

$$u = \frac{r^2}{4\mu} \frac{dP}{dx} [1 - (\frac{r_c}{r})^2], \qquad (2.55)$$

the characteristic paraboloidal velocity distribution in a pipe.

At $r = 0$, $u = U$, the maximum velocity in the center of the tube.

$$U = - \frac{r_c^2}{4\mu} \frac{dP}{dx} \,,$$

a positive quantity since dP/dx is negative.

The average velocity is one-half the maximum velocity in a paraboloid: (as opposed to 2/3 for a parabola)

$$V = \frac{1}{2} U = - \frac{r_c^2}{8\mu} \frac{dP}{dx} \qquad (2.56)$$

and the volume flow, $Q = V A$:

$$Q = (- \frac{r_c^2}{8\mu} \frac{dP}{dx}) (\pi r_c^2) = - \frac{\pi r_c^4}{8\mu} \frac{dP}{dx} \qquad (2.57)$$

Using the perfect gas law,

$$Q_0 = Q_s (\frac{P_s}{P})^{1/m}$$

where $m = 1$ for isothermal flow, $m = \gamma$ for adiabatic flow, and $m = \infty$ for compressible flow. Equation (2.57) becomes

$$Q_s (\frac{P_s}{P})^{1/m} = - \frac{\pi r_c^4}{8\mu} \frac{dP}{dx} \,.$$

Integrating

$$Q_s P_s^{1/m} x = - \frac{\pi r_c^4}{8\mu} \cdot \frac{m}{m+1} P^{(m+1)/m} + C \qquad (2.58)$$

At $x = 0$, $P = P_s$. Therefore

$$C = \frac{\pi r_c^4}{8\mu} \frac{m}{m+1} P_s^{(m+1)/m}$$

and (2.58) is now

$$Q_s P_s^{1/m} x = \frac{\pi r_c^4}{8\mu} \frac{m}{m+1} (P_s^{(m+1)/m} - P^{(m+1)/m})$$

At $x = l_c$, $P = P_0$:

$$Q_s P_s^{1/m} l_c = \frac{\pi r_c^4}{8\mu} \frac{m}{m+1} (P_s^{(m+1)/m} - P_0^{(m+1)/m}$$

The volume rate for isothermal flow: $(m = 1)$:

$$Q_s = \frac{\pi r_c^4}{16\mu l_c} \frac{(P_s^2 - P_0^2)}{P_s} \qquad (2.59)$$

and the mass flow: $(M = \rho_s Q_s)$

$$M = \frac{\pi r_c^4}{16\mu l_c} \frac{\rho_s}{P_s} (P_s^2 - P_0^2) \qquad (2.60)$$

Expressions could be derived for the pressure distribution along the length of the tube and for the force on the walls of the tube, but the only matter of interest here is the pressure drop in the tube from entrance to exit.

Turbulent tubular flow. The same procedure is used as for turbulent longitudinal flow, but a different empirical relationship was found by Blasius for the friction coefficient of smooth pipes:[14]

$$\lambda = \frac{0.3164}{R_e^{1/4}} \tag{2.61}$$

where the Reynolds number is based on the diameter of the pipe.

$$Re = \frac{DV}{\nu} = \frac{\rho DV}{\mu} = \frac{2\rho r_c V}{\mu}$$

$$Re^{1/4} = \frac{1.18 \rho^{1/4} r_c^{1/4} V^{1/4}}{\mu^{1/4}} \ . \tag{2.62}$$

The equation defining the friction coefficient was given previously as

$$- \frac{dP}{dx} = \frac{\lambda}{d} \frac{\rho}{2} V^2 = \frac{\lambda}{4r_c} \rho V^2 \ . \tag{2.32}$$

Combining equations (2.61) and (2.62) and substituting in (2.32):

$$- \frac{dP}{dx} = \frac{.3164 \, \mu^{1/4} \rho V^2}{4.72 \rho^{1/4} r_c^{1/4} V^{1/4} r_c} \ .$$

[14]Hermann Schlichting, op. cit., p. 401. (valio for 2000<Re<100,000).

Now, using the relationship $M = g\rho \pi r_c^2 V$;

$$V^2 = M^2/g^2 \rho^2 \pi^2 r_c^4 \text{ and } M^{1/4} = g^{1/4} \rho^{1/4} \pi^{1/4} r_c^{1/2} V^{1/4}:$$

$$-\frac{dP}{dx} = \frac{.3164\mu^{1/4} M^2 g^{1/4} \pi^{1/4} r_c^{1/4}}{g^2 \rho \pi^2 r_c^4 (4.72) M^{1/4} r_c} = \frac{.3164\mu^{1/4} M^{7/4}}{\pi^{7/4}(4.72)g^{7/4} \rho r_c^{19/4}}$$

and multiplying both sides by $P = g\rho R T$ and separating variables:

$$(\pi^{7/4} = 7.414)$$

$$- PdP = \frac{0.00904\mu^{1/4} M^{7/4} RT}{g^{3/4} r_c^{19/4}} dx .$$

Integrating from P_s at $x = 0$ to P at $x = x$:

$$P_s^2 - P^2 = \frac{0.01808 \mu^{1/4} M^{7/4} RT}{g^{3/4} r_c^{19/4}} x .$$

At $x = l_c$, $P = P_0$:

$$P_s^2 - P_0^2 = \frac{0.01808 \mu^{1/4} M^{7/4} RT}{g^{3/4} r_c^{19/4}} lc .$$

Solving for the mass flow

$$M = \left[\frac{g^{3/4} r_c^{19/4}}{0.01808 \mu^{1/4} lc} \cdot \frac{(P_s^2 - P_0^2)}{RT} \right]^{4/7} \tag{2.63}$$

an equation for turbulent mass flow in a tube analogous to equation (2.60) for laminar flow.

V. SPRING CONSTANT

Static spring constant. The static spring constant is defined by

$$\text{Stiffness} = \frac{\Delta w}{\Delta h}$$

where Δw is the load in lbs. required to produce the deflection, Δh in inches. The load supported by a bearing is given by the lift equations derived in the previous sections. Calculations which must be performed in order to obtain the static spring constant for a given bearing are:

a. For a given supply pressure, P_s, and gap height, h, calculate the lubricating film pressure, P_1, using the equations for mass flow. The mass flow into the bearing equals the mass flow out of the bearing in steady state.

b. Calculate the load w supported by pressure, P_1, using the equations for lift.

c. Vary the gap height by an amount Δh.

d. Calculate the pressure P_1, as in step a, for the new gap height, h + Δh.

e. Calculate the load supported by the new pressure P_1, w + Δw.

f. Form the ratio $\Delta w / \Delta h$ to determine the stiffness of the bearing at the given supply pressure and gap height.

Grinnell[15] uses a different method of indicating stiffness. He forms a ratio of dimensionless load, termed efficiency, to dimensionless displacement, termed attitude:

$$\text{efficiency} = \frac{\text{Total load on bearing}}{\text{Supply pressure x area of bearing}},$$

$$\text{attitude} = \frac{\text{Displacement from original gap height}}{\text{Original gap height}},$$

$$\text{stiffness measure} = \frac{\text{Attitude}}{\text{Efficiency}}.$$

A stiffness measure of 2 indicates a stiff bearing.

Dynamic spring constant. The dynamic spring constant is a function of the volume of gas in the lubricating film and recess, and the frequency of the disturbing force. If the bearing is subjected to a sinusoidal force, the spring constant and natural frequency it exhibits depend on the compressibility of the gas trapped between the bearing and the bearing pad.

All other parameters being equal, the bearing with a higher static spring constant will have a higher dynamic spring constant. However if one bearing has a large volume of trapped gas, (either because of a large recess or large gap height) it will have a much lower dynamic spring constant than a bearing with the same static spring constant, but a smaller volume of gas.

[15] Sherman K. Grinnell, "A Study of pressurized Air Bearing Design, Steady Loading-No Rotation," (M. S. Thesis, Massachusetts Institute of Technology, Cambridge, Massachusetts, 1954), p. 59.

The type of compensation also has a great influence on the

dynamic spring constant--capillary compensation, in general, is bad

because of the large volume of gas in the capillary tube. It should

be noted here that although the bearing in this study uses capillary

tube restrictors, the bearing is not capillary-compensated.. The

tubes are less than one inch long, therefore the volume of gas in

the tubes is small compared to the volume present in a true capillary-

compensated bearing which has tubes about ten feet long. The rate

of gas flow in the bearing under study is controlled by the annular

ring surrounding the tube at its exit, not by the capillary tube;

therefore the bearing is inherently-compensated. This point is

discussed further in Chapter V, page 110, in the course of analyzing

the results of experimental work.

VI. VIBRATIONS

Background vibrations, transmitted through the base to the

air-bearing, could be a source of major error if the vibrations are

transmitted to the model by the bearing. If the background vibrations

are near the natural, or resonant, frequency of the air-bearing

assembly, they are amplified as well as transmitted and could cause

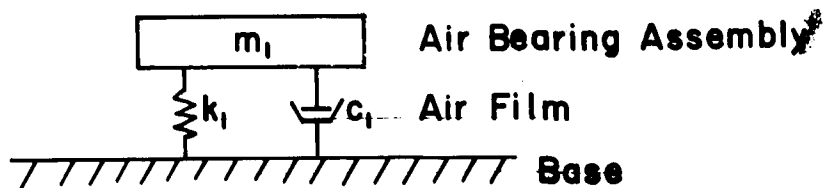the bearing to be unstable. In the unstable state, the glass bearing,
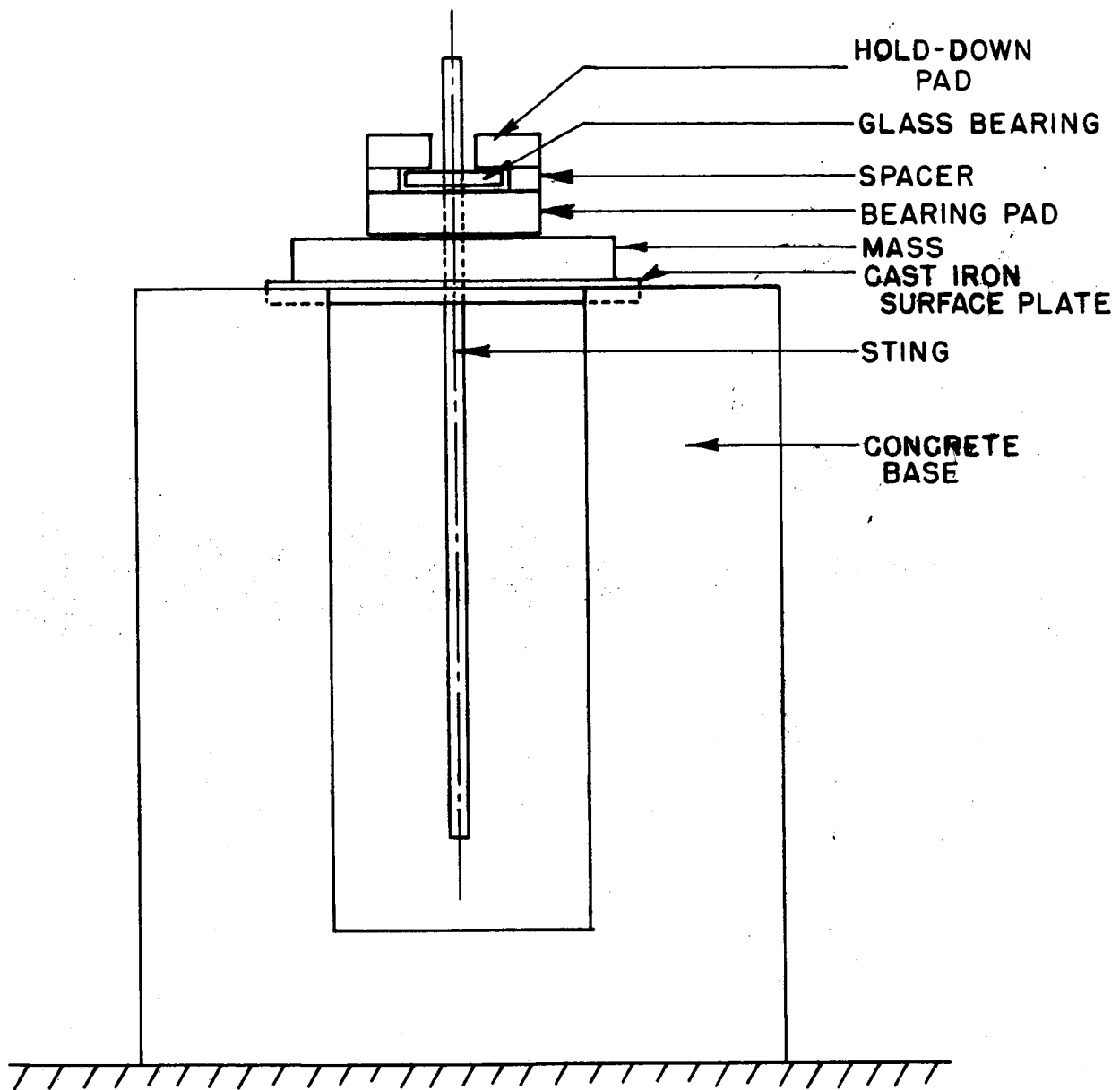

Figure 8. Equivalent Spring-Mass-Damper System

Figure 9. Air Bearing and Base Assembly

sting, and model oscillate continuously because of the background

vibrations. It is possible to calculate the theoretical natural

frequency of the air-bearing assembly. Figure 9 is a sketch of

the bearing and base. Figure 8 is the equivalent spring-mass-

damper system.

Eliminating effect of background vibrations. One may

eliminate the effect of background vibrations by isolating the base

from outside vibration--building it on bed-rock. The only vibrations

transmitted would be earth tremors--building movements are

eliminated. However, this air-bearing will eventually be placed

on top of a wind-tunnel and subjected to a large background vibratory

field; therefore the base was poured on the floor of the laboratory.

Background vibrations are present and their effect is studied.

There is a vibration-damping material, Isomode[16], that can

be used to reduce the natural frequency of the air-bearing assembly.

It is placed between the bearing and the base. The equivalent spring-
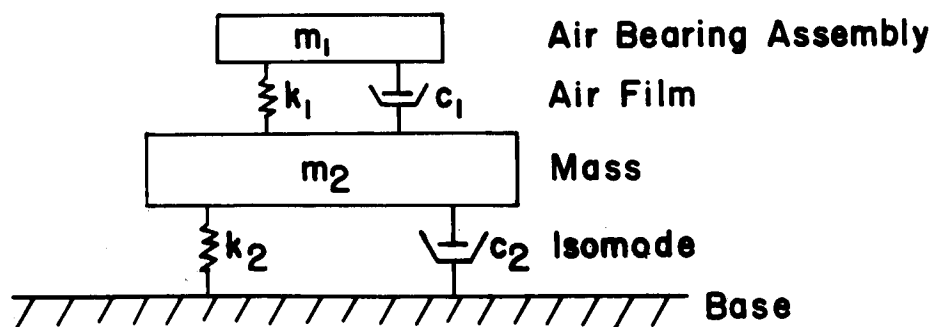
mass-damper system is now:

Figure 10. Equivalent Spring-Mass-Damper System with Isomode

This method is useful if the background frequencies and the natural frequency of the m_1--k_1--c_1 system are high. By placing a soft spring and damper (k_2--c_2) into the system, the natural frequency is lowered and the high background frequencies are not transmitted to the bearing.

There is a problem created however--the bearing supports a model--the purpose of the air-bearing system is to measure forces on the model by sensing deflections and measuring the force required to reduce the deflections to zero. If the spring constant k_2 is much lower than k_1, as it must be to lower the natural frequency appreciably, then any vertical force on the model causes a deflection of the entire system by compressing the spring k_2. The position sensors do not pick up the displacement because they are mounted on the air-bearing assembly.

If there are no vertical forces and no yaw moments, the method could be used, but leveling the system is a problem with a soft spring support. The best way to eliminate the effect of background vibrations is to design the bearing so that its natural frequency is not near the frequencies present in the background vibrations. This may be accomplished by changing the mass, m_1, or the spring constant, k_1, or both.

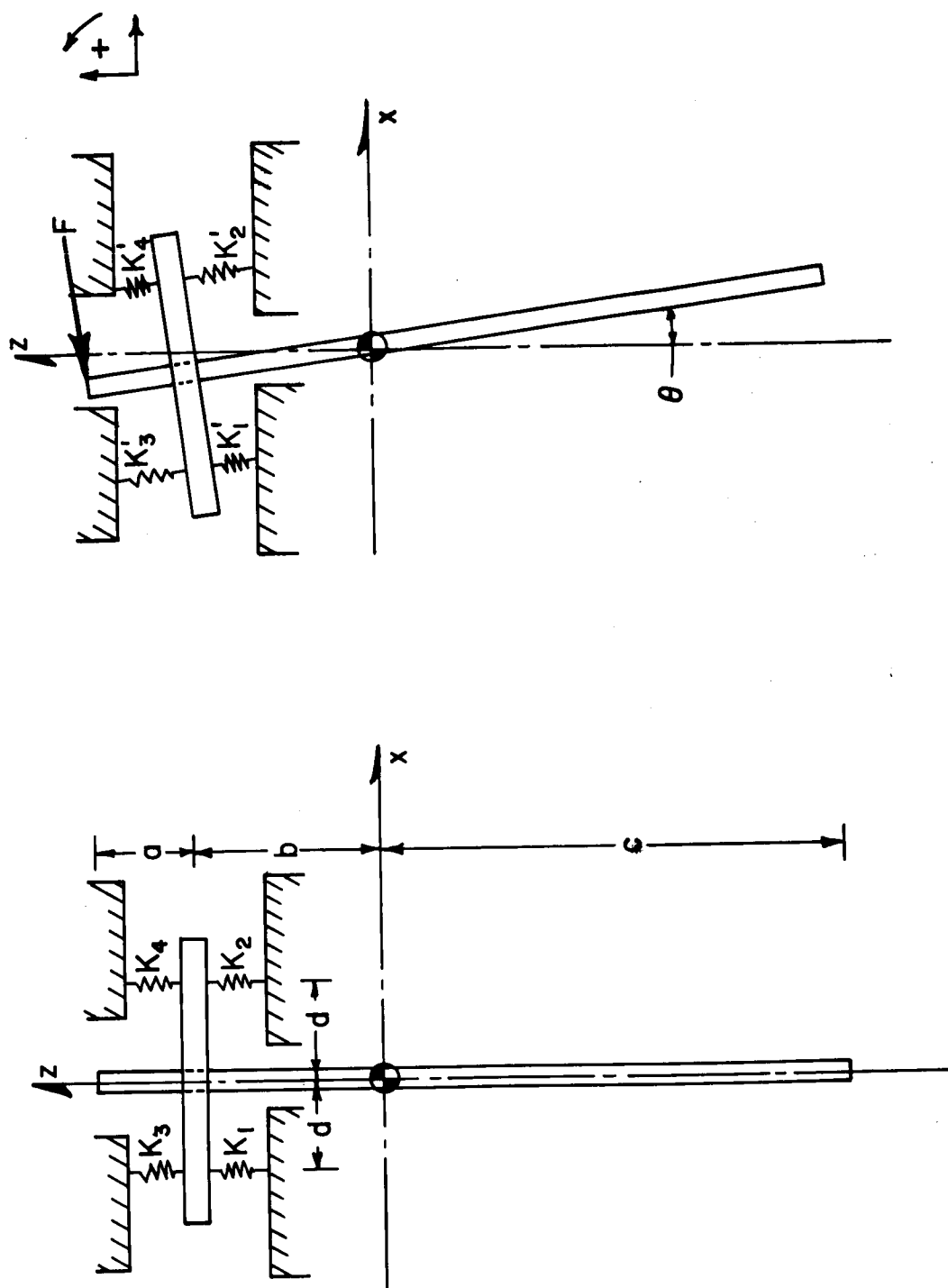Equations of motion. A sketch of the air-bearing spring-mass system is shown in Figure 11 .

Figure 11. Air Bearing Spring-Mass System

Figure 11 (a) is the equivalent spring--mass system for the air-bearing in equilibrium. The equivalent spring constants $K_1 = K_2 > K_3 = K_4$ depend on the gap height and supply pressure. The numerical values may be calculated as outlined previously.

Suppose the system is disturbed by a horizontal force, F, applied at the end of the sting, as by motors correcting a bearing displacement. The disturbed spring--mass system is sketched in Figure 11 (b). The spring constants are now $K_1' > K_4' > K_2' > K_3'$. Spring constants K_1 and K_4 increase to K_1' and K_4' because the gap height is decreased; K_2 and K_3 decrease to K_2' and K_3' because the gap height is increased.

Assuming no vertical displacement of the bearing and a small rotation about the center of gravity, θ, the equations of motion are:

$$m \ddot{x} = -K_1' \ (d \ \text{Sin} \ \theta) \ \text{Sin} \ \theta \ -K_2' \ (d \ \text{Sin} \ \theta) \ \text{Sin} \ \theta$$
$$+K_3' \ (d \ \text{Sin} \ \theta) \ \text{Sin} \ \theta \ +K_4' \ (d \ \text{Sin} \ \theta) \ \text{Sin} \ \theta$$
$$- F \ \text{Cos} \ \theta$$

$$J_\theta \ \ddot{\theta} = -K_1' \ (d \ \text{Sin} \ \theta) \ d \ +K_2' \ (d \ \text{Sin} \ \theta) \ d$$
$$+K_3' \ (d \ \text{Sin} \ \theta) \ d \ -K_4' \ (d \ \text{Sin} \ \theta) \ d$$
$$+F \ (a + b)$$

Linearizing, for small displacements, $\text{Sin } \theta = \theta$, $\text{Cos } \theta = 1$, and $\text{Sin}^2 \theta \approx 0$. The equations of motion become:

$$m \ddot{x} = -F \qquad (2.64)$$

$$J_\theta \ddot{\theta} = (K_2' + K_3') d^2 \theta - (K_1' + K_4') d^2 \theta + F(a + b) \qquad (2.65)$$

Taking the Laplace Transforms:

$$m s^2 X(s) = -F$$

$$X(s) = -F / ms^2 \qquad (2.66)$$

$$\left\{ J_\theta s^2 + [(K_1' + K_4') - (K_2' + K_3')] d^2 \right\} \theta(s) = F(a + b)$$

$$\theta(s) = \frac{F(a + b)}{J_\theta s^2 + [(K_1' + K_4') - (K_2' + K_3')] d^2} \qquad (2.67)$$

The inverse Laplace transforms yield:

$$x(t) = -\frac{F}{m} \cdot t \qquad (2.68)$$

$$\theta(t) = \frac{F(a + b)}{d \sqrt{J_\theta [(K_1' + K_4') - (K_2' + K_3')]}} \, \text{Sin } \omega t \qquad (2.69)$$

$$\text{where } \omega = d \sqrt{\frac{(K_1' + K_4') - (K_2' + K_3')}{J_\theta}} \quad .$$

The spring constants K_1', K_2', K_3', and K_4' depend on the corresponding gap heights and the distributed pressure, P. The determination of P, which depends on gas flow in converging and diverging gaps, is outside the scope of this thesis.

CHAPTER III

DESIGN AND FABRICATION

The prime objective is to have a bearing with a high equivalent spring constant. Little thought was given to the load it must support, since the load is of the order of 10 pounds and the target spring constant is to be about 100,000 pounds per inch.

The decisions leading to the final design and fabrication of the air-bearing support are presented in the order in which they were considered.

I. DESIGN

Gap height. As indicated in Chapter II, the theoretical relationships between pressure, gap height, flow rate, and supported load are all interdependent. The pressure distribution was shown to be independent of the gap height, though the actual pressure at a given point is dependent on the gap height. As a point of departure, the gap height was fixed arbitrarily at 0.0005 inch. This height is one of many used by authors who have conducted experiments with air bearings and seems to give good results. Careful and precise lapping produces a smooth surface finish to allow operation at this small gap. A small gap height ensures that viscous forces dominate and that the gas flow rate will be kept to a minimum, since it varies with the cube of the gap height.

51

Size and pressure. The next consideration was the pressure
required to give sufficient lift and produce a stiff equivalent spring
constant. The total lift of the bearing varies directly with the pressure
providing lift and with the square of the radius (assuming a circular
bearing). Consequently, the bearing surface and the pressure over
that surface should be large to obtain maximum lift and maximum
equivalent spring constant. A bearing five inches in diameter was
chosen for the following reasons:

a. Sufficient area to provide lift--approximately twenty
square inches with only five pounds pressure will provide one
hundred pounds lift.

b. A five-inch diameter bearing is easily mounted on top
of the wind-tunnel; it is neither too large nor too heavy.

c. A lapped and polished surface is available commercially
in the form of an optically flat piece of glass--flat to one-tenth
wave length (0.000002 inch) with parallel top and bottom surfaces
to two seconds of arc. [17]

A definite supply pressure was not set at this time, although an
upper limit of thirty pounds per square inch was set for testing
purposes. The actual pressure used will depend on the results
of tests conducted with the bearing.

---

[17]Original plans were to measure deflections by optical
means and feed back the information to pressure regulators to
keep a constant gap height. An air gage was used to measure
deflections which obviated the optical method.

Geometry. As mentioned earlier, it is desirable to have a large pressure acting over as large an area as possible to provide lift. The geometry of the bearing pad controls the area over which pressures act:
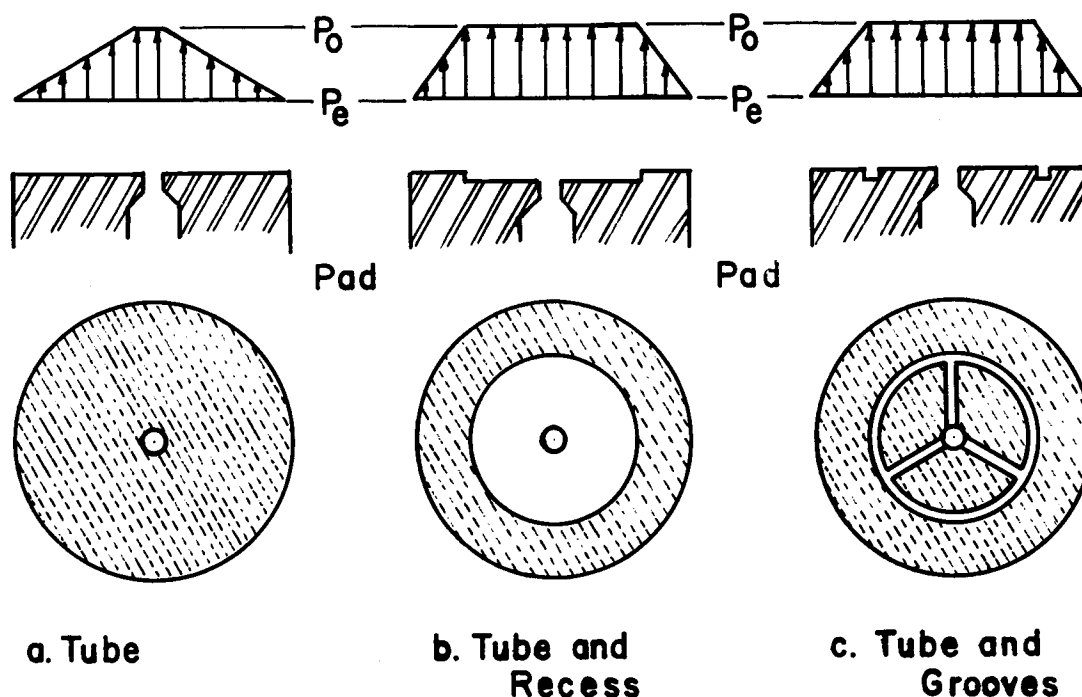
Figure 12 Three possible geometric configurations for bearing pad.

The three configurations drawn schematically above are possible radial geometric designs for a circular bearing. The pressure profile for each geometry is shown above the end view of the bearing pad. The total lift provided is the integral of the distributed pressure over the area; therefore, the area under each profile is an indication of the relative lift for each configuration. Configuration "a" has the least lift; configurations "b" and "c"

have identical lift. Many authors[18] have analyzed the effect of the enclosed volume of gas on the stability of the bearing. All state that a bearing with a minimum volume of enclosed gas (in the film and recess) is the most stable. A recess depth roughly equivalent to the film thickness will be stable. A way to reduce the gas volume to a minimum and still have a large high-pressure area is with grooves, as indicated in Figure 12c.

Grooves are used for the bearing tested in this thesis. The geometrical design is sketched on the next page. As indicated, there are four identical quadrants, each designed to act independently of the other. The model is affixed to a sting, normal to the paper, and is subjected to forces along the x and y axes and also to a moment about the z axis (normal to the paper). The bearing provides virtually no resistance to these forces[19], but does resist motion along the z axis and resists moments about the x and y axes. The four quadrants act independently to restrain the bearing to an equilibrium point on the z axis in the xy plane.

---

[18]William A. Gross, Gas Film Lubrication (New York: John Wiley and Sons, 1962), p. 366.

L. Licht, D. D. Fuller, and B. Sternlicht, "Self Excited Vibrations of an Air-Lubricated Thrust Bearing," Transactions ASME, Vol. 80, pp. 411-414.

W. H. Roudebush, "An Analysis of the Effect of Several Parameters on the Stability of an Air-Lubricated Hydrostatic Thrust Bearing," NACA TN-4095.

L. Licht and H. Elrod, "A Study of the Stability of Externally Pressurized Gas Bearings," Journal of Applied Mechanics, Trans. ASME, Vol. 82, pp. 250-258.

[19]The forces are in the range of 0.005 to 0.5 pound and are to be measured electronically with equipment to be developed.
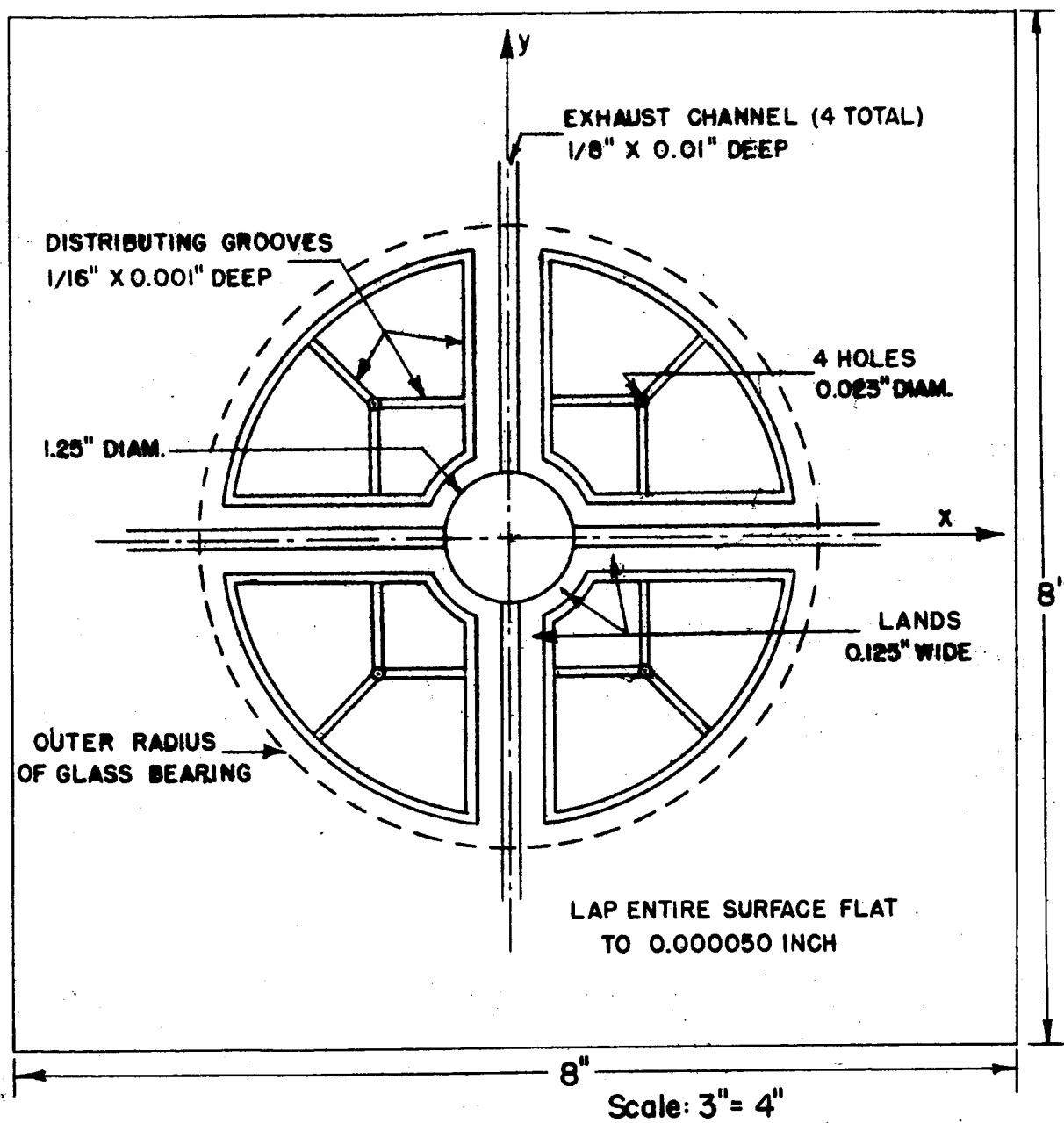
Figure 13. Configuration of Bearing Pad

Four exhaust grooves are cut along the x and y axes to isolate each quadrant. Gas enters through the hole in the center of the quadrant after passing through the restrictor. It changes direction ninety degrees, then expands radially until it meets the grooves. From this point outward, the flow is partly radial (over the pie-shaped land areas between the grooves) and partly channel flow (through the grooves).

$r_o = 0.006''$

$0.0625''$

Outer limit of
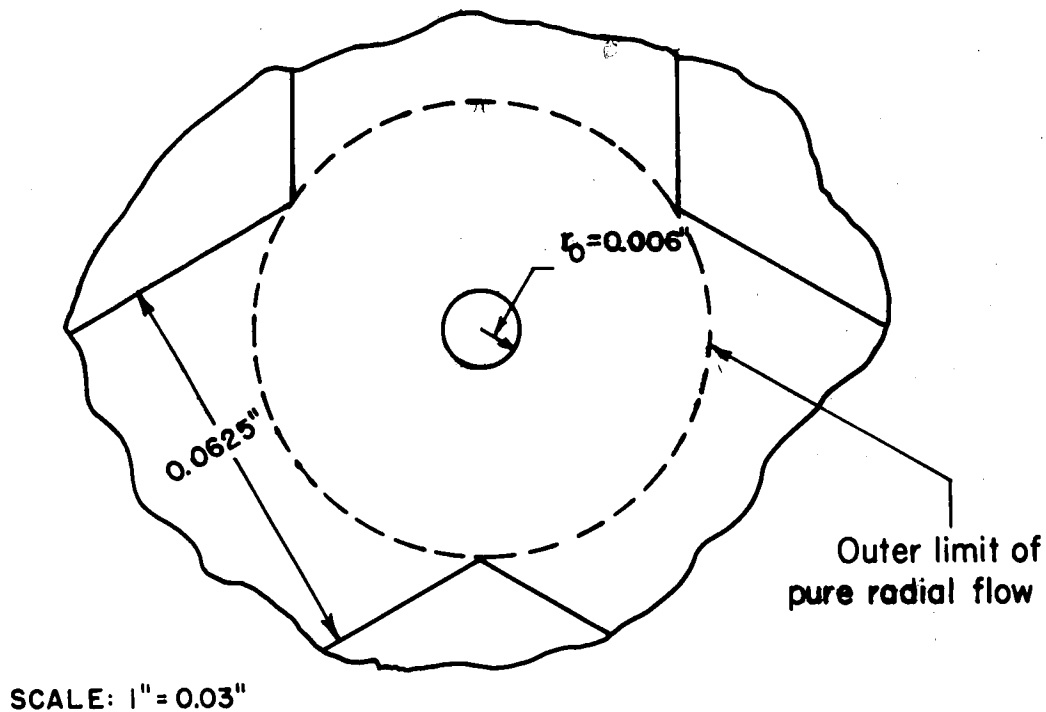pure radial flow

SCALE: 1" = 0.03"

Figure 14. Enlarged view of tube entrance area.

Referring to Figures 13 and 14, the combined flow is initially mostly channel flow since the cross-sectional area presented to the flow is larger through the grooves. The cross-sectional area of the

grooves for steady-state operation is constant, given by:

$$A_g = 3 \, b(d + h) = 3 \, (.0625)(.001 + .0005) = \underline{.000282}'' \text{ sq. in.}$$
(3.1)

where b is groove width, 0.0625 inch,

d is groove depth, 0.001 inch, and

h is gap height, 0.0005 inch.

The cross-sectional area of radial flow over the lands:
(where r is the radial distance from the center of the entrance tube)

$$A_l = 2\pi \, r \, h - 3 \, b \, h \text{ (approximately)}$$

$$= 2 \, (3.1417)(.0005) \, r - 3 \, (.0625)(.0005)$$

$$A_l = \underline{0.00314 \, r - 0.000094} \text{ (varies with the distance, r, from}$$

the entrance tube). (3.2)

The radius, r, at which the cross-sectional areas over the lands and through the grooves are equal is:

$$r = \frac{.000282 + .000094}{.00314} = \underline{0.1197 \text{ inch}}$$
(3.3)

Up to this distance, resistance to flow is less through the grooves, therefore the pressure drop at that radius in the grooves is less, and the pressure at the center of the grooves is higher than the pressure at the center of the land area. Beyond this distance, gas will flow from the groove over its lip and into the land area as well as along the grooves. This flow pattern is very complex. A theoretical analysis will not be attempted, but the pressure in the outer groove must be determined to calculate the amount of lift

provided by the bearing pad.

The gas is now at some pressure P_1, $P_0 > P_1 > P_e$, in the outer periphery of the grooves and it exhausts over the land area surrounding the grooves to the ambient pressure, P_e. For laminar flow over the lands, the ratio of gap height to exhaust land length (in the direction of flow) should be: [20]

$$\frac{\text{Gap Height}}{\text{Land Length}} \geqslant \frac{1}{1000} \; , \qquad\qquad (3.4)$$

To obtain this ratio, the exhaust land length is

$$L \geqslant 0.0005 \, (1000) = \underline{0.5 \text{ inch}} \qquad\qquad (3.5)$$

Fully developed flow (unchanging velocity profile), either laminar or turbulent, is obtained for a lateral distance of:[21]

$$L \geqslant 10 \, h \; = \; 10 \, (0.0005) = 0.005 \text{ inch.} \qquad\qquad (3.6)$$

which represents an h/L ratio of 1/10.

A value of L = 0.125 in., between the extremes given by equations (3.5) and (3.6), was chosen as close to that given by equation (3.5) as practical to allow easy machining, give as much lift as possible, and ensure fully developed flow. Thus the h/L ratio for this bearing is 1/250, which ensures fully that viscous forces dominate over the exhaust lands.

---

[20]Sherman Grinnell, op. cit., p. ii.
[21]Raymond Comolet, op. cit., p. 19.

One-sixteenth inch was selected as the width of the grooves to provide easy machining and to allow sufficient area for gas flow to the outer perimeter groove--no theoretical considerations were made for this part of the geometry. Grooves were positioned to allow accurate machining: all grooves are concentric to the sting hole or at angles of 90° and 45° to each other. The areas enclosed by the grooves determine the lift of the bearing; therefore, it is imperative that the four areas be equal. All equal radii were cut at the same time and the horizontal, vertical, and 45° grooves were cut for two quadrants with each pass of the cutting tool.

The width (perimeter) of the exhaust land and the area enclosed by the grooves are needed to calculate the flow rate and lift. The sketch below is used to determine the width and enclosed area:
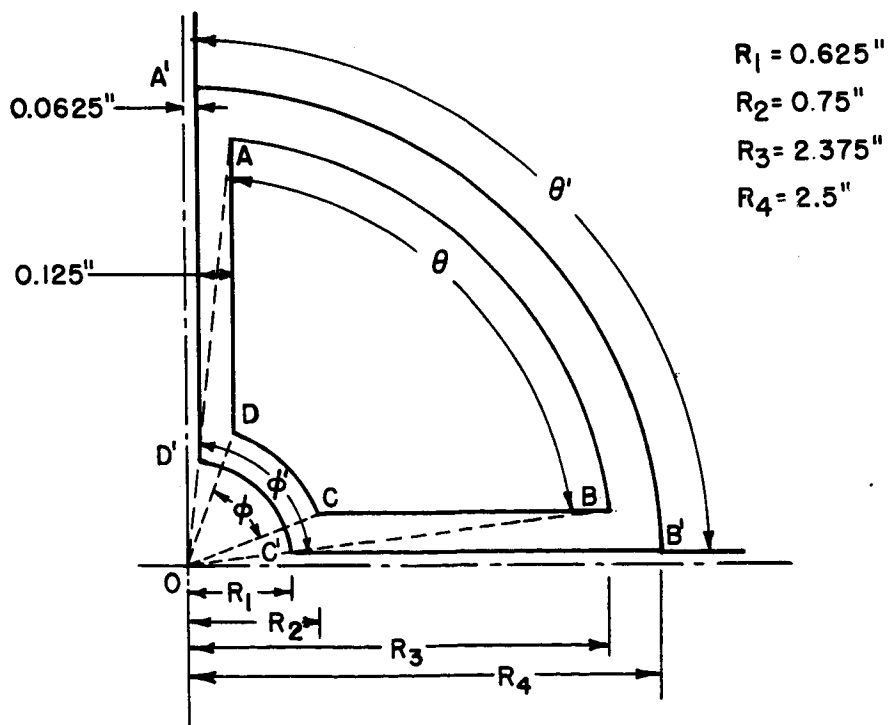

Figure 15. Geometry of Single Quadrant of Bearing Pad

Perimeter ABCD = width, b, in equation (2.18):

$$\overline{ABCD} = \frac{2 \pi R_3 \theta}{360} + \frac{2 \pi R_2 \phi}{360} + 2 \overline{CD} = \underline{7.43 \text{ inches}}$$

where $\theta = 90° - 2 \sin^{-1} (.1875/R_3) = 81°$,

$\phi = 90° - 2 \sin^{-1} (.1875/R_2) = 61°$,

and $\overline{CD} = R_3 \cos (\sin^{-1} .1875/R_3) - R_2 \cos (\sin^{-1} .1875/R_2)$

$\overline{CD} = R_3 \cos 4.5° - R_2 \cos 14.5° = 1.64 \text{ inches.}$

Area ABCD = area acted on by P_1:

$$\text{Area}_{ABCD} = \text{Area}_{AOB} - \text{Area}_{DOC} - 2 \text{Area}_{OCB}$$

$$= \pi R_3^2 \theta / 360 - \pi R_2^2 \phi / 360 - R_3 R_2 \sin \left(\frac{\theta - \phi}{2}\right)$$

$$\text{Area}_{ABCD} = \underline{3.36 \text{ sq. inches}}$$

Area A' B' C' D' - Area ABCD = area of exhaust land:

$$\text{Area}_{A'B'C'D'} = \text{Area}_{A'OB'} - \text{Area}_{D'OC'} - 2 \text{Area}_{OC'B'}$$

$$= \pi R_4^2 \theta' / 360 - \pi R_1^2 \phi' / 360 - R_4 R_1 \sin(\theta - \phi/2)$$

$$= 4.365 \text{ sq. inches}$$

where $\theta' = 90° - 2 \sin^{-1} (.0625/R_4) = 87.1°$,

$\phi' = 90° - 2 \sin^{-1} (.0625/R_1) = 78.5°$,

and area of exhaust land = 4.365 - 3.36 = $\underline{1.005 \text{ sq. inches}}$.

Discussion of the geometry of the pad is now complete.
Dimensions decided are indicated in Figure 13..

Restrictors. At steady state operation with no bearing oscillations, the mass flow through the restrictors must equal the mass flow out of the bearing over the exit land area. The mass flow into the bearing through one restrictor is given by:

$$M_{in} = \frac{\rho \pi r_0^4}{16 \mu lc} \frac{(P_s^2 - P_0^2)}{P_s} . \qquad (2.60)$$

The mass flow out of the bearing through one quadrant is given by:

$$M_{out} = \frac{\rho bh^3}{24 \mu l} \frac{(P_1^2 - P_e^2)}{P_1} \qquad (2.18)$$

For low pressures, the flow may be considered incompressible, assuming the density of the gas does not vary from entrance to exit. [22,23] Equations (2.60) and (2.18) become:

$$M_{in} = \frac{\rho \pi r_0^4}{8 \mu l_c} (P_s - P_0); \quad M_{out} = \frac{\rho bh^3}{12 \mu l} (P_1 - P_e) \qquad (3.7)$$

Setting the two equations equal and canceling like terms:

$$\frac{\pi r_0^4}{2 l_c} (P_s - P_0) = \frac{bh^3}{3 l} (P_1 - P_2)$$

---

[22] Kenneth Stark, "The Design of Various Types of Air Bearings for Frictionless Environments" NASA TN D-1100, May, 1962, pp. 2, 5.

[23]This is hardly an exact approach, but it gives good results.

After substituting known dimensions, a relationship for the length of the tube restrictor, l_c, in terms of the radius of the tube restrictor, r_c, is obtained:

$$l_c = 634 \times 10^6 \, r_c^4 \qquad (3.8)$$

Fully developed flow is obtained for $l_c > 116 \, r_c$, or 58 diameters for a Reynolds Number of 1000, based on the diameter of the tube.[24] Therefore, equation (3.8) must yield $l_c > 116 \, r_c$ to ensure fully developed flow in the entrance tube. A table of commercially-available hypodermic tubing follows:

TABLE I

BISHOP HYPODERMIC TUBING

Gauge	Inside diameter	Shortest length = 58 D
22	0.016"	0.928"
23	0.013	0.754
24	0.012	0.696
25	0.010	0.58

Substituting the inside diameters from Table I into equation (3.8) yields:

For 22 gauge: $r_c = .008$; $l_c = 2.60$ inches,

---

[24]Salamon Eskinazi, op. cit., p. 355.

for 23 gauge: $r_c = .0065$; $l_c = 1.13$ inches,

for 24 gauge: $r_c = .006$; $l_c = 0.821$ inches,

and for 25 gauge: $r_c = .005$; $l_c = 0.396$ inches.

All except 25 gauge exceed the minimum length. All of the above combinations of length and radius will provide equal pressure drops in the restrictor and across the exhaust land area, assuming incompressible flow. The tubing chosen for this bearing was 24 gauge because its relatively short length allowed the thinnest bearing pad, since the tube must be inserted normal to the bearing pad surface. The method of insertion is shown:
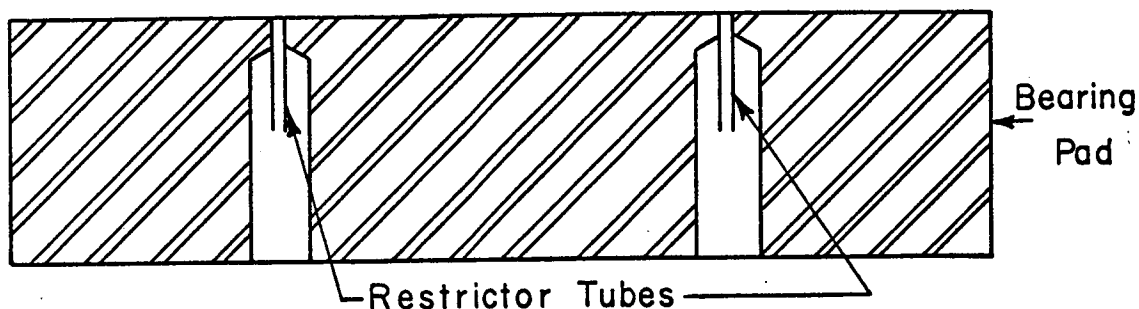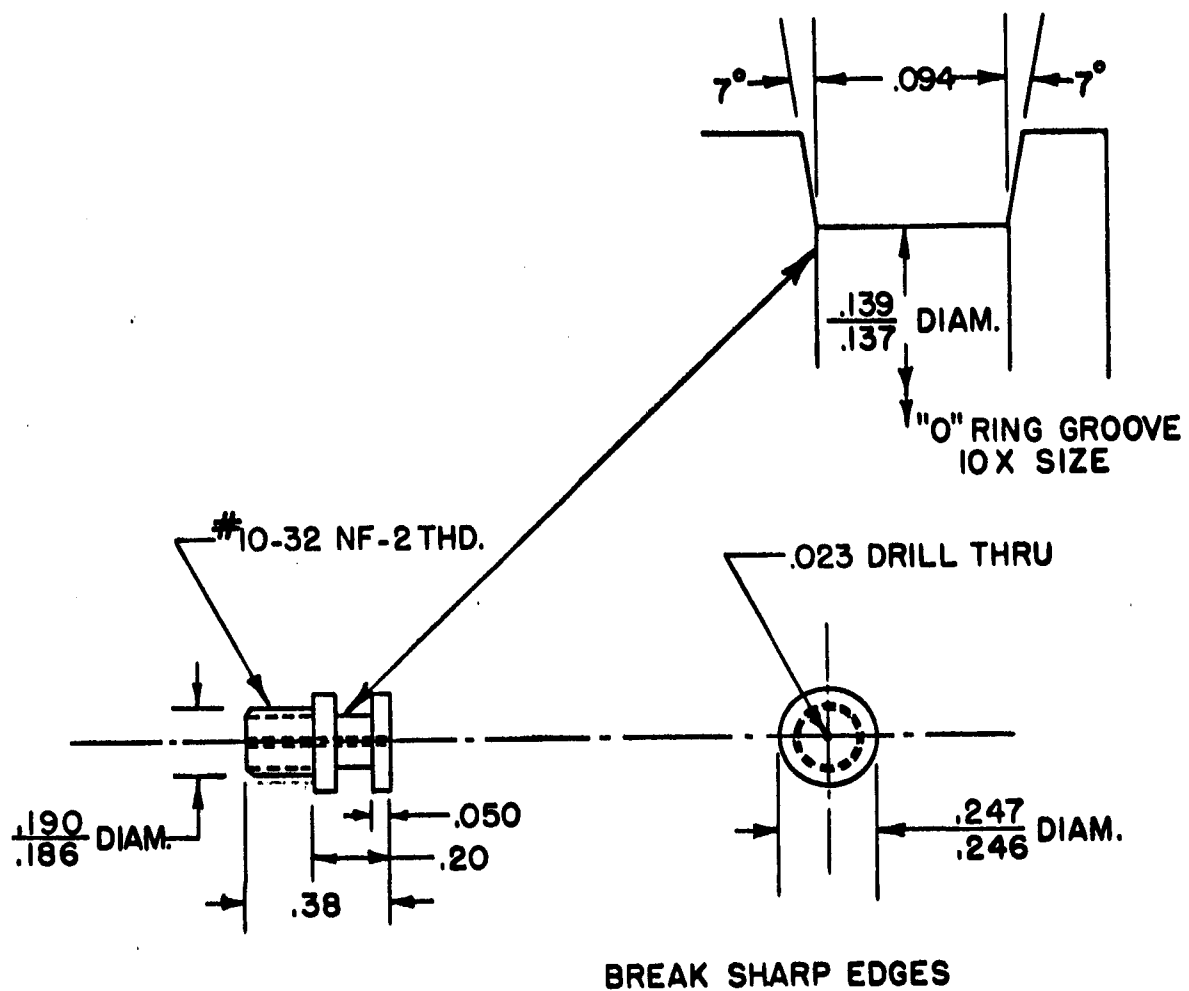

Figure 16. Restrictor Insertion

The next problem to be solved is purely mechanical-- mounting the restrictors in the bearing pad. The best method is to glue, weld, or silver-solder the tubes in place prior to lapping the surface. However, the length and radius of the tubes were picked based on incompressible flow theory, therefore they may

have to be changed if tests indicate the need for a different size restrictor. One good solution to this problem is to solder the tubes in a holder: Figure 17, next page.

The holder is inserted into an opening drilled in the bottom of the bearing pad (see Figure 16). The O-ring acts as a seal between the lower end of the tube and the top of the bearing pad. It is necessary to put packing in the space above the holder to prevent the top of the tube from being forced above the bearing pad surface by the supply pressure, P_s. The packing used is made in Great Britain under the trade name "Apiezon". It is primarily intended as a vacuum seal, however it performed well as a packing compound; it does not "run" or compress to any noticeable degree. The threads on the bottom of the holder facilitate its insertion into and removal from the bearing pad.

Hold-down pads. Original design specifications have a gap height of 0.0005 inch--all the remaining design features depend on that gap height. The gap must be maintained at 0.0005 inch, regardless of the supply pressure, to obtain maximum stiffness and low flow rates. Two ways to maintain constant gap height are:

a. Increase the weight of the bearing to reduce the gap height as the bearing pad supply pressure is increased, or

b. Install a hold-down pad above the glass bearing to supply a controlled, variable, downward force counter-acting the increased lift and thus reduce the gap height as the lower bearing pad pressure

Figure 17. Restrictor Tube Holder

is increased. The downward force is varied by changing the hold-down pad supply pressure.

The latter method is used for this bearing. The size is specified[26] and by following the design procedure outlined previously, the geometry for the hold-down pad is determined:

Figure 18. Hold-Down Pad Design

---

[26] Size of the upper bearing was limited to four pads each 4 x 1-1/4 inches. Space was reserved between the pads for position-sensing and measuring equipment to be installed later.

To calculate the perimeter of the land area and the area enclosed by the grooves with this geometry, the sketch below is used to determine the distance OY:
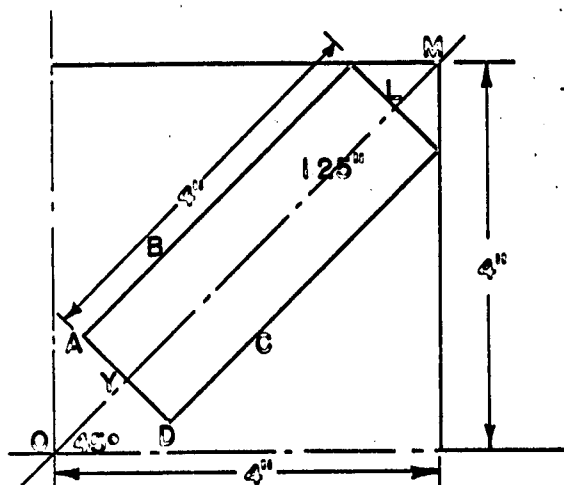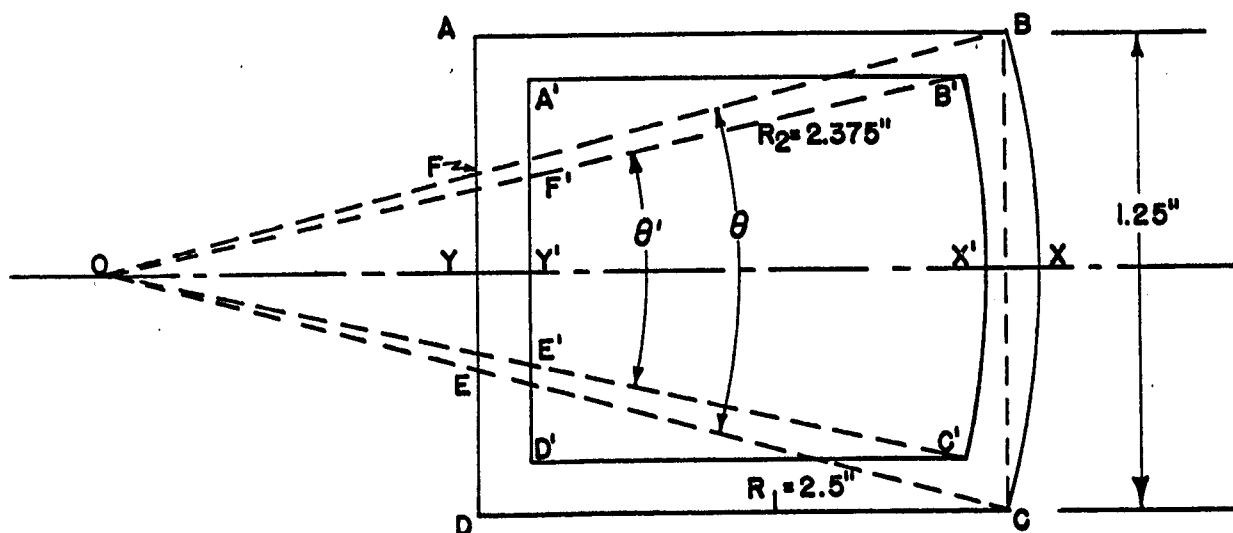

Now, using the distance OY and Figure 19,

Figure 19. Simplified Geometry of Hold-Down Pad

the perimeter of the grooved area is

$$\overline{A'B'C'D'} = \frac{2\pi R_2 \theta'}{360} + 2\overline{A'B'} + \overline{A'D'} = \underline{4.333 \text{ inches}} \quad ;$$

where $\theta' = 2 \sin^{-1} \dfrac{\overline{B'X'}}{\overline{O''B'}} = 2 \sin^{-1} \dfrac{.5}{2.375} = 24.3° \quad ,$

$$\overline{A'B'} = \overline{OX'} - \overline{OY'} = \overline{OB'} \cos \frac{\theta'}{2} - (\overline{OY} + .125) = 1.163" ,$$

$$\overline{A'D'} = \overline{AD} - 2(.125) = 1.00" \quad ;$$

the area enclosed by the grooves is

$$\text{Area}_{A'B'C'D'} = \text{Area}_{OB'C'} + 2 \text{ Area}_{A'B'F'} - \text{Area OE'F'}$$

$$= \frac{\pi R_2^2 \theta'}{360} + (\overline{A'B'} \times \overline{A'F'}) - \frac{1}{2}(\overline{OY'} \times \overline{E'F'}) = \underline{1.198 \text{ sq.inches}} ,$$

where $\overline{E'F'} = 2\left[\dfrac{\overline{OY'}}{\cos \theta'/2} (\sin \theta'/2)\right] = 2\left[1.186 \left(\dfrac{.5}{2.375}\right)\right] = .499" ,$

$$\overline{A'F'} = .5 - \frac{\overline{E'F'}}{2} = .2505" \quad ;$$

and the area of the exhaust lands is

Exhaust land area $= \text{Area}_{ABCD} - \text{Area}_{A'B'C'D'}$

$$\text{Area}_{ABCD} = \frac{\pi R_1^2 \theta}{360} + (\overline{AB} \times \overline{AF}) - \frac{1}{2}(\overline{OY} \times \overline{EF}) = 1.801 \text{ sq. inches} ,$$

where $\overline{AB} = \overline{OX} - \overline{OY} = OBCos\dfrac{\theta}{2} - 1.035 = 1.385''$,

$$\overline{EF} = 2\left[\dfrac{OY}{Cos\frac{\theta}{2}}(Sin\ \dfrac{\theta}{2})\right] = 2\left[1.0692\left(\dfrac{.625}{2.5}\right)\right] = .5346 ,$$

$$\overline{AF} = .625 - \dfrac{EF}{2} = .3577''\qquad \theta = 2sin^{-1}\dfrac{\overline{BX}}{\overline{OB}} = 2sin^{-1}\dfrac{.625}{2.5} = 29° ;$$

Exhaust land area = 1.801 - 1.198 = <u>0.603 sq. inches.</u>

Restrictor length and diameter are found in the same manner as for the bearing pad restrictors, using equation (3.7):

$$r_c = 0.006'', l_c = 1.41''$$

for 24 gauge hypodermic tubing.[25] The longer length (1.41" as compared to 0.821" for the bearing pad restrictor) is due to a shorter perimeter and, therefore, more resistance to flow in each hold-down pad.

Restrictors are installed in the same manner as for the bearing pad. A completed hold-down pad without grooves is shown:

---

[25]An upper gap of 0.00075 was used for the tested bearing due to incorrect spacer height--discussed later in this chapter. The restrictor length for a gap of .00075 in. is 0.72 inches.
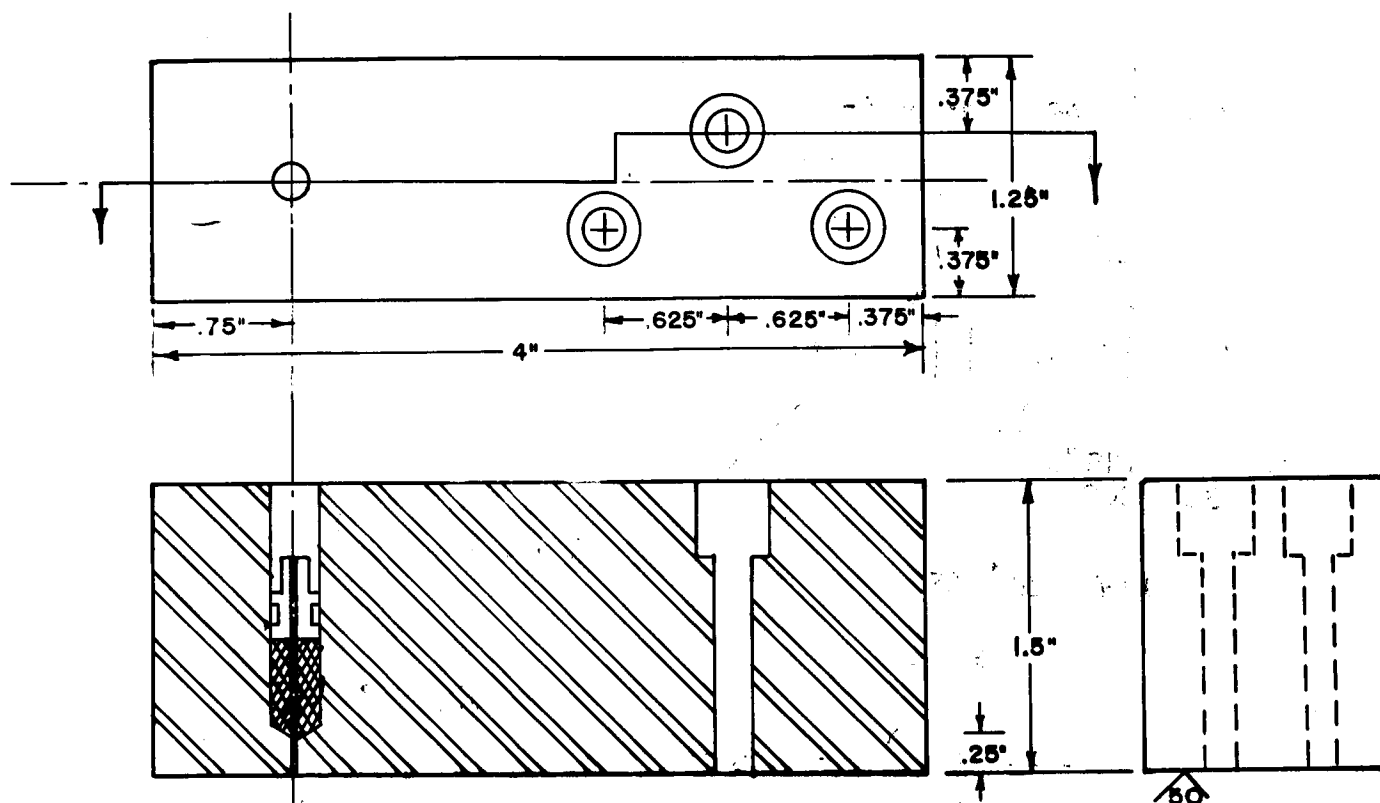
Figure 20. Hold-Down Pad Dimensions

The three holes in the right-hand end are to bolt the hold-down pads to the bearing pad in assembly.

Spacers. The hold-down pads must be assembled 0.001 inch above the glass bearing to ensure a gap height of 0.0005 inch on the top and bottom of the bearing when in operation. Spacers are placed between the hold-down pads and the bearing pad surface. They were lapped flat and parallel to a thickness of 0.001 inch greater than the thickness of the glass bearing. The glass supplied is 0.9405" thick; therefore the spacers were lapped to 0.9415" as sketched:
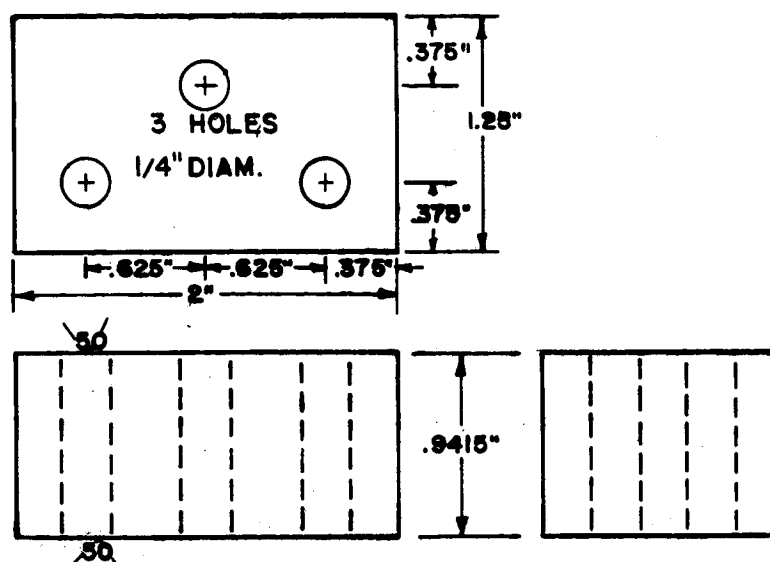
Figure 21. Spacer Dimensions

Precise lapping of the spacers to the exact dimension
and exactly parallel is important. This matter is discussed in
detail later in this chapter.

Gas supply. Gas is supplied to the hold down pads and
to the bearing pad at different pressures through separate pressure
regulators. The total cross-sectional area of the restrictors is:

$$4 \pi r_c^2 = .000452 \text{ sq. inch. .}$$

Gas is supplied through Tygon tubing 3/16" in diameter.
The cross-sectional area of the supply line is:

$$\frac{\pi D^2}{4} = .0276 \text{ inch,}$$

or about 61 times the cross-sectional area of the restrictors.

Therefore, there should be no pressure loss between restrictors and all restrictors operate at the same constant supply pressure.

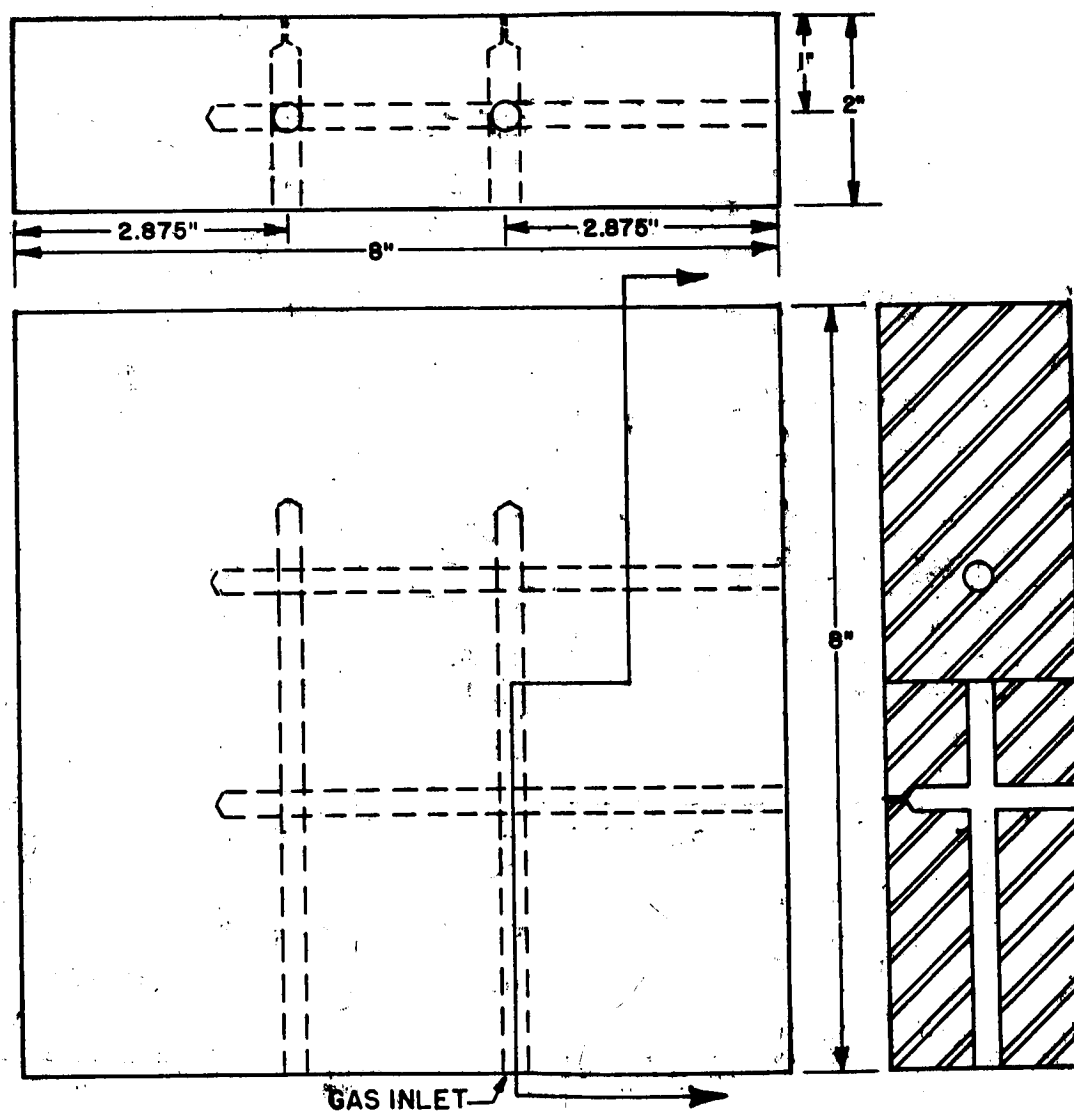Gas is supplied to the bearing pad through tunnels drilled into the pad:

Figure 22. Bearing Pad Gas Supply Channels

All tunnels except the one connected to the supply line are plugged after drilling.

II. FABRICATION

Material. Stainless steel was the natural choice because it is scratch- and corrosion-resistant. Type 410 stainless is machined easily and does not gall readily, therefore it may be lapped to a smooth surface. The steel was ordered, but after three months had passed without delivery, the pads and spacers were made of tool steel purchased locally. A second complete set of pads and spacers was made of aluminum at about the same time.

The aluminum pads and spacers would permit easy changes to the geometry (if testing indicated the need), but aluminum scratches easily. It may be made more scratch-resistant by anodizing the surface. Another advantage of aluminum is that it is not magnetic, therefore will not interfere with electrical equipment mounted on the bearing.

The stainless steel arrived about two weeks after the tool steel and aluminum pads and spacers had been completed. All tests were performed with the tool steel pads and spacers.

Sources. The glass bearing was purchased from the 3-B Optical Company, Gibsonia, Pennsylvania. All other parts were

manufactured locally to specifications. Lapping was accomplished with diamond lapping compound. U.S. Bureau of Standards No. 30 grade (22 to 36 micron particle size) was used to start and No. 3 grade (2 to 4 microns) was used for the final lap. Figure 23 is a photograph of the lapped bearing pad. Figure 24 is one hold-down pad. [26]

Assembly. The assembled bearing is photographed in Figures 25 and 26. Tygon tubing shown supplies gas to the pads.

A running bolt was used as a sting for the tests. A platform and an accelerometer were attached to the running bolt at various stages of the test. The method of attaching the glass bearing to the sting is shown in Figure 27.

III. PROBLEM AREAS

Spacers. The spacers were specified to be flat to 0.000050 inch with parallel top and bottom surfaces. At the time of lapping to this dimension, the most accurate instrument available was a micrometer which measured to the nearest ten-thousandth of an inch (0.0001"). Half-tenths (0.00005") could be estimated, therefore the spacers were lapped, measured with the micrometer and relapped until all measurements with the micrometer were within

---

[26]The hold-down pads in the tested bearing had no grooves-- therefore the gas flow is purely radial.
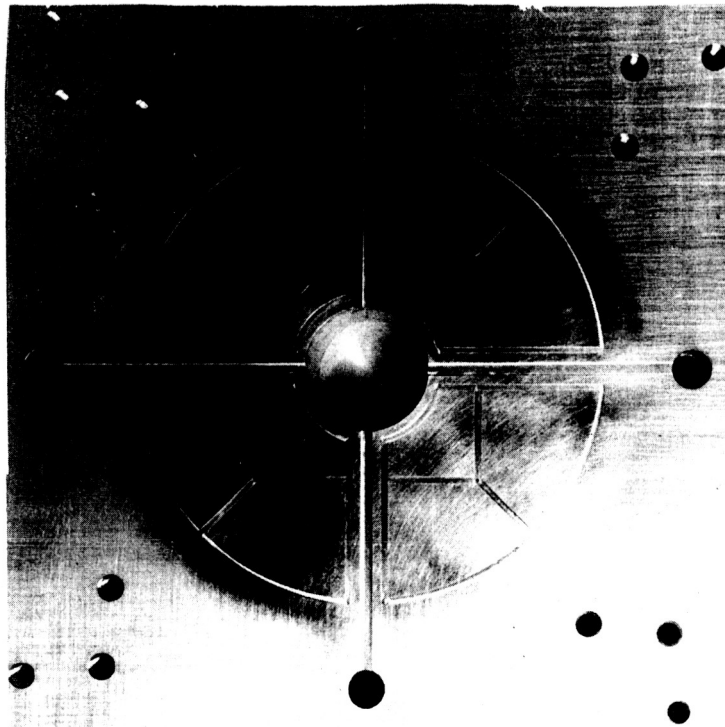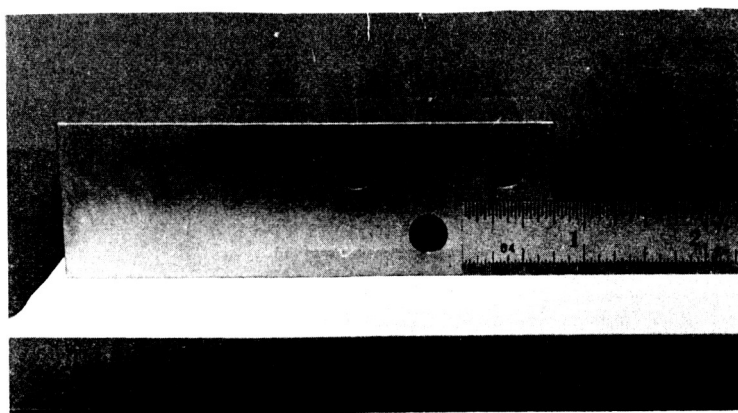
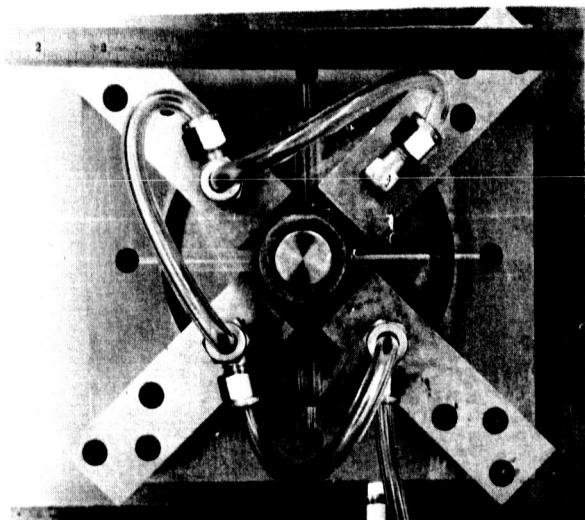Figure 23   Bearing Pad

Figure 24   Hold Down Pad
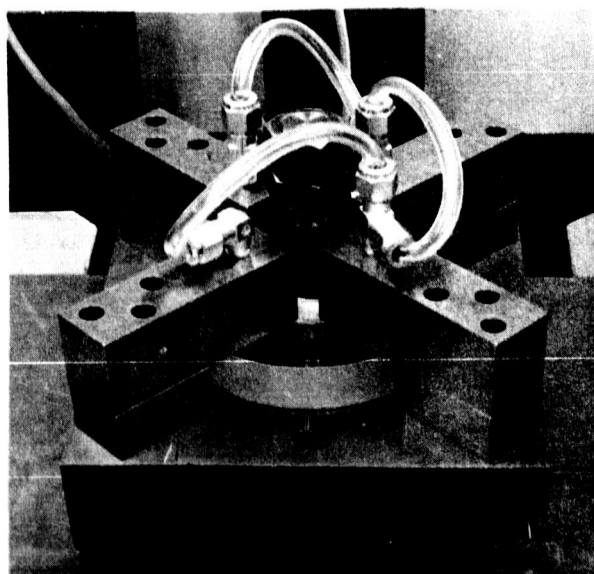
Figure 25   Assembled Bearing, Top View
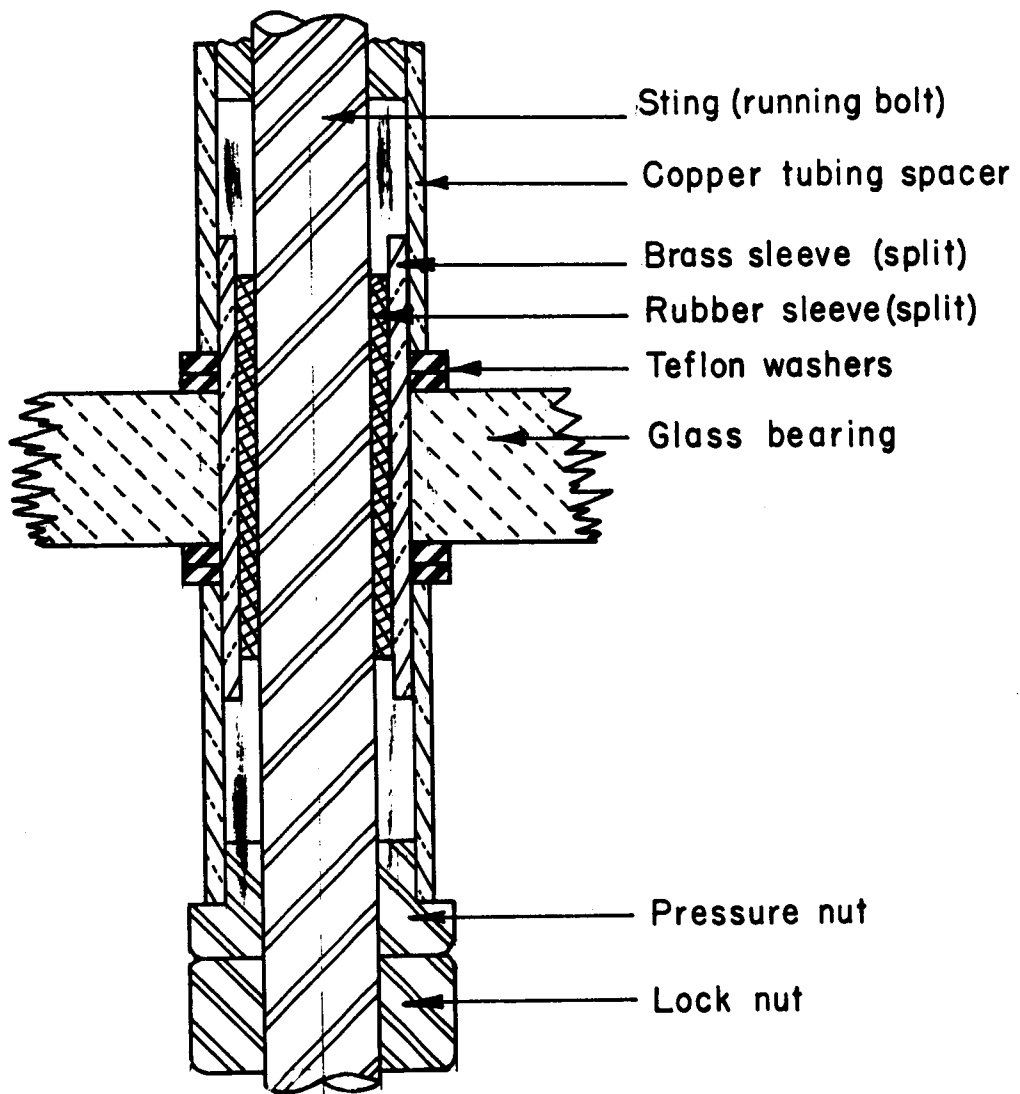

Figure 26   Assembled Bearing, 3/4 Front View

Figure 27. Manner of Attaching Sting to Bearing

0.00005 inch. An air gage[27] was not available at this time. The bearing was then assembled.

As gas is supplied to the bearing pads, the glass bearing floats between the two gas films flowing over its surfaces. A turbine torque was noticed--the glass bearing was rotating on its own accord, with no external disturbance. The rotation was eliminated by adjusting the torque on the bolts connecting the hold-down pads to the bearing pad. By tightening the single bolt on one side or the two bolts on the other side, the rotation could be eliminated or could be made to act in the other direction. This action was controlled by a single hold-down pad. The turbine torque was eliminated by adjusting the bolts and testing proceeded.

During the tests it was noted that even though the upper gap was reduced to zero, by increasing the bearing pad supply pressure and decreasing the hold-down pad supply pressure, gas continued to flow through the hold-down pads. The flow was less than 1.4 cubic inches per second and could not be measured by the flowmeter, but the disturbing fact remained that the flow could not be completely stopped by pressure of the glass bearing on the hold-down pads. The converse was not true--flow of gas through the bearing pad could be stopped by a large downward force on the bearing.[28]

---

[27]See Appendix C.

[28]The amount of force required for various supply pressures is discussed in detail in Chapter IV.
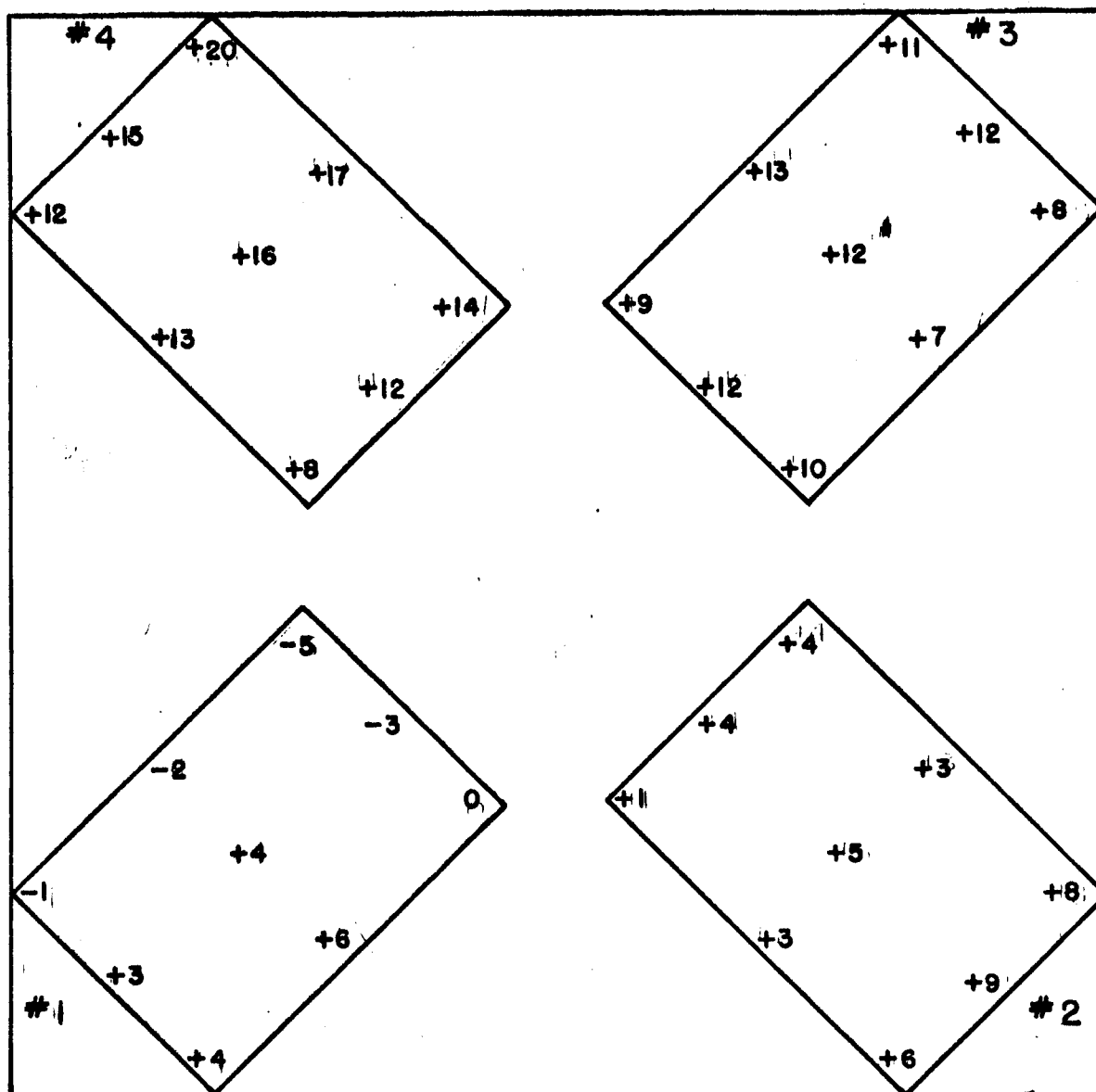
Figure 28. Results of Spacer Air-Gaging

After all tests were completed, the bearing was disassembled and the spacers were measured with the air gage, which arrived while vibration-sensitivity tests were being conducted.

The results of the air-gaging are shown in Figure 28, as readings above and below the specified dimension in ten-millionths of an inch. Thus the figure +20 indicates a thickness of 0.9417 and the figure -5 indicates a thickness of 0.94145" -the maximum and minimum readings. The position of the spacers in Figure 28 is the same as their relative location on the bearing pad. Note that No. 3 is high in the center. This is the spacer that controls the turbine torque. The jet could be directed to the right or left by adjusting bolts on one side or the other.

Leveling. A hole is drilled in the center of each side of the bearing pad to permit initial leveling of the bearing. A 1/4" -20 machine screw is placed through the hole and a rubber spacer inserted between the bottom of the pad and the base support:
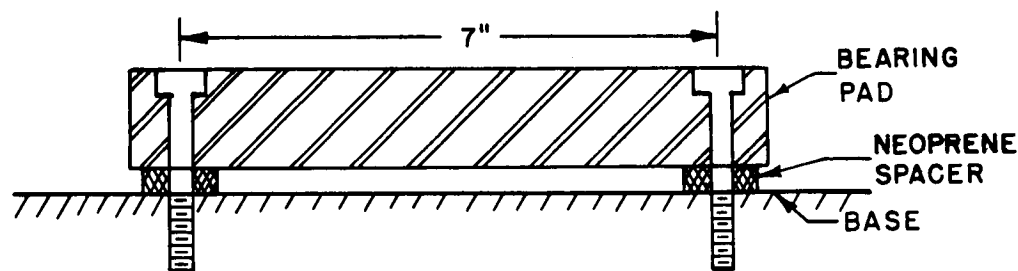
Figure 29. Leveling Bearing Pad

One turn of the screw will move the base up or down 1/20". The distance between centers is 7". Therefore, the angle per turn of the screw is

$$\theta = \tan^{-1} \frac{.05}{7} = 0° -- 24.5'$$

or, for one-eighth turn, approximately 3 minutes.

A machinist's level, with each division representing 0.0005 inch per foot or an angle of

$$\tan^{-1} \frac{.0005}{12} = \tan^{-1} .0000417 = .417 (57.294) \times 10^{-4°} = .0023° = 8.28''$$

was used to level the pad initially. The 1/4"-20 screws were satisfactory to 8 seconds, but if greater accuracy is required, either micrometer screws or differential screws should be used. The bearing did not stay in the center of the pad at times during the tests--it had to be re-leveled. Leveling by centering the bearing itself is as accurate as using the machinists' level.

Deflection of the glass bearing under load. No problem was encountered due to deflection of the glass; that is, the glass did not strike the bearing pad in the center while still supported at the outer perimeter, but it is a possible problem area with smaller gap heights and is discussed.

Deflection of the glass may be approximated by

a. Deflection of a circular plate supported at 3 points,

120° apart:[29]

$$\delta = 0.0670 \frac{Pa^2}{D}; \quad P = \pi a^2 q; \quad D = \frac{Eh^3}{12(1-\nu^2)};$$

where a is radial distance from center of plate to

supports = 1.57" (CG of area enclosed by grooves),

q is load in center of plate = 20 pounds (high est.),

E is Young's modulus = 9.8 x 10⁶ lb/in² for Pyrex, 7740 glass[30],

h is thickness of plate = 0.9405 inch,

and ν is Poisson ratio = 0.22, for all glass[31],

Substituting the above values and solving:

δ = 438 x 10⁻⁶ inch (three simple supports).

b. Deflection of a circular plate simply supported all around edge: [32]

$$\delta = \frac{(3 + \nu)Pa^2}{16\pi(1+\nu)D}$$

Using the same values as given in a:

δ = 23 x 10⁻⁶ inch (supported all around edge).

[29]S. Timoshenko and S. Woinowsky-Kreiger, Theory of Plates and Shells (second edition; New York, McGraw-Hill Book Company Inc., 1952), p. 295.

[30]Corning Glass Works, "Properties of Selected Commercial Glasses," Handbook B-83 (Corning, New York, 1949) p. 9.

[31]Ibid., p. 4.

[32]S. Timoshenko and S. Woinowsky-Kreiger, op. cit., p. 68

With four simple supports, the deflection of the glass bearing would be somewhere between 23×10^{-6} and 438×10^{-6} inch. However, the supports in the air bearing are not simple supports--the support is distributed over a radius of 0.75 to 2.375 inches. Therefore the deflection of the glass bearing is much less than 23×10^{-6} inch. Deflection of the glass bearing presented no problem.

CHAPTER IV

EXPERIMENTAL WORK AND RESULTS

The purpose of the experimental work was to test the design
and to determine

    a. the equivalent spring constant, and

    b. the effect of background vibrations on the air-bearing
assembly.

Related tasks were the measurement of gas flow rates,
observation of the stability, and the ability of the bearing to support
loads.

The bearing pad was tested with supply pressures from 4 to
20 psig and the hold-down pads with supply pressures from 0 to 30
psig, each in 2 psig increments. Loads on the bearing were varied
from +30 pounds (down) to -25 pounds (up) to test both the hold-down
pads and bearing pad operation.

Temperatures were kept stable at 71 to 73° F. The laboratory
is air-conditioned, therefore all apparatus was kept within that
temperature range at all times. Temperature changes could have
a great effect on bearing operation because of the small clearances
and relatively large metal surfaces involved.

The gas used for all tests was bottled super-dry nitrogen--
primarily because it is clean and requires no filter, also because
its properties are close to those of air and, being dry, corrosion
of the machined surfaces of the bearing would not occur.

I. DESCRIPTION OF EQUIPMENT

Pressure measurement. Supply pressures to the bearing
pad and hold-down pads were regulated and measured with KGM
single stage nitrogen flow regulators. Graduations are in 2 psi
divisions. One gauge measures from 4-60 psi; the other from
4-100 psi.

Flow measurement. Volume flow rates were measured with
a Monostat Predictability Flowmeter, described in Appendix A, and
a standard Fisher and Porter rotameter. Both instruments were
calibrated with a wet test meter as explained in Appendix B.
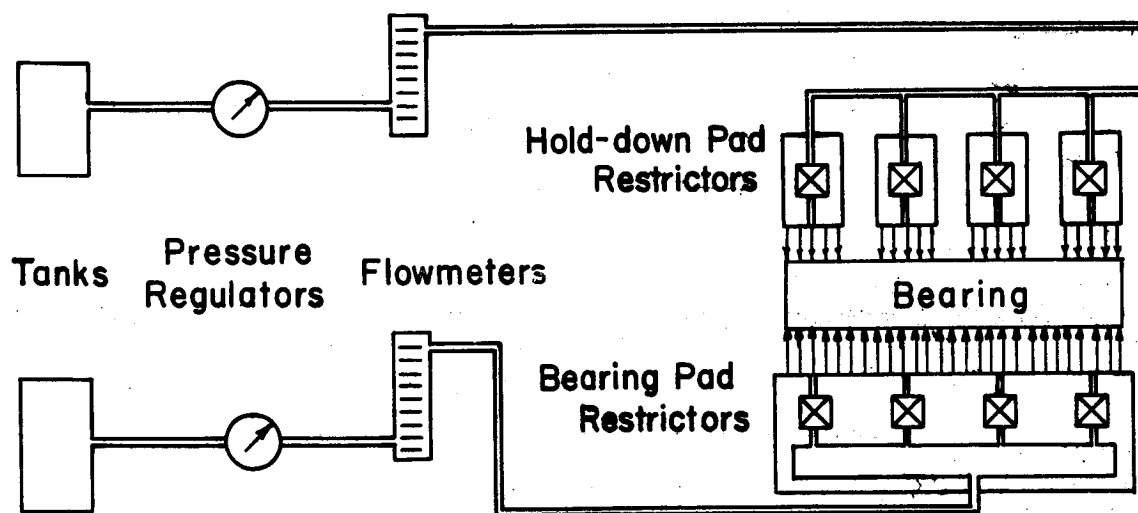
Figure 30. Schematic Gas Flow Rate and Pressure Measurement

Loading. The bearing was loaded in the vertical plane only.

A platform is attached to the end of the sting and weights were placed

on the platform in pairs, equidistant from the centerline of the sting.

This provides downward forces to examine the spring constant of the

bearing pad. Upward forces, to determine the spring constant of the

hold-down pads, were obtained with a platform-lever apparatus

sketched in Figure 31.
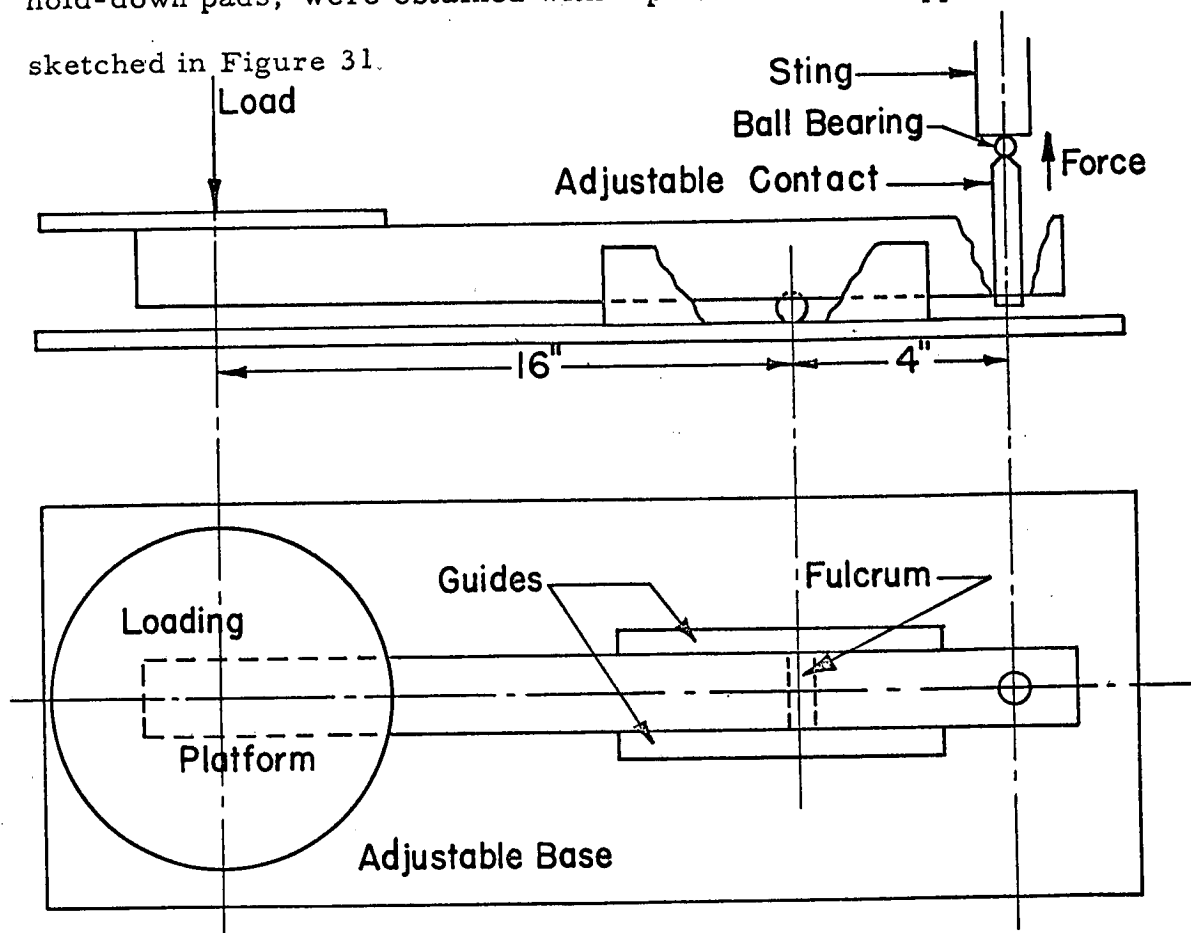
Figure 31. Platform lever apparatus-upward forces.

The contact transmits the force to the bearing and is adjustable so the apparatus may be leveled when the load (and thus the gap height) is changed. Without this device, there would be a horizontal force-component transmitted and the bearing would be cocked to one side or the other. The result would be an erroneous reading of gap height and non-parallel gas flow. The entire base on which the apparatus is mounted is movable to permit positioning directly under the center of the sting.

The apparatus is designed to magnify platform loads by four due to the unequal arm length. The bearing is made weightless by balancing its weight with this apparatus. A photograph of this device appears as Figure 32.

Gap height measurement. Gap heights are measured to the nearest twenty millionths of an inch (0.000020") with a Precisionaire air gage. Calibration and use of the gage is explained in Appendix C. The air jet is placed directly above the glass bearing. Movements of the bearing up or down result in varying positions of the float in the air column of the air gage--in that respect it acts as a rotameter. As the bearing moves up, the float moves down.

The gage is shown in position on the bearing in Figures 33 and 34. Note that the gage in Figure 34 indicates a bottom gap height 0.0001" less than the gage in Figure 33. Air flow is from bottom to top of the gage. Upward movement of the float indicates a decreasing bottom gap height; that is, the top of the glass bearing is moving
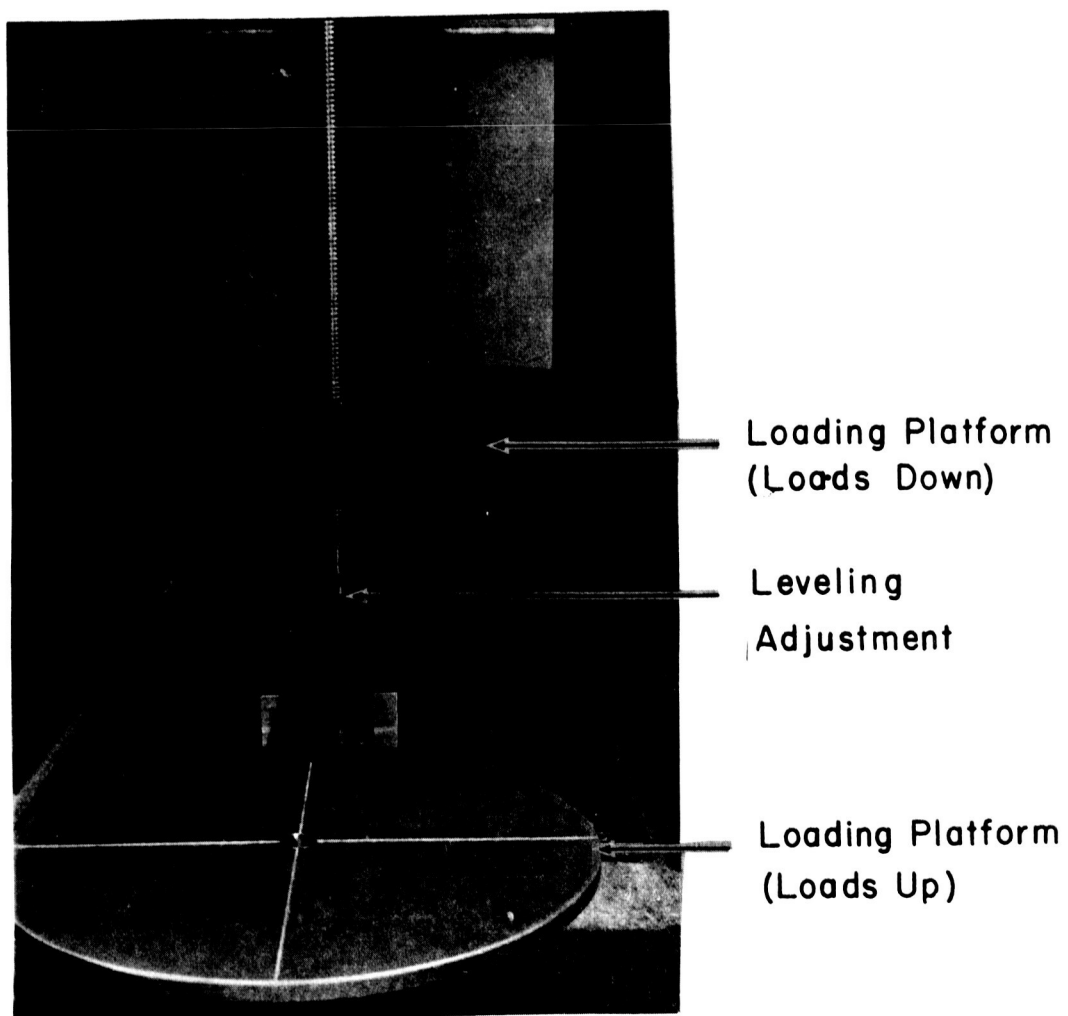
Loading Platform
(Loads Down)

Leveling
Adjustment

Loading Platform
(Loads Up)

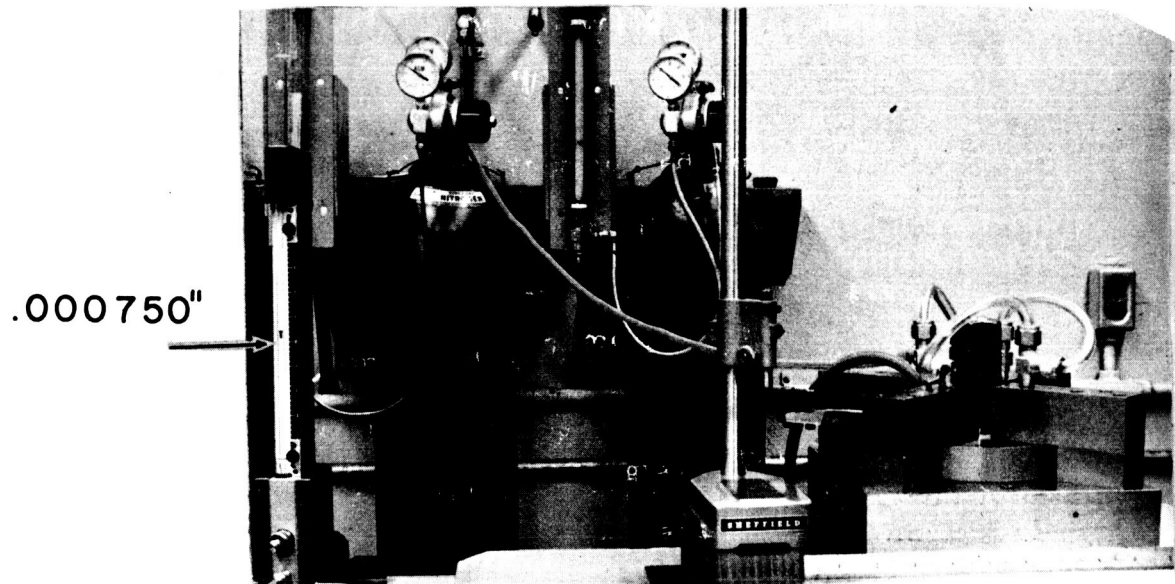Figure 32   Platform Lever Apparatus

.000750"

Figure 33   Gap Height Measurement I

.000650"
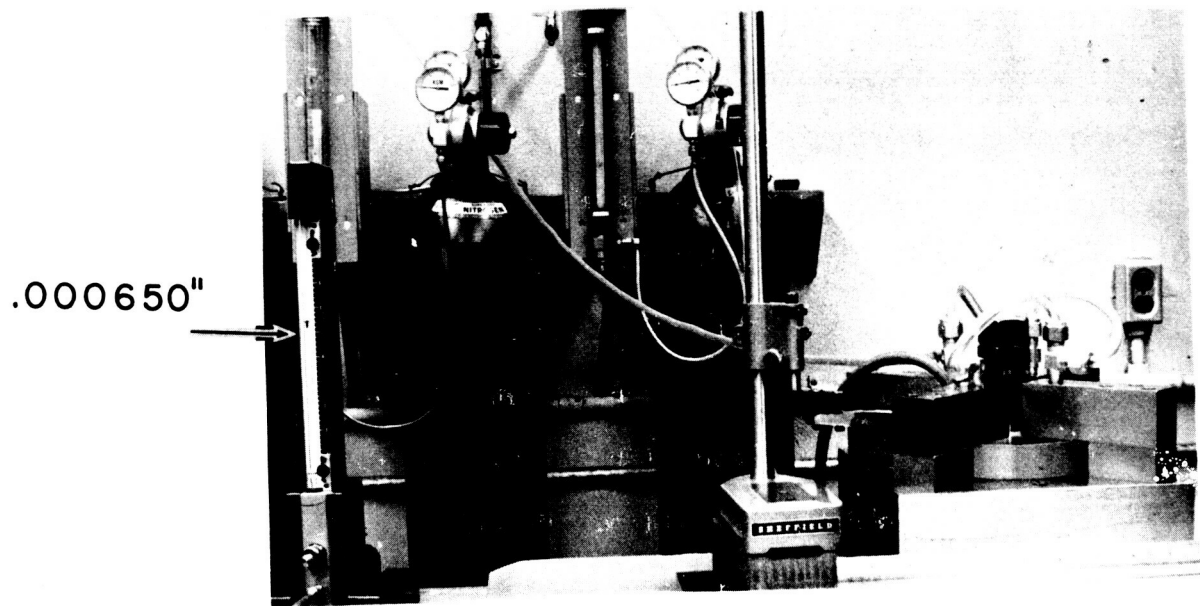
Figure 34   Gap Height Measurement II

away from the air gage jet. The pressures indicated are 30 psig

(left regulator) to the hold-down pads, 20 psig to the bearing pad

in Figure 34; and 20 psig to the hold-down pads, 10 psig to the

bearing pad in Figure 34.

The total gap in the bearing is measured with no pressure

in the hold-down pads. The pressure to the bearing pad is gradually

increased until further increases in pressure cause no movement of

the bearing. The total movement indicated on the air gage is the total

gap.

Vibration analysis. A General Radio Corporation vibration

pickup was clamped to the base, the bearing pad, and at two locations

on the sting to detect vibrations at those points. A vibration analyzer

indicated the relative magnitude and frequency components of the

vibrations, from 2.5 to 750 cycles per second. The equipment is

described in Appendix D. The equipment is shown connected to an

Offner Type R Dynograph recorder in Figure 35. The vibration

pickup is on the platform at the bottom of the sting.

II. EXPERIMENTAL RESULTS

Flow rates. Mass flow rates through the bearing pad, hold-

down pads, and the combined total flow rates through the bearing are

shown in Figures 36 through 39.

Figure 36 indicates the bearing pad mass flow rate for extreme

loading conditions. Note that for a load of 33.8 pounds down, the

Recorder

Vibration Meter
and Analyzer

Piezo-Electric
Vibration Pickup

Figure 35   Vibration Analysis

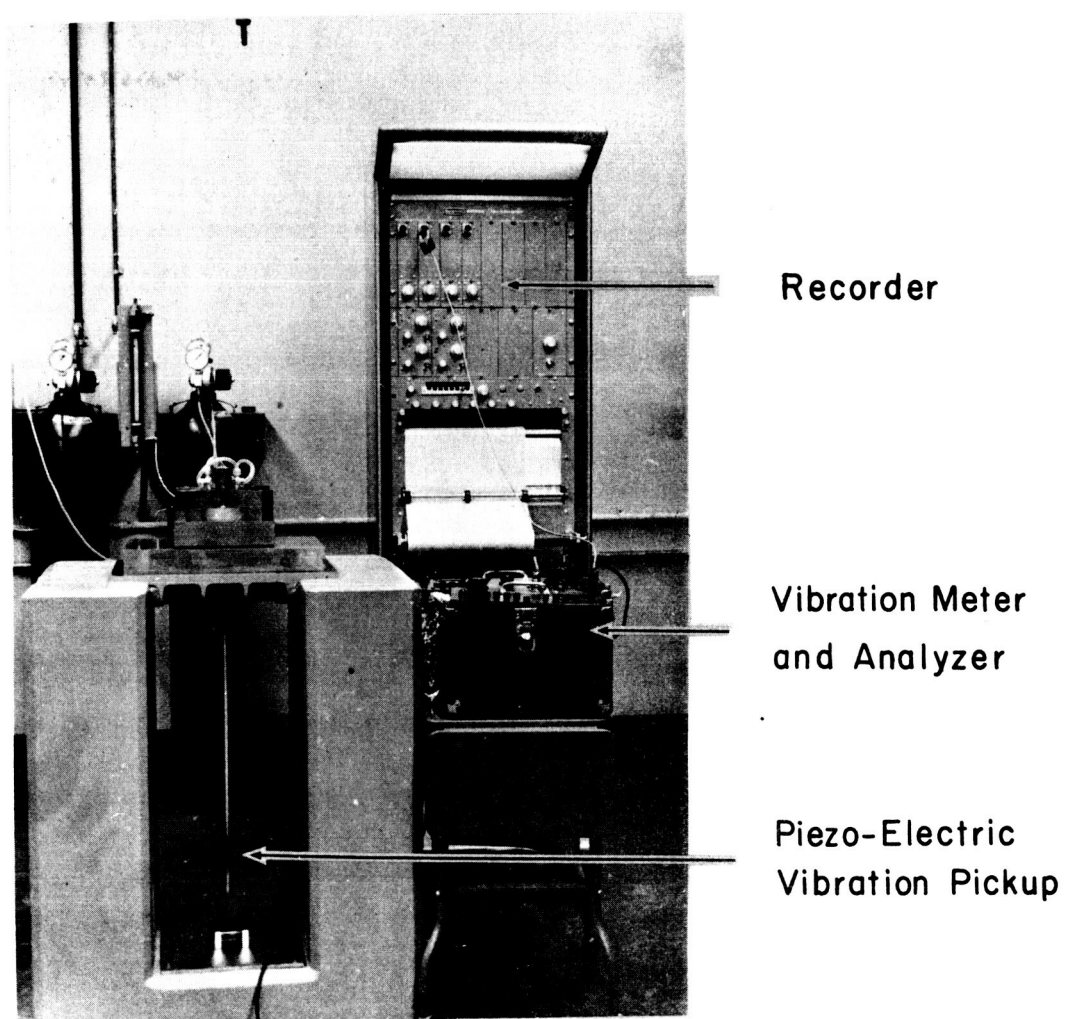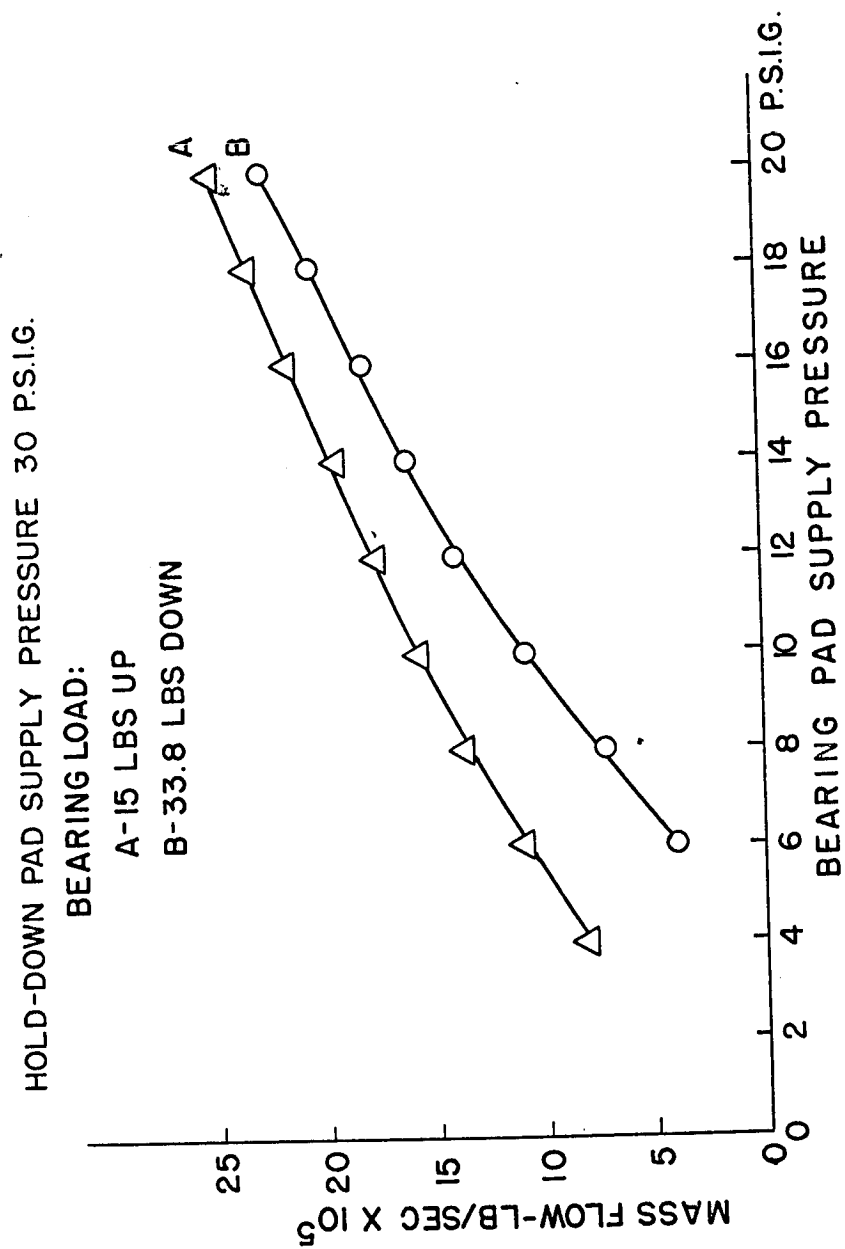Figure 36. Mass Flow Rate vs Supply Pressure, Bearing Pad

flow rate decreases more rapidly than for a load of 15 pounds up at low bearing pad supply pressures. This indicates a more rapidly changing lower gap height and consequently a softer spring at the lower supply pressure. Hold down pressure is held constant at 30 psig for this plot.

Figure 37 shows the hold-down pads mass flow rates for various loads and pressures. Curves A and D represent mass flow at extreme loading conditions. Note that in curve D the flow rates were too low to be measured for supply pressures less than 20 psig. The flow was less than 0.00005 pound per second (1.11 cubic inch per second at S.T.P.) at that pressure.

Curves B and C of Figure 37 indicate the lift provided by a bearing pad supply pressure of 10 psig--a little less than 12.8 pounds at a hold-down pad supply pressure of 30 psig. Note that the lift provided by the bearing pad varies as the hold-down pressure decreases and at hold-down pressures less than 20 psig, the lift provided is greater than 12.8 pounds. This is because the lower gap is changing at a different rate for each curve. Curve B has only a varying down-ward load while curve C has a varying downward load plus a constant load of 12.8 pounds. Therefore the lower gap height, and consequently the lift provided by the bearing pad, changes at a lower rate than in curve B; as indicated by the intersection of the two curves at 20 psig hold-down pad supply pressure.

The total flow through both gaps in the bearing assembly is reproduced graphically in Figure 38. The notable feature in this

Figure 37.   Mass Flow Rate vs Supply Pressure.

Hold-Down Pads

BEARING PAD SUPPLY PRESSURE	LOAD
A 6 PSIG,	33.8 LBS DOWN
B 10 PSIG,	BALANCED
C 20 PSIG,	12.83 LBS DOWN
D 20 PSIG,	22.5 LBS UP

94
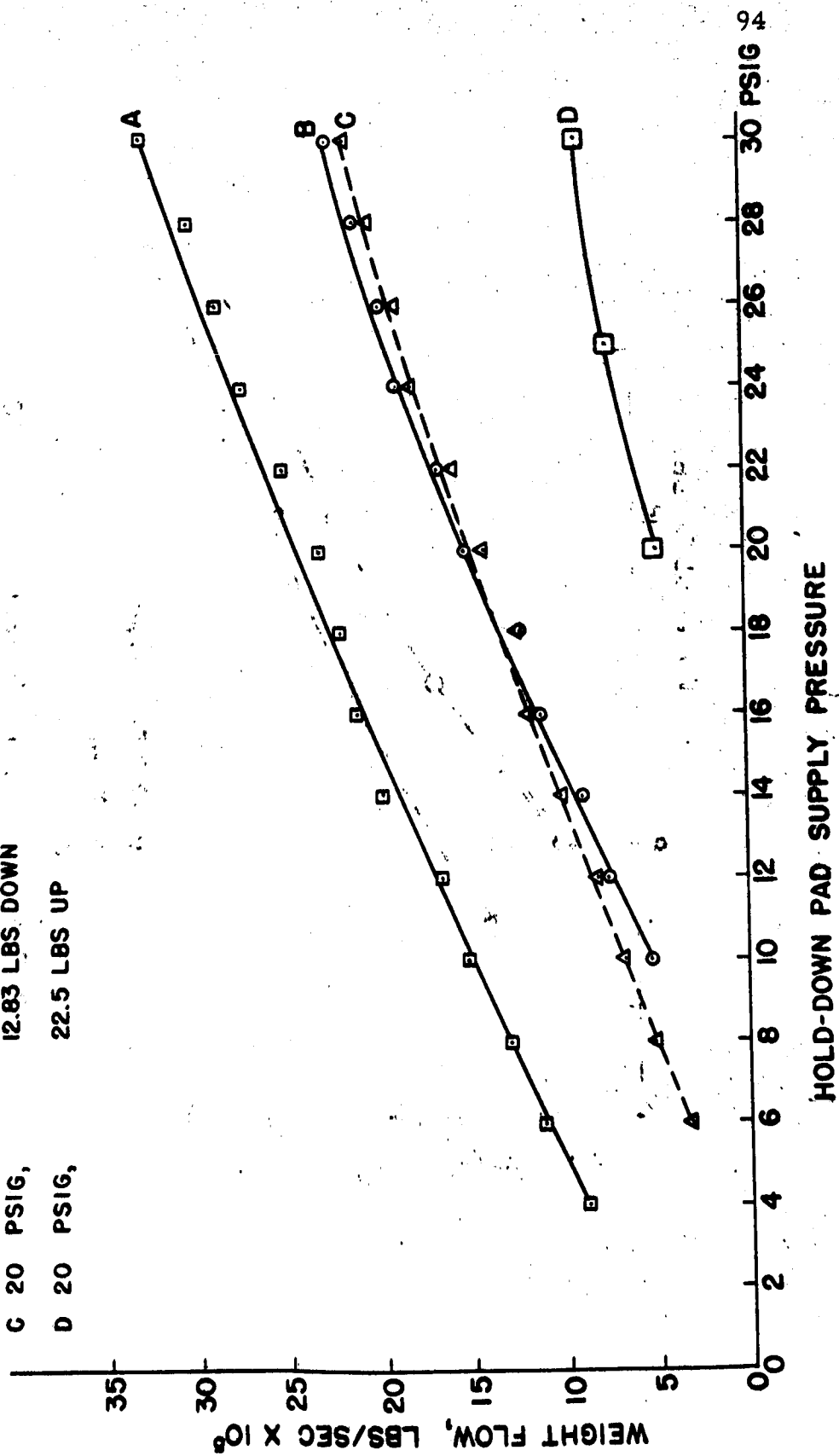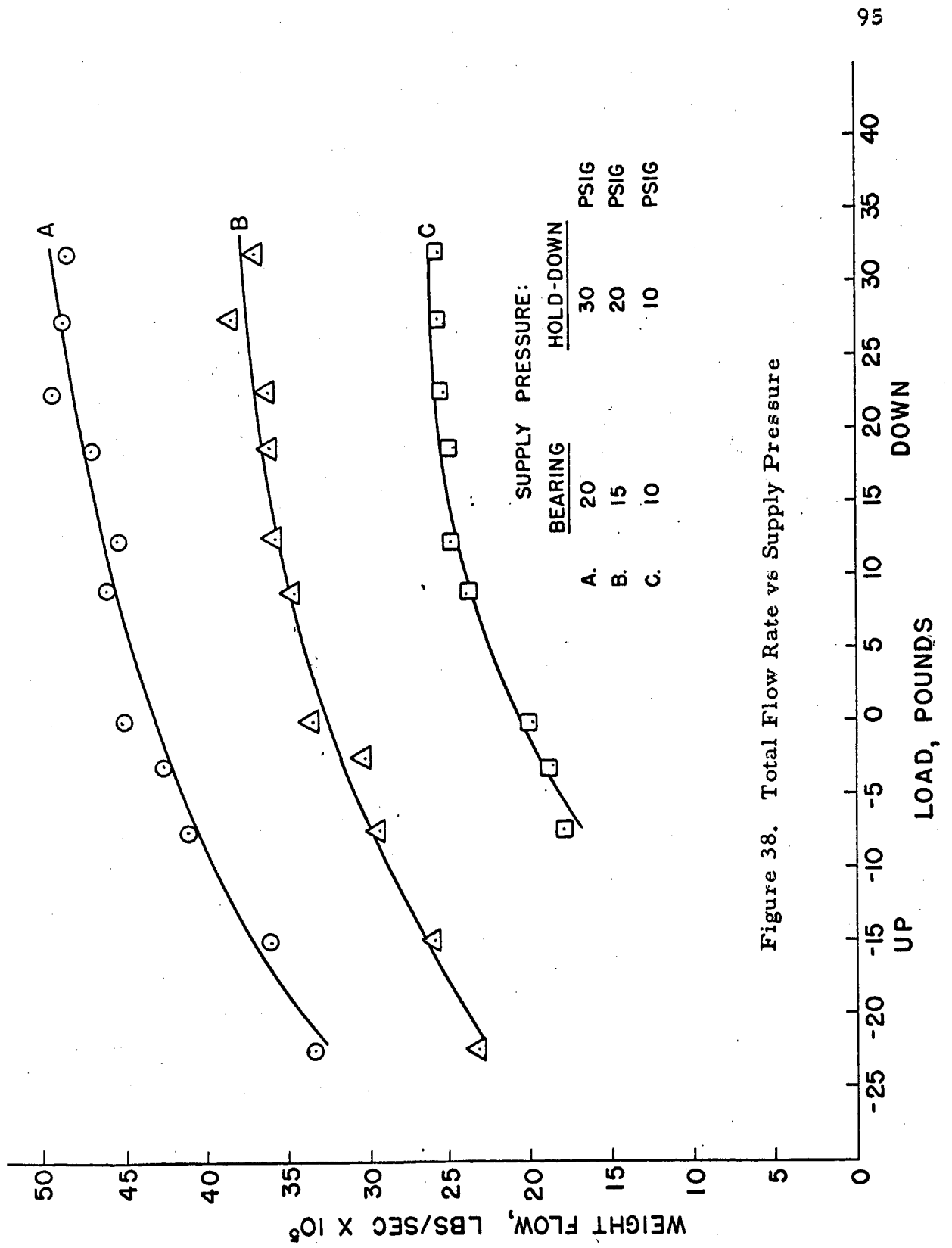
Figure 38. Total Flow Rate vs Supply Pressure

figure is the indication of a maximum rate of flow in the bearing
assembly for any given load--about 0.00(5 pound per second. This
maximum flow rate depends entirely on the total gap and supply
pressures. Theory states that the flow rate will approach a maximum
as the velocity of the gas approaches the speed of sound.

The maximum possible flow through the restrictors is shown
in Figure 39, under conditions of no load and infinite gap height,
exhausting to free atmosphere. The maximum flow rate would be
obtained when the supply pressures are above the critical pressure
(the pressure required to accelerate the gas in the tube to the speed
of sound and produce a shock wave). The continuously increasing
mass flow rate curves indicate that the experimental pressures
are below critical for gas flow in the tubes, even when exhausting
to atmospheric pressure, therefore the maximum flow rate
approached in Figure 38 must be due to a sonic neck at some other
point in the bearing assembly. This point is discussed in the next
chapter.

Stiffness. The static stiffness, or static equivalent spring
constant, was determined for the bearing pad and hold-down pads
separately as shown in Figures 40 and 41. A combined stiffness
diagram is given by Figure 42.

The experimental work shown i . Figure 40 was conducted
with the hold-down pads ren .ed. The   .p height at light
loads was greater than the tota. gap in tl   ing assembled with
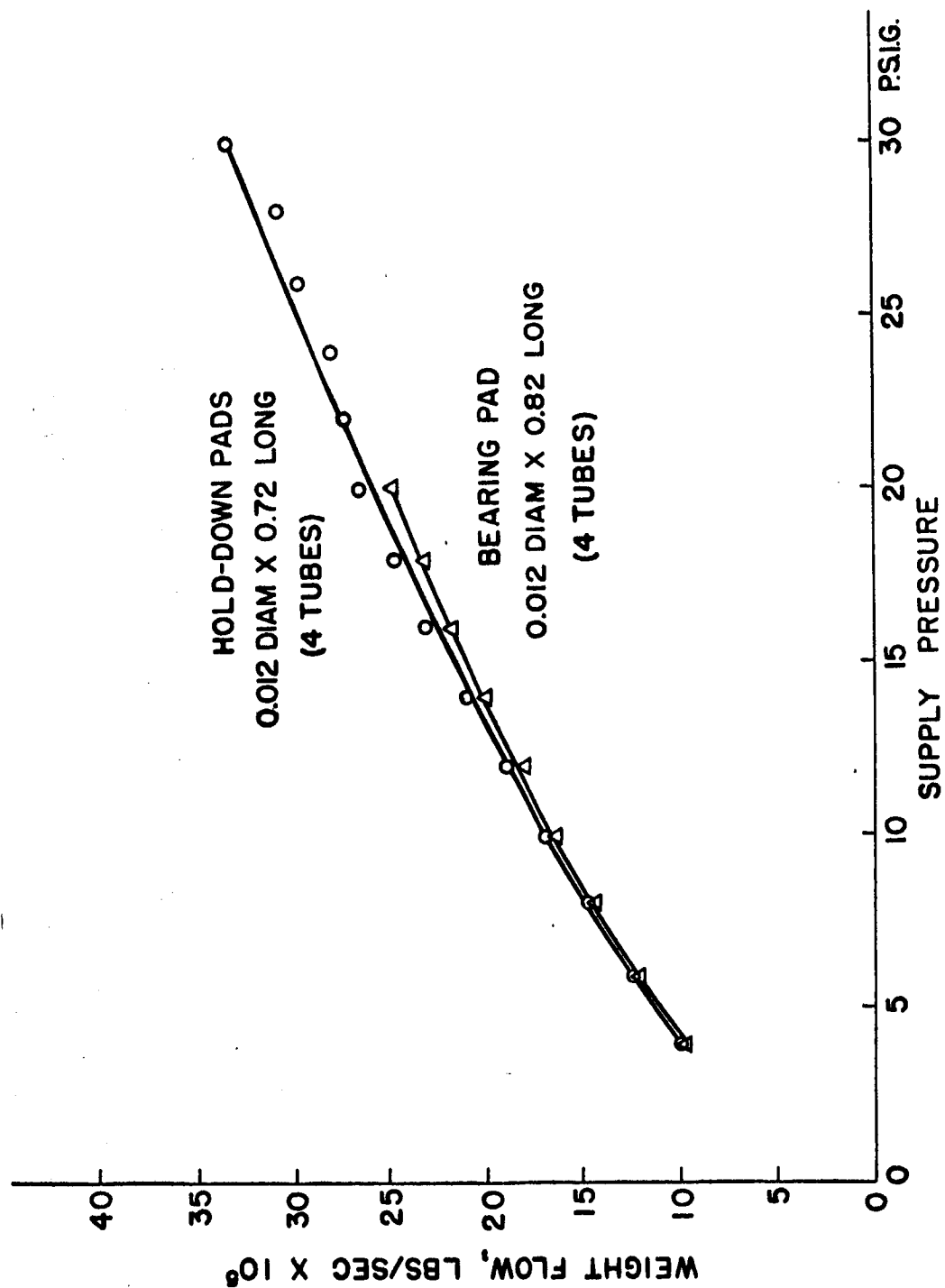
Figure 39. Maximum Restrictor Flow vs Supply Pressure
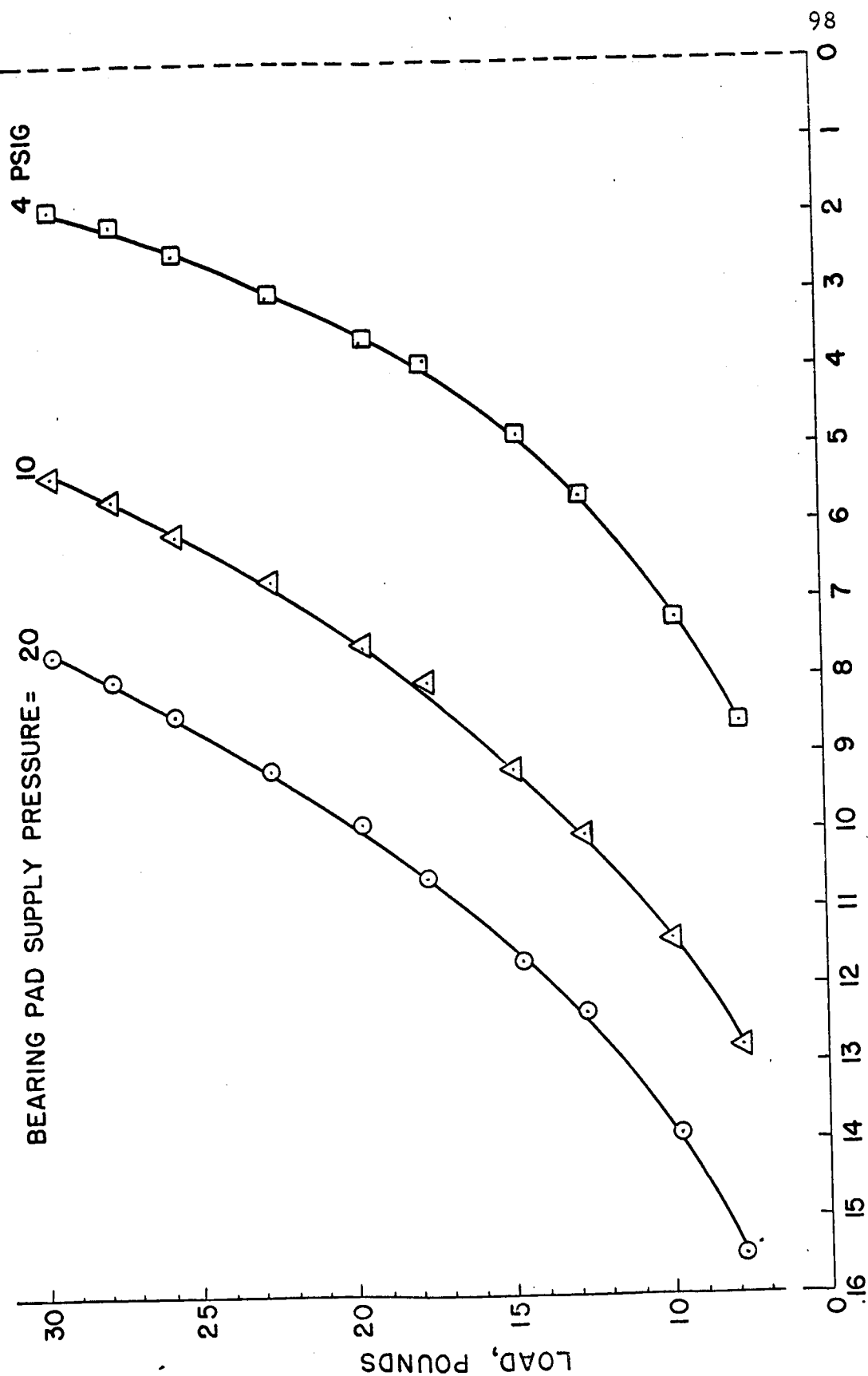
Figure 40. Stiffness, Bearing Pad

hold-down pads. As expected, the higher the pressure, the greater the stiffness of the bearing pad. An interesting point is that all three pressures indicate approximately the same stiffness (slope of the load-deflection curve) for heavy loads. However, the gap height at 4 psi is less than 0.0002 inch for a thirty pound load; while at 20 psig the gap height is 0.00085 for the same load--a gap over four times greater. For a given gap height and given load, higher supply pressures yield higher static spring constants. Operation at 4 psig would be dangerous; a suddenly applied load is likely to cause the bearing to strike the pad because the lower gap is very small. In the region of 20 to 25 pounds load, the equivalent static spring constant is about 40,000 pounds per inch. The bearing pad stiffness curves resemble the curve characteristic of a hard spring--as the gap decreases, the spring constant increases. Theory predicts this also-- as the gap height decreases, the pressure P_1 increases, and the lift increases, with the cube of the gap height.

Figure 41 also indicates a hard-spring characteristic for the hold-down pads at supply pressures over 20 psig, and almost a linear spring for a supply pressure of 10 psig. The static spring constant at 30 psig is about 40,000 pounds per inch, and at 10 psig is about 20,000 pounds per inch.

With the bearing completely assembled and pressurized on the top and bottom, the curves in Figure 42 were obtained. The total gap is 0.001360 inch. The top portion of the figure is for loads down and indicates stiffness of the bearing pad. The bottom portion is for loads
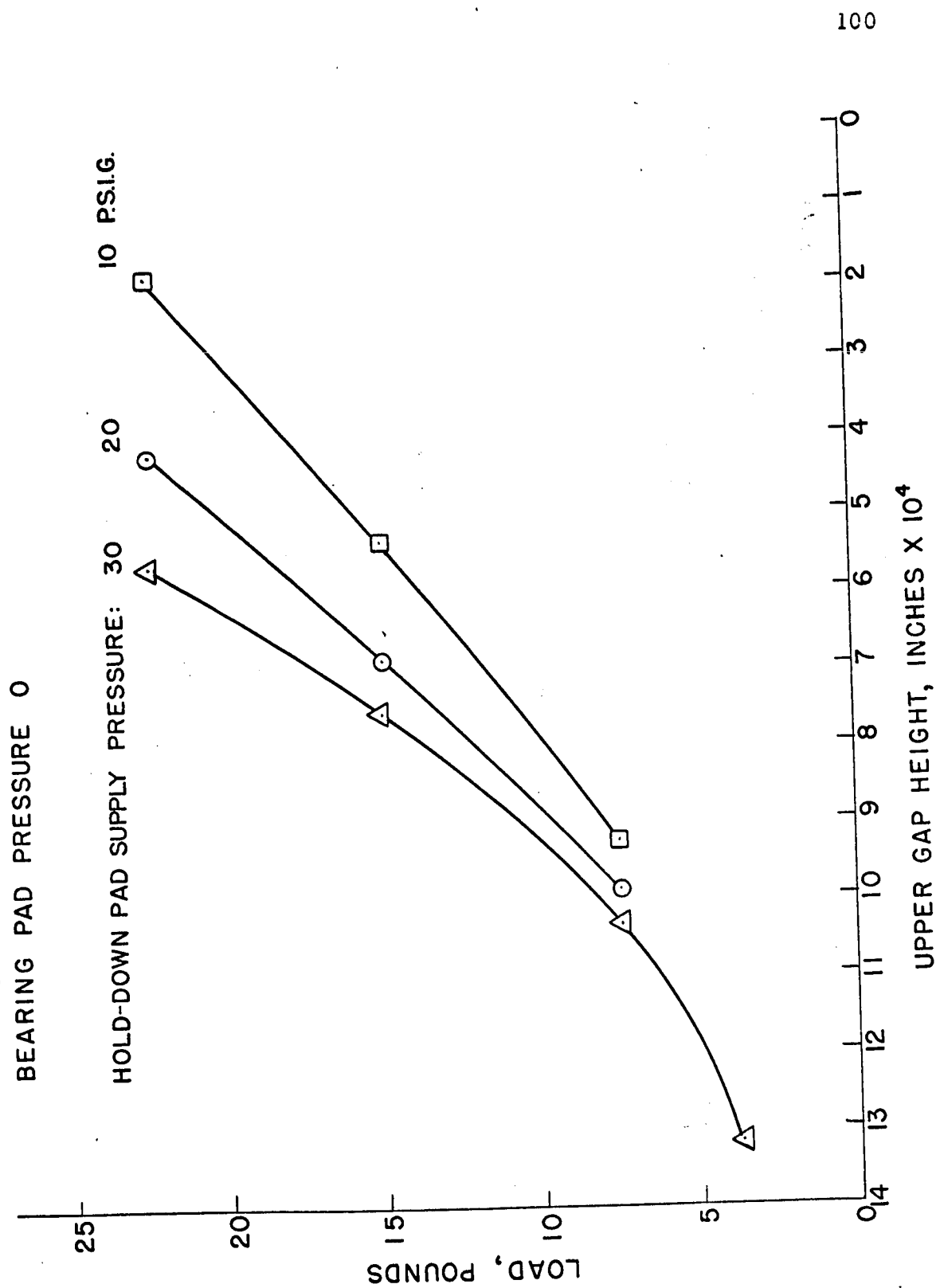
Figure 41. Stiffness, Hold-Down Pads
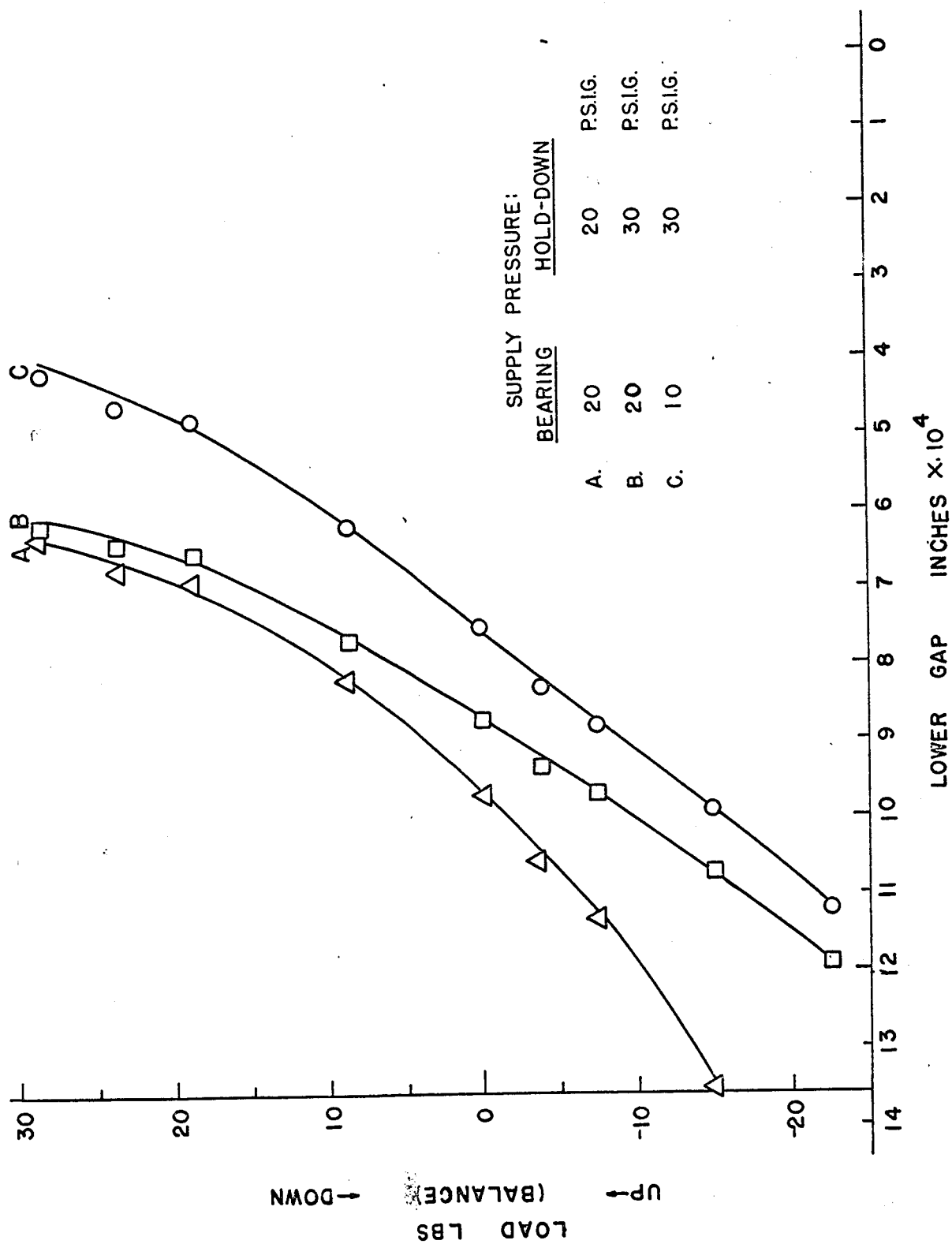
Figure 42. Stiffness, Assembled Bearing

up and indicates the hold-down pads stiffness. The curves again are those characteristic of a hard spring.

Curves A and B indicate approximately the same stiffness for the bearing pad (top half), but curve A indicates a softer spring constant for the hold-down pads at a supply pressure of 20 psig. Curve A also shows the closure load for the hold-down pads as 15 pounds upward force plus the lift provided by a bearing pad pressure of 20 psig.

Curves B and C indicate approximately the same spring constant for the hold-down pads at 30 psig supply, but curve C shows a softer spring for the bearing pad at 10 psig.

The maximum stiffness of the bearing is given by curve B, operating at the highest supply pressures used in the tests--30 psig to the hold-down pads and 20 psig to the bearing pad. The static spring constant of the bearing with no preload--only the tare weight of 8.875 pounds down--is 91,000 pounds per inch. With a preload of 20 to 25 pounds, the spring constant is raised to 150,000 pounds per inch, and the upper and lower gap heights are equal.

Additional hold-down pressure will move curve B to the right (decrease the lower gap) and will increase the stiffness. Increased hold-down pressure would thus have the same effect as preloading without the disadvantage of attaching weights to the bearing.

The effect of reducing the total gap height, by making the spacers smaller, would be to increase the stiffness--the curves would be squeezed closer together and would assume a more vertical attitude.

Vibrations. Readings were made of vibrations of the base (SUPT) and of the bearing pad (PAD) separated from the base by Isomode. The results are shown in Figure 43. All vibrations of the base were reduced by the Isomode material except the vibration at 30 cps which was transmitted unchanged. This figure indicates the vibration damping qualities of Isomode very well. The material was not used however, due to problems in force measuring and leveling that would arise with a soft spring under the bearing assembly, mentioned in Chapter II.

Figure 44 was made with the accelerometer clamped to the end of the sting, as pictured in Figure 35. The recording on the left is of the unsupported bearing, the center recording with the bearing supported by 4 psig through the bearing pad and hold-down pads, and the recording on the right is with 30 psig supply pressure to the hold-down pads and 20 psig to the bearing pad. Vibrations at 90 cps were magnified when the pad was just barely supported (center) and attenuated slightly at full support.

Vibrations at 500 cps, not indicated for the unsupported bearing are very pronounced when the bearing is just supported (center) and have almost disappeared at full support. The tick marks at 75 cps and 250 cps occurred when the frequency range of the vibration meter was changed--they were not sensed by the accelerometer.

Figure 45 was recorded with the accelerometer at the center of gravity of the bearing and sting assembly--about 18 inches below the bearing. Vibrations of 75 cps are attenuated by the supported bearing,
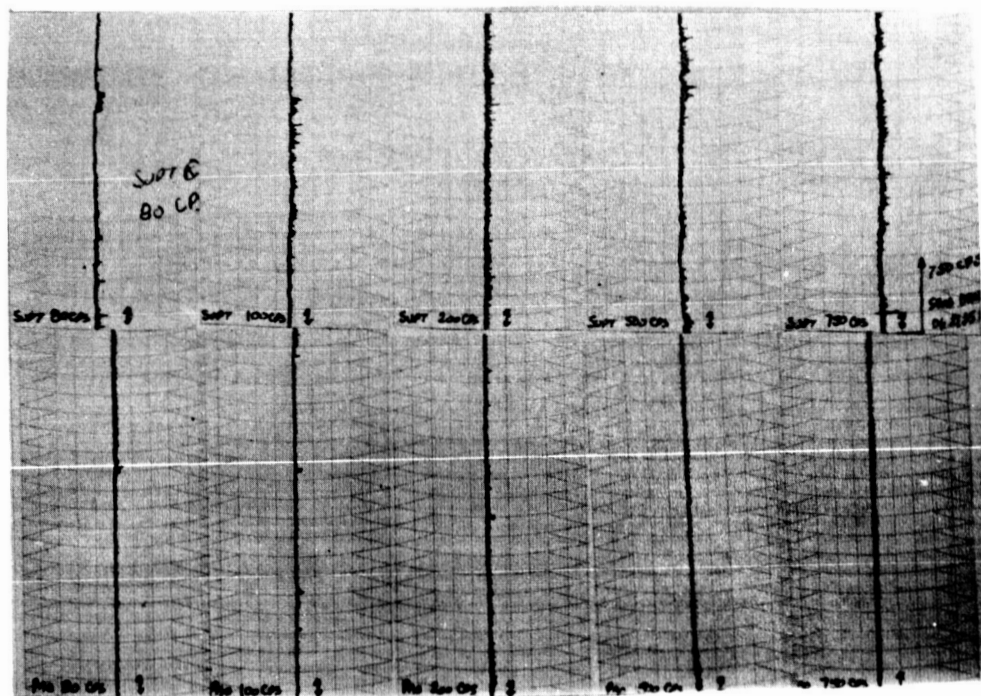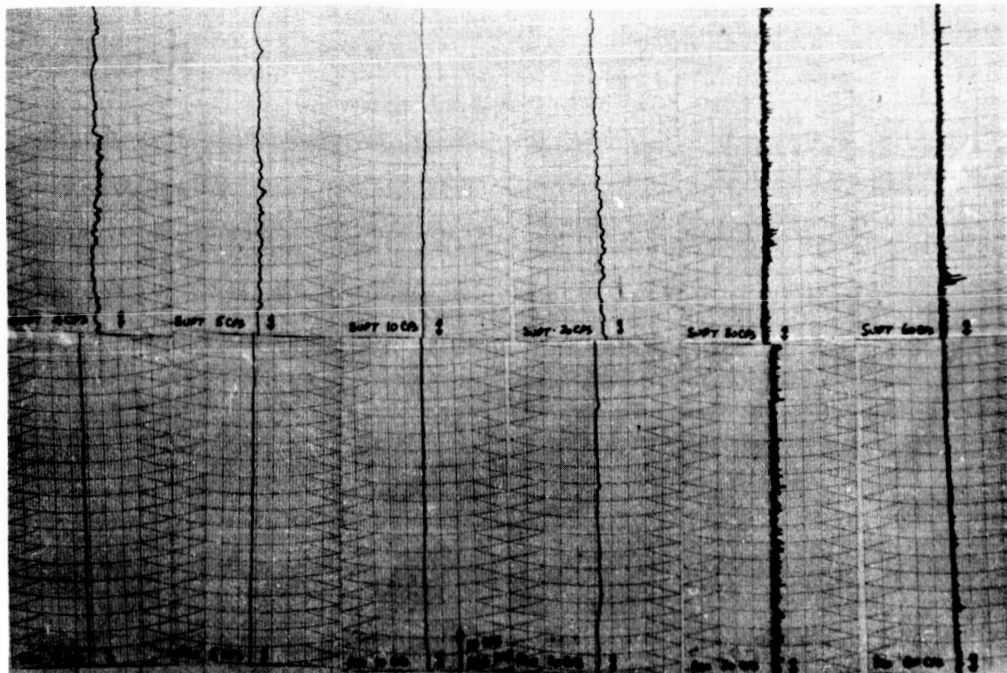
Figure 43   Vibration Transmission, Base to Bearing Pad
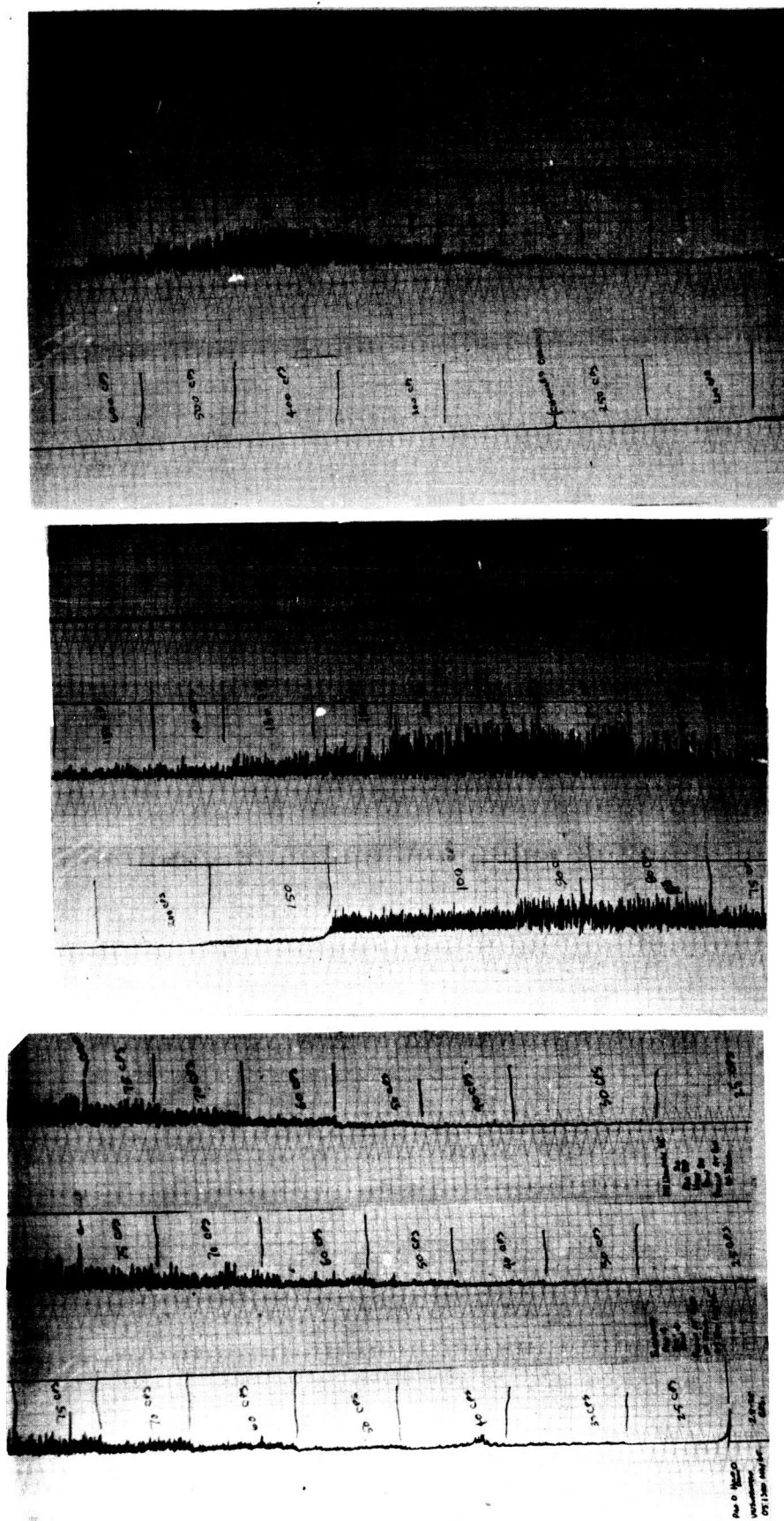
Figure 44   Vibrations, End of Sting
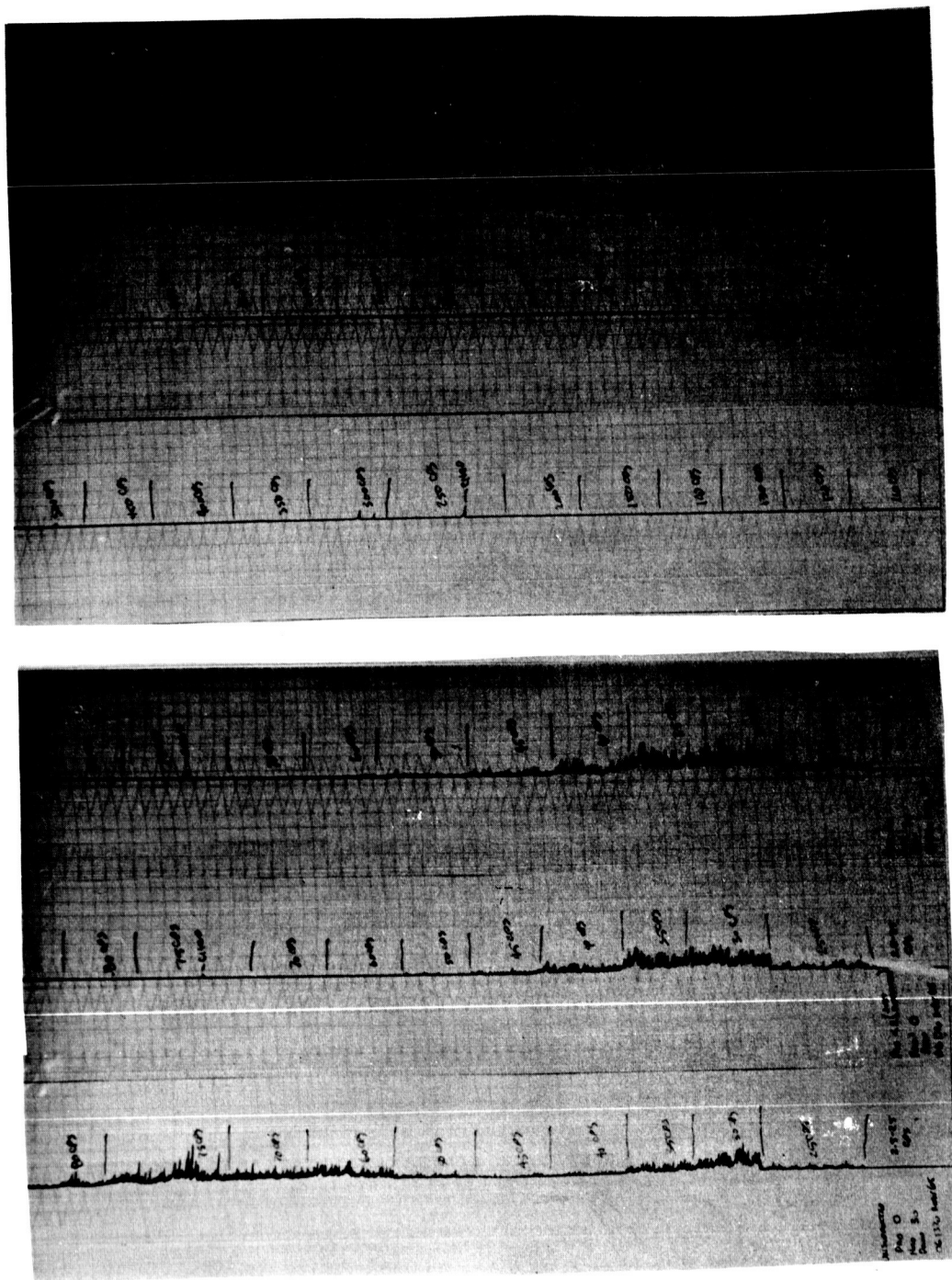
Figure 45   Vibrations, Center of Gravity of Bearing Assembly

but disturbances at 30 cps are present in all three bearing attitudes.
Note that vibrations at 500 cps do not appear in any of the recordings.

The critical frequencies of the supported bearing as indicated
by experiment:

    a. 90 and 500 cps at the end of the sting, and

    b. 30 cps at the center of gravity of the bearing and sting
assembly.

The results indicate that the supply pressure (and consequently
the spring constant) have a great influence on the vibration-sensitivity
of the bearing. Once the vibratory field at the site is known, the
bearing can be designed with no critical frequencies at or near the
known background vibrations.

CHAPTER V

COMPARISON OF RESULTS WITH THEORY

Equations were developed for the theoretical lift of a bearing with radial or longitudinal flow in Chapter II. The equations of motion were stated, from which the natural frequencies of the system may be obtained. In this chapter the lift and critical frequencies observed experimentally are compared with theory.

I. LIFT

The incorrect dimensions of the spacers makes an analysis of the gas flow and calculation of the lift for the top of the bearing impossible; therefore the hold-down pads were removed and the lower gap height was measured at various loads to obtain a relationship between theoretical lift and actual lift of the bearing pad. The results are tabulated in Table II, also plotted in Figure 40, Chapter IV.

The actual lift provided by each quadrant of the bearing pad is the total lift divided by 4. Theoretical lift is calculated by assuming that the pressure at the entrance of the exhaust land acts over the entire area enclosed by the grooves. A theoretical value of the distributed pressure, $P_0 > P > P_1$, from the tube exit to the outer perimeter of the grooves was not derived due to the complexity of flow.

Theoretical lift is the pressure $(P_1 - P_e)$ times the area enclosed by the grooves (3.36 square inches), plus the lift provided by the pressure $P_1 > P > P_e$ over the area above the lands, given by

TABLE II

LOAD, GAP HEIGHT, AND MASS FLOW RATES
DETERMINED EXPERIMENTALLY

A. FOR BEARING PAD SUPPLY PRESSURE 20 PSIG

Load, pounds	Gap height, inch x 10^6	Flowmeter reading	Volume flow rate, in^3/sec	Mass flow rate lb/sec x 10^5
7.85	1540	13.4	5.60	25.3
9.85	1390	13.4	5.60	25.3
12.85	1225	13.3	5.55	25.1
14.85	1150	13.3	5.55	25.1
17.85	1055	13.3	5.55	25.1
19.85	990	13.2	5.50	24.8
22.85	920	13.2	5.50	24.8
25.85	840	13.0	5.45	24.6
27.85	805	12.9	5.40	24.4
29.85	775	12.8	5.35	24.2
31.85	750	12.7	5.30	23.9
36.85	685	12.5	5.25	23.7

B. FOR BEARING PAD SUPPLY PRESSURE 10 PSIG

Load, pounds	Gap height, inch x 10^6	Flowmeter reading	Volume flow rate, in^3/sec	Mass flow rate lb/sec x 10^5
7.85	1295	10.7	3.55	16.0
9.85	1135	10.5	3.50	15.8
12.85	980	10.4	3.45	15.6
14.85	895	10.25	3.35	15.1
17.85	795	10.1	3.30	14.9
19.85	740	9.9	3.20	14.4
22.85	670	9.7	3.15	14.2
25.85	610	9.5	3.05	13.8
27.85	580	9.3	2.95	13.3
29.85	540	9.0	2.80	12.6
31.85	515	8.8	2.75	12.4
36.85	460	8.5	2.15	12.0

equation (2.40).

The pressure, P_1, at the entrance to the lands is calculated by:

$$M = \frac{bh^3}{24\mu l} \frac{\rho_1}{P_1} (P_1^2 - P_e^2)$$

or $\quad P_1^2 = P_e^2 + \dfrac{24\mu l M}{bh^3 \; \rho_1/P_1}$ \hfill (5.1)

where $\mu = 2.6 \times 10^{-9}$ reyn

$l = 0.125$ inch

$M =$ mass flow, lb per second, from Table II.

$b = 7.43$ inches

$h =$ lower gap height from Table II

$P_e = 14.7$ psi

$\rho_1/P_1 =$ constant, 2.8417×10^{-6}.

Substituting the known values, equation (5.1) becomes:

$$P_1 = \left[216 + \left(\frac{.37M}{h^3} \times 10^{-9} \right) \right]^{1/2} \hfill (5.2)$$

The lift provided by the pressure P_1 acting on the area enclosed by the grooves is

$$\text{Lift}_I = 3.36 (P_1 - P_e) \hfill (5.3)$$

The lift provided by the pressure $P_1 > P > P_e$ acting on the area above the lands is (using equation 2.40):

$$\text{Lift}_{II} \ = \ 0.93 \ P_1 \ \left[\frac{2}{3} \cdot \frac{[1 - (\frac{P_e}{P_1})^3]}{[1 - (\frac{P_e}{P_1})^2]} - \frac{P_e}{P_1} \right] \qquad (5.4)$$

Theoretical lift calculated with equations (5.2, 5.3, and 5.4) is plotted versus observed load in Figure 46 for a supply pressure of 20 psig and in Figure 47 for 10 psig supply pressure. Computed data are tabulated in Table III.

Figure 46 shows the actual lift larger than that predicted by theory. Therefore, the pressure under the bearing is larger than the pressure P_1 calculated by equation (5.2). This is also true in Figure 47 for gap heights greater than 6.3×10^{-4} inch.

The pressure P_1 is controlled by the annular ring surrounding the entrance tube in the center of each quadrant. As the gap height increases, the area of the annular ring is larger. This results in a smaller pressure drop at the tube exit, therefore the lift is greater than predicted. As the gap height decreases, as shown in Figure 47 for gap heights less than 6.3×10^{-4} inch, a greater pressure drop occurs, and the lift is less than that predicted by theory.

The areas presented to gas flow at critical points in the bearing pad are drawn in Figure 48. Log-log paper is used to emphasize the inherent compensation at the end of the entrance tube. Gas flow is controlled by the gap height. The maximum gap height in the assembled bearing is 0.0014" and at that gap height, the area

TABLE III

THEORETICAL LIFT

A. SUPPLY PRESSURE 20 PSIG = 34.7 PSIA

Gap height x 10^6	Mass flow per quadrant lbs/sec x 10^5	Pressure P_1 lbs/in^2	Lift$_I$ lbs	Lift$_{II}$ lbs	Total lift, lbs
1540	6.58	14.89	0.64	0.11	0.75
1390	6.32	14.96	0.87	0.12	0.99
1225	6.28	15.10	1.34	0.18	1.52
1150	6.28	15.19	1.65	0.22	1.87
1055	6.28	15.33	2.12	0.30	2.42
990	6.20	15.48	2.62	0.37	2.99
920	6.20	15.66	3.22	0.44	3.66
840	6.15	15.94	4.17	0.58	4.65
805	6.10	16.10	4.70	0.66	5.36
775	6.05	16.21	5.07	0.71	5.78
750	5.98	16.39	5.68	0.80	6.48
685	5.92	16.85	7.22	1.02	8.24

B. SUPPLY PRESSURE 10 PSIG = 24.7 PSIA

Gap height x 10^6	Mass flow per quadrant lbs/sec x 10^5	Pressure P_1 lbs/in^2	Lift$_I$ lbs	Lift$_{II}$ lbs	Total lift, lbs
1295	4.00	14.89	0.64	0.10	0.74
1135	3.95	15.03	1.11	0.17	1.28
980	3.90	15.19	1.65	0.22	1.87
895	3.78	15.32	2.08	0.29	2.37
795	3.72	15.60	3.02	0.42	3.44
740	3.60	15.78	3.63	0.51	4.14
670	3.55	16.10	4.70	0.66	5.36
610	3.45	16.46	5.91	0.83	6.74
580	3.32	16.66	6.58	0.93	7.51
540	3.15	17.00	7.73	1.10	8.83
515	3.10	17.26	8.60	1.22	9.82
460	3.00	18.42	12.50	1.79	14.29

113
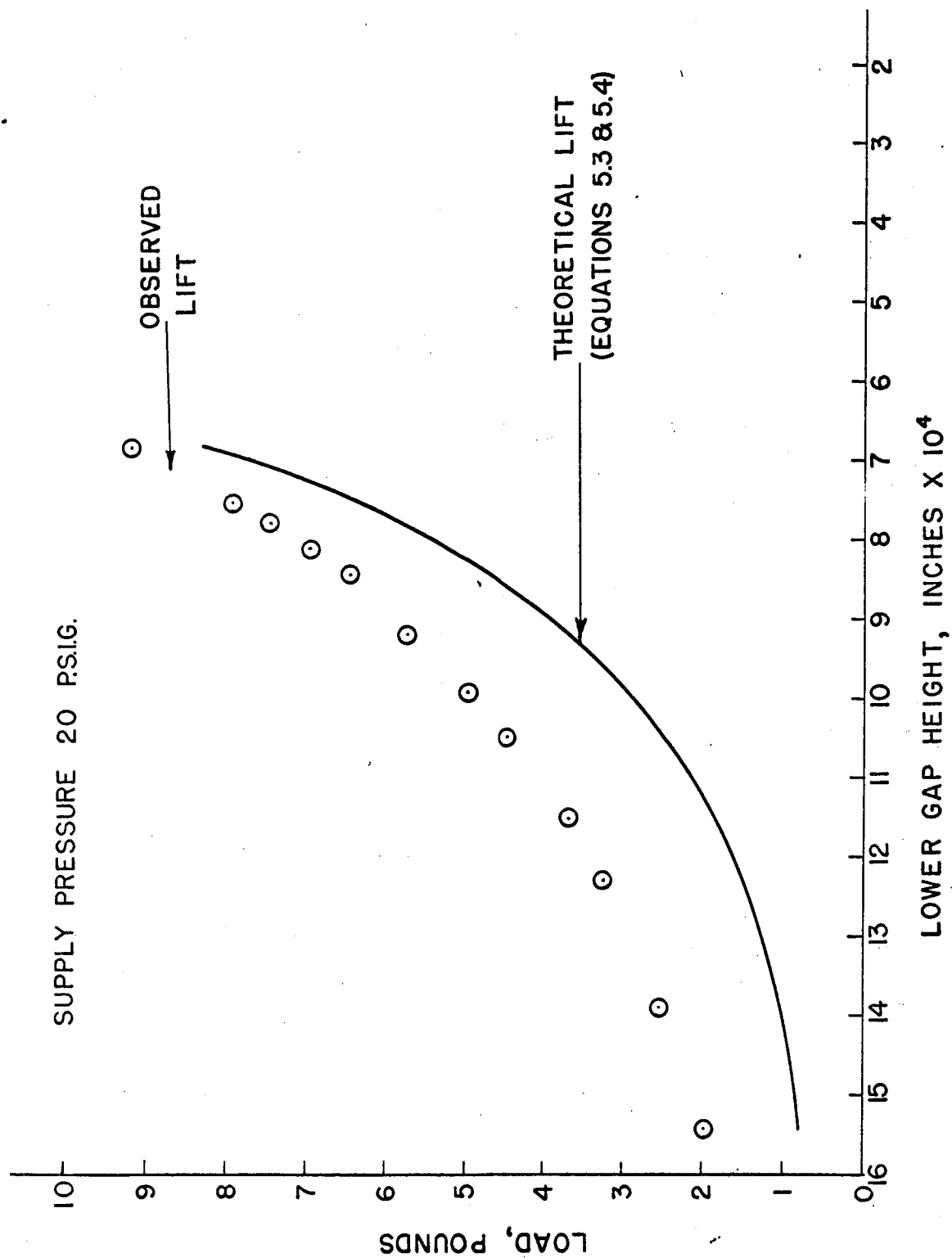
Figure 46. Theoretical and Actual Lift, 20 psig
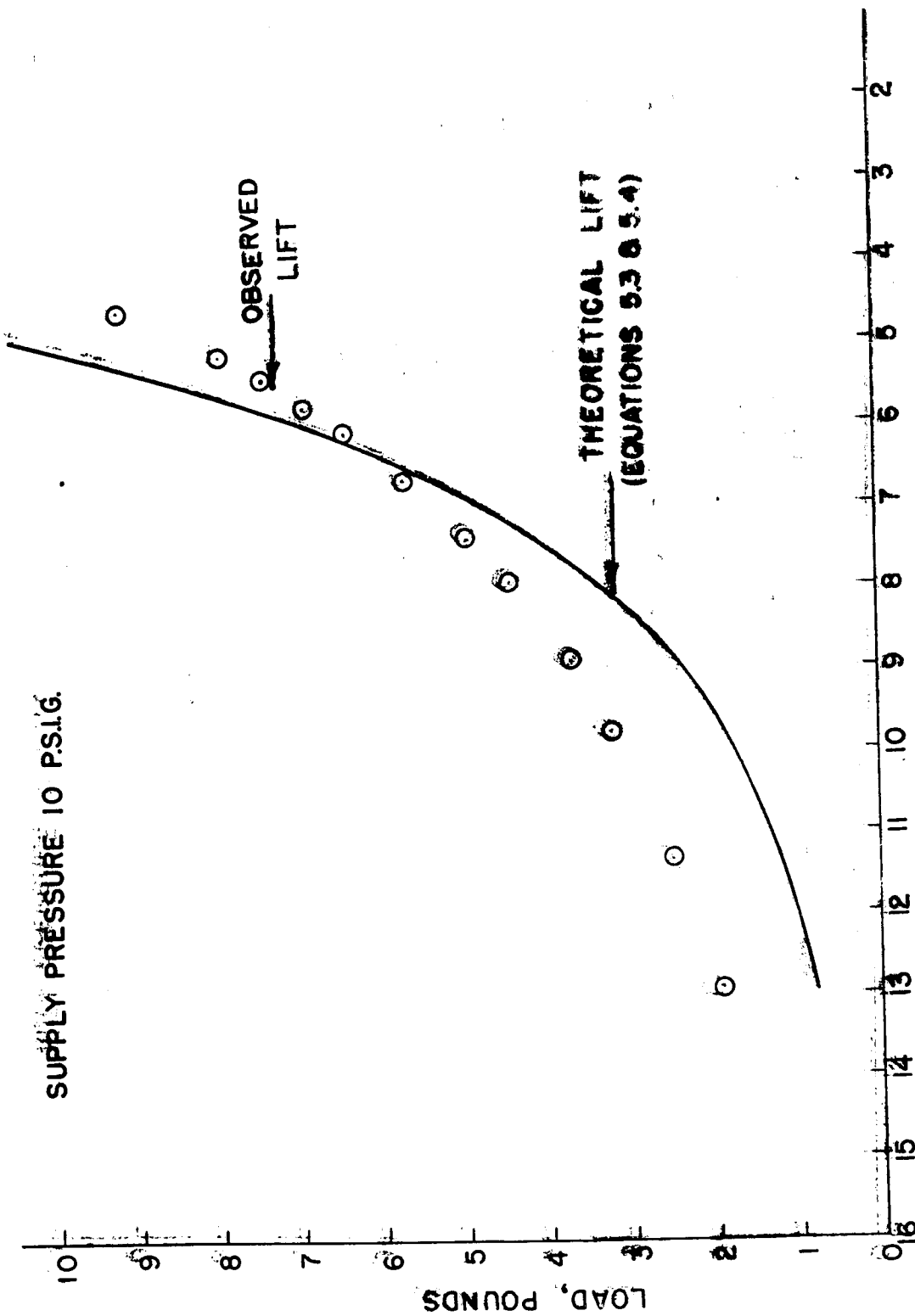
Figure 47. Theoretical and Actual Lift, 10 psig
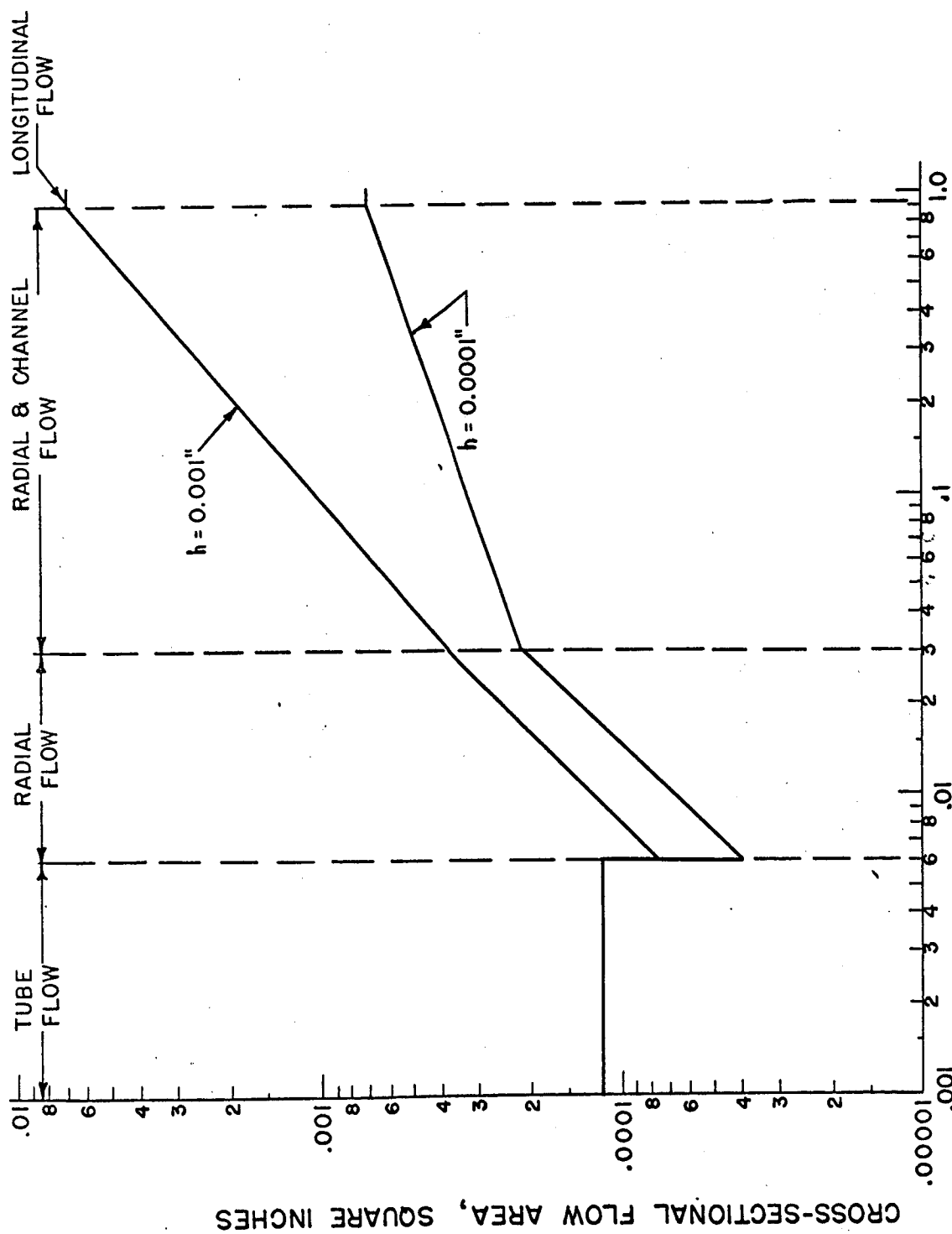
Figure 48. Cross-Sectional Area vs Distance from Entrance Tube

of the annular ring is less than the area of the entrance tube, therefore

the bearing with hold-down pads is inherently compensated for all

supply pressures. Types of flow are indicated at specific radial

distances from the entrance tube in Figure 48.

Comolet has measured the distributed pressure, P, at

specified radial distances from the entrance tube for various Mach

numbers.[35] His results are reproduced in Figure 49. Note that at

a distance 0.25 inch from the entrance tube, the pressure is less

than ambient at Mach 0.19 speeds. The gap height for Comolet's

curve is larger than the lower gap of the bearing in this study--

0.0039 inch as compared to 0.0024 inch, therefore the Mach number

in our case is larger and the pressure drop even greater than the

curve obtained by Comolet.

The curves of Figure 49 support Figures 46 and 47 in that

the pressure calculated for the outermost groove is not equal at

all points in the enclosed area.

II. NATURAL FREQUENCIES

The static natural frequency of the bearing, sting, and

attachments in the vertical plane is:

---

[35]Raymond Comolet, op. cit., p. 55.

Figure 49. Distributed Pressure vs Distance from Entrance Tube

○ MACH 0.19
□ MACH 0.105
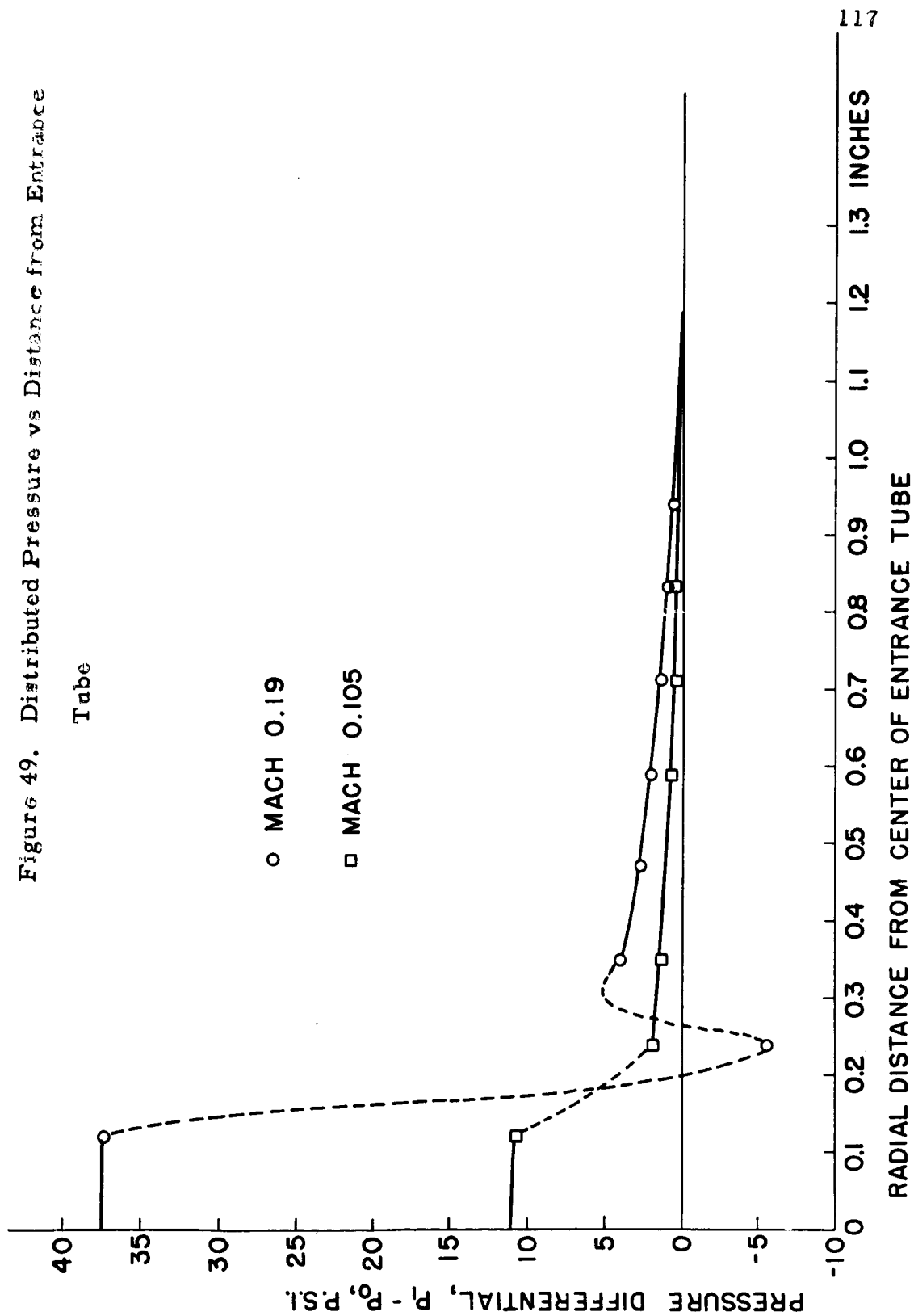
$$\omega_n = \sqrt{\frac{K}{m}} \qquad (5.4)$$

where K is the static spring constant determined experimentally, and m is the mass of the bearing assembly.

At 20 psig bearing pad and 30 psig hold-down pads supply pressures, the observed spring constant for a load of 8.875 pounds (the weight of the bearing assembly) is 91,000 pounds per inch (see Figure 42). The undamped natural frequency under these conditions is

$$\omega = \sqrt{\frac{91000 \ (386)}{8.875}} = 1990 \ \text{Rad/Sec} = 317 \ \text{cps},$$

for the spring--mass system.

The critical speed of the sting is[36]

$$\omega_{cr} = \sqrt{\frac{gk}{W}} \qquad (5.5)$$

where g is the acceleration due to gravity,

k is the shaft spring constant, and

W is the load on the shaft.

In equation (5.5), k is given by $\frac{3 E I1}{a^2 b^2}$, [37] where E is Young's modulus, 29,000,000 lb/in,

---

[36]Lionel S. Marks, (ed.), <u>Mechanical Engineer's Handbook</u> (fourth edition; New York: McGraw Hill Book Company, Inc., 1949), p. 519.

[37]<u>ibid</u>, p. 520.

I is the moment of inertia of the shaft about its axis,

l is the length of the shaft, and

a, b are distances from the end of the shaft to the point

of loading, W.

The moment of inertia of the shaft is

$$I = \frac{m r^2}{2} = \frac{5.125 (.375)^2}{2 (386)} = .933 \times 10^{-3}$$

The shaft spring constant,

$$k = \frac{3EIl}{a^2 b^2} = \frac{3 (29 \times 10^6)(.933 \times 10^{-3})(36)}{(4.25)^2 (31.75)^2} = 160.5 \text{ LB/inch}$$

and finally, the critical speed of the shaft:

$$\omega_{cr} = \frac{gk}{W} = (\frac{386 (160.5)}{2.75})^{1/2} = 150.1 \text{ Rad/Sec} = 23.9 \text{ cps.}$$

The predicted critical frequency of 24 cps was shown

experimentally by the observed response at 30 cps (Figure 45).

The dynamic spring constant, which depends on the flow

of gas through converging and diverging gaps, is outside the scope

of this thesis and has not been stated theoretically. The responses

noted at 90 and 500 cps indicated at the end of the sting are, in all

likelihood, due to the dynamic spring constant.

As shown in Figure 11, the forces K_1 and K_2 act to restrain

rotation about the center of gravity of the bearing assembly. There-

fore, as the forces K_1 and K_2 vary due to a slight displacement, the

end of the sting experiences the greatest vibration.

Assume that the natural dynamic frequency is the observed response at 90 cps = 565.2 rad/sec. Then the _dynamic_ spring constant is

$$k = \frac{J_\theta}{1.11} \omega_n^2 = \frac{2.32}{1.11} (565.2)^2 = \underline{668,000 \text{ lb/inch.}}$$

at supply pressures 30 psig to the hold-down pads and 20 psig to the bearing pad.

The moment of inertia J_θ is taken about the center of gravity of the bearing and sting assembly, calculated below:

$$J_\theta = I_B + m_B a^2 + I_S + m_S d^2$$

$$= \frac{m_B}{4} \left[r_B^2 + \frac{l_B^2}{3} \right] + m_B a^2 + \frac{m_S}{4} \left[r_S^2 + \frac{l_S^2}{3} \right] + m_S d^2$$

where m_B is the bearing mass = $2.75/g$,

r_B is the bearing radius = 2.5 in.,

l_B is the length of the bearing = 0.94 in.,

a is the distance from bearing CG to assembly CG = 8.845 in.,

m_S is the mass of the sting = $5.12/g$,

l_S is the length of the sting = 36 in., and

d is distance from sting CG to assembly CG = 4.805 in.

therefore J_θ = 2.32.

From Equation (2.70):

$$\omega_\theta = d \sqrt{\frac{(K_1' + K_4') - (K_2' + K_3')}{J_\theta}} .$$

As stated previously, the exact values of K_1', K_2', K_3', and K_4' depend on combination radial and channel gas flow through a converging or diverging gap and are not determined theoretically. However, an approximation of the angular natural frequency may be made by linearizing the experimentally-obtained stiffness for a fixed upper and lower gap height and reading the values of K from Figures 40 through 42 .

Assume an equilibrium gap height of 0.0007 inch and a force, F, sufficient to cause changes in the gap height of 0.0001 inch on the right and left sides of the bearing. Linearizing for a gap height of 0.0006 inch:

$2 K_1' = 300,000;$ $K_1' = 150,000$ lb/in (curve B, Figure 42),

$2 K_4' = 38,000;$ $K_4' = 19,000$ lb/in (curve A, Figure 41),

and for a gap height of 0.0008 inch:

$2 K_2' = 50,000;$ $K_2' = 25,000$ lb/in (curve A, Figure 40),

$2 K_3' = 30,000;$ $K_3' = 15,000$ lb/in (curve A, Figure 41).

Geometry of the bearing pads yields $d = 1.11$ inches, and

$$\omega_\theta = 1.11 \sqrt{\frac{129,000}{2.32}} = 262 \text{ rad/sec} = 41.7 \text{ cps,}$$

near the observed response at 30 cps.

III.   ERROR ANALYSIS

Gap height.   An error of 10% measurement of gap height
will result in a 30% error in calculation of the pressure drop.
Using equation (3.7)   :

$$M = \frac{\rho_1 bh^3}{12\mu 1} (P_1 - P_2)$$

or

$$\frac{K}{(P_1 - P_2)} = h^3$$

where

$$K = \frac{12\mu 1 M}{b\rho_1} .$$

Taking the logarithm of both sides,

$$\ln K - \ln (P_1 - P_2) = 3 \ln h$$

and differentiating,

$$- \frac{d (P_1 - P_2)}{(P_1 - P_2)} = 3 \frac{dh}{h} .$$

Let dh be the error in measuring gap height.   For a 10% error
in measuring h, dh/h = 0.1, and

$$- \frac{d(P_1 - P_2)}{(P_1 - P_2)} = 3(0.1) = .30 \text{ or } 30\% \text{ error in computing the}$$

pressure drop.

The same relationship holds for the pressure drop across the entrance tube--exact measurement of the gap height is very important for calculation of the pressure P_0 at the tube exit and the pressure P_1 at the entrance to the exhaust lands.

The air gage used to measure gap height is accurate to the nearest 0.000020 inch. For a gap height of 0.0005" the measurement is within 4% of the actual gap height.

Incompressible flow assumption. Volume flow through a longitudinal gap is given by:

$$Q = \frac{b\,h^3}{12\,\mu\,l}\,(P_1 - P_2) \text{ for incompressible flow,}$$

and

$$Q_1 = \frac{b\,h^3}{24\mu\,l}\,\frac{(P_1^2 - P_2^2)}{P_1}$$

$$= \frac{b\,h^3}{12\mu\,l}\,(P_1 - P_2)\,\frac{(P_1 + P_2)}{2\,P_1} \text{ for compressible flow.}$$

The two equations are equal iff:

$$\frac{P_1 + P_2}{2P_1} = 1, \text{ or iff } P_2/P_1 = 1.$$

But $P_1 > P_2$ and for a ratio of $P_2/P_1 = 0.90$, the error in assuming incompressible flow will be

$$0.5 + 0.45 = .95,$$

or 5% less than the actual compressible flow through the bearing.

The ratios of the pressure differential across the entrance tube, P_0/P_s, and across the exhaust land, P_e/P_1, for this bearing ranged from 0.98 to 0.80; therefore the incompressible flow assumption is accurate to 10% at the lowest pressure ratio. This corresponds to a gap height measuring accuracy of 3.3%, which is within the accuracy obtainable with the air gage. Moreover, the lapping tolerance specified is 0.000050 inch which also justifies a compressible flow assumption in the design stage.

Small angle assumption. The angle, θ, about the center of gravity of the bearing assembly, was assumed small when deriving the equations of motion for the system. The maximum possible angle is governed by the radius of the bearing and the gap height. For the bearing studied, the total gap height was .001360 inches, and the radius of the bearing was 2.5 inches. Therefore the maximum angle, θ, is:

$$\theta_{max} = Sin^{-1} \frac{0.00068}{2.5} = 0.000272 \ radians,$$

and the assumptions that $Sin \theta = \theta$ and $Sin^2 \theta \approx 0$ are valid.

CHAPTER VI

CONCLUSIONS AND RECOMMENDATIONS

I. CONCLUSIONS

Based on the experimental work described and analyzed in Chapters IV and V, the following conclusions are made:

a. The design procedures outlined in Chapter III have resulted in an air-bearing suitable for use as a support for a wind-tunnel balance.

b. Stiffness of the air-bearing is primarily a function of the gap height--maximum stiffness is obtained for minimum gap height; the limiting factors in reducing the gap height are the anticipated shock load and the machining and lapping flatness obtainable.

c. The gap height is best held to a minimum through the use of a hold-down pad (or pads) which supplies the required downward force on the bearing, but great care must be exercised in the fabrication and assembly stages to ensure parallel and properly spaced pads.

d. An optically flat glass disc provides the optimum flatness and parallelism required in an air-bearing.

e. The weight flow of gas was well below the maximum flow allowed--0.002 lb/ sec as opposed to 0.01 lb/ sec allowed.

f. Theoretical determination of the lift provided is inaccurate, due to a non-uniform pressure distribution in radial flow which results

in pressures below ambient in some portions of the gas flow area.

II. DESIGN RECOMMENDATIONS

The following recommendations for changes in the design of the bearing are made:

a. Silver solder the restrictors in their access holes prior to machining and lapping the surface of the pads. This will eliminate the need for packing compound and special holders; it will also allow higher pressures to be used without danger of forcing the restrictor tubes above the bearing pad surface.

b. Increase the effective area of the hold-down pads to obtain equal gap heights, and the same spring constant, on the top and bottom of the bearing. A design similar to that used for the bearing pad would be effective. The area of the bottom pad should be slightly greater than that of the hold-down pad to overcome gravity forces of the sting and bearing assembly. Supply pressure to both pads could then be equal.

c. Machine and lap the spacers to uniform heights. If design recommendation b, above, is adopted, the spacer should be one piece, shaped as an annulus. The top and bottom should be lapped parallel to 0.001 inch larger than the thickness of the glass bearing for a top and bottom gap height of 0.0005 inch. A single spacer will reduce the possibility of misalignment of the top and bottom bearing pads by unequal torque on the connecting screws.

d. Use higher pressures--of the order of 50 psig--to increase

the stiffness of the bearing assembly. The gas flow rate will still be below the maximum allowable.

III. FUTURE STUDY RECOMMENDATIONS

Gas flow through comparatively rough channels in combination with radial flow over a smooth surface leads to the following recommendations:

a. Measure the distributed pressure over the lands and grooves, with a movable pressure tap mounted in the glass bearing, or mounted in a metal bearing machined and lapped to the exact dimensions of the glass bearing.

b. Develop empirical relationships between the groove width, groove depth, gap height, and supply pressure to predict gas flow rates and pressure distribution for geometrical configurations as used in this thesis.

The dynamic spring constant of the air-bearing assembly is not the same as the static spring constant. A study of the dynamic spring constant will involve gas flow through converging or diverging gaps in addition to the complex flow study recommended in the pre-ceeding paragraph.

BIBLIOGRAPHY

BIBLIOGRAPHY

A. BOOKS

Crede, Charles E. <u>Vibration and Shock Isolation</u>. New York: John
    Wiley and Sons, Inc., 1951.

den Hartog, J. P. <u>Mechanical Vibrations</u>. New York: McGraw-Hill
    Book Company, Inc., 1956.

Eskinazi, Salamon. <u>Principles of Fluid Mechanics</u>. Boston: Allyn
    and Bacon, Inc., 1962.

Gross, W. A. <u>Gas Film Lubrication.</u> New York: John Wiley and
    Sons, Inc., 1962.

Hodgman, Charles D. (ed.) <u>Handbook of Chemistry and Physics</u>.
    Twenty-ninth edition. Cleveland, Ohio: Chemical Rubber
    Company Publishing Company, 1945.

Hunsaker, J. C. and B. G. Rightmire. <u>Engineering Applications of
    Fluid Mechanics.</u> New York: McGraw-Hill Book Company,
    Inc., 1947.

Korn, Granino A. and Theresa M. Korn. <u>Mathematical Handbook
    for Scientists and Engineers</u>. New York: McGraw-Hill
    Book Company, Inc., 1961.

Marks, Lionel S. (ed.) <u>Mechanical Engineer's Handbook.</u> Fourth
    Edition, Twelfth Printing. New York: McGraw-Hill Book
    Company, Inc., 1949.

Peterson, Arnold P. G. and Leo L. Beranak. <u>Handbook of Noise
    Measurement and Measurement of Vibration.</u> Third edition,
    Cambridge, Massachusetts: General Radio Corporation, 1956.

Pinkus, Oscar and Beno Sternlicht. <u>Theory of Hydrodynamic
    Lubrication.</u> New York: McGraw-Hill Book Company, Inc.,
    1961.

Schlichting, Hermann. <u>Boundary Layer Theory</u>. New York: McGraw-
    Hill Book Company, Inc., 1955.

Timoshenko, S. and S. Woinowsky-Kreiger. <u>Theory of Plates and
    Shells</u>. Second edition. New York: McGraw-Hill Book
    Company, Inc., 1952.

Zucrow, M. J. <u>Principles of Jet Propulsion and Gas Turbines.</u>
New York: John Wiley and Sons, Inc., 1948.

B. PUBLICATIONS OF THE GOVERNMENT, LEARNED
SOCIETIES, AND OTHER ORGANIZATIONS

Boeker, G. F., D. D. Fuller, and C. F. Kayan. "Gas Lubricated
Bearings--A Critical Survey." Wright-Patterson Air
Force Base, Ohio: WADD Technical Report 58-495. July
1958.

Cetiner, Ayhan "Influence of Elastomeric and Conventional
Bearing Plates on Beam Vibrations." <u>MS Thesis.</u> Char-
lottesville, Virginia: University of Virginia, 1963.

Comolet, Raymond. "Ecoulement d'un Fluide Entre Deux Plans
Paralleles, Contribution a l'Etude des Butees d'Air. "
<u>Publication Scientifiques et Techniques du Ministere de
l'Air.</u> No. 334. Paris: Au Service de Documentation
et d'Information Technique de l'Aeronautique, 1957.

Corning Glass Works. "Properties of Selected Commercial
Glasses." <u>Handbook B-83.</u> Corning, New York: Corning
Glass Works, 1949.

Graneek, M. and J. Kerr. "Air Bearings--Research and Appli-
cations at National Engineering Laboratory, Scotland. "
Paper presented to First International Symposium on
Gas-Lubricated Bearings, Washington, D.C., 1959
pp. 71-91.

Grinnell, Sherman K. "A Study of Pressurized Air Bearing
Design, Steady Loading, No Rotation. " <u>MS Thesis.</u>
Cambridge, Massachusetts: Massachusetts Institute of
Technology, 1954.

_____, "Flow of a Compressible Fluid in a Thin Passage, "
<u>Transactions of the ASME,</u> Vol. 78, 1956. New York:
The American Society of Mechanical Engineers, 29 West
Thirty-Ninth Street, pp. 765-711.

Laub, J. H. "Hydrostatic Gas Bearings, " <u>Transactions of the
ASME,</u> Vol. 82, June 1960, pp. 276-286.

_____, "Externally Pressurized Journal Gas Bearings, "
<u>ASLE Transactions,</u> Vol. 4, 1961, pp. 156-171.

Laub, J. H. and R. H. Norton. "Externally Pressurized Spherical Gas Bearings," ASLE Transactions, Vol. 4, 1961, pp. 172-180.

Laub, J. H. "Gas Lubrication in Instruments and Control Devices," ISA Transactions, Vol. 1, No. 4, October 1962, Pittsburgh: Instrument Society of America, 530 William Penn Place, pp. 305-314.

_____, and H. D. McGinness. "Gas Floated Spinning Spheres," ASME--ASLE Paper, No. 60, LC-16, 1961.

Licht, L. and H. Elrod. "A Study of the Stability of Externally Pressurized Gas Bearings," Transactions of the ASME, Journal of Basic Engineering, Series D, Vol. 82, 1960, pp. 250-258.

_____, D. D. Fuller, and B. Sternlicht. "Self Excited Vibrations of an Air-Lubricated Thrust Bearing," Transactions of the ASME, Vol. 80, 1958, pp. 411-414.

Ling, M. T. S. "On the Optimization of the Stiffness of Externally Pressurized Bearings," Transactions of the ASME, Series D, Vol. 84, March 1962, pp. 119-122.

Malanoski, S. B. and A. M. Loeb, "The Effect of the Method of Compensation on Hydrostatic Bearing Stiffness," Transactions of the ASME, Series D, Vol. 83, June 1961. pp. 179-187.

Pigott, J. D. and E. F. Macks. "Air Bearing Studies at Normal and Elevated Temperatures," Lubrication Engineering, Vol. 10, 1954, pp. 29-32.

Proceedings of the First International Symposium on Gas-Lubricated Bearings, Office of Naval Research, ACR-49. Washington, D. C.: Superintendent of Documents, 1959.

Richardson, H. H. "Static and Dynamic Characteristics of Compensated Gas Bearings," Transactions of the ASME, Vol. 80, 1958, pp. 1503-1509.

Roudebush, W. H. "An Analysis of the Effects of Several Parameters on the Stability of an Air-Lubricated Hydrostatic Thrust Bearing," NACA TN-4095, October 1957. Washington, D. C.: National Advisory Committee for Aeronautics (now National Aeronautics and Space Administration, NASA).

Stark, Kenneth W. "The Design of Various Types of Air Bearings for Simulating Frictionless Environments," <u>NASA TN D-1100</u>, May 1962. Washington, D. C.: National Aeronautics and Space Administration, May, 1962.

Wunsch, H. L. "Design Data for Flat Air-Bearing when Operating under Steady Conditions of Load," <u>Metalworking Production</u>, Vol. 102, 1958, pp. 1697-1709. London: McGraw-Hill Publishing Company, Ltd., Farringdon Street.

_____, "Flat Pad Bearings," <u>Scientific Lubrication</u>, Vol. 14, No. 4, April 1962, pp. 14, 16, 18, 20-23. Broseley-Shropshire, England: Scientific Publications.

APPENDICES

APPENDIX A

PREDICTABILITY FLOWMETER

The predictability flowmeter is manufactured for the Manostat Corporation by the Fisher and Porter Company. The instrument is available in four sizes and measures gas flow rates from 1.3 to 68,000 milliliters per minute. The size used for this experiment measured gas flows from 1350 to 34,500 milliliters per minute (1.4 to 35.1 cubic inches per second) with a glass float provided with the flowmeter.

The flowmeter tube has a circular cross-section at the bottom which gradually changes to a triangular cross-section at the top as the length of the tube is traversed.
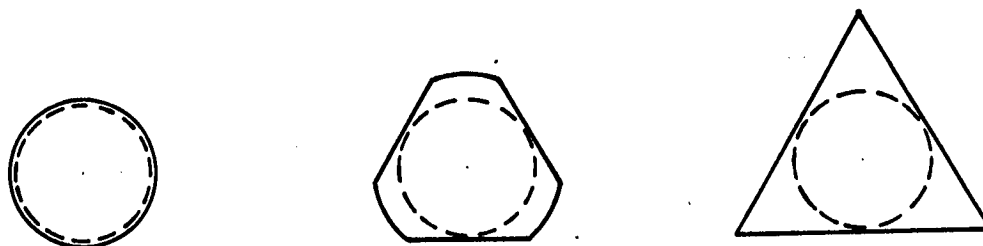

Figure 50. Cross-Section of Flowmeter Tube

The spherical float rests snugly against the sides of the tube at all times since the sides of the equilateral triangle are tangent to the sphere. The float comes to an equilibrium position at the point

in the tube where the weight of the float equals the force of the gas

flowing through the annular area. Graduation marks on the tube

indicate the percentage increase in the diameter of the tube over

that of the float:

$$\text{Reading} = \frac{D_t - D_f}{D_f} \times 100,$$

where D_t is the effective diameter of the tube at the point of reading

(effective diameter is the diameter of an equivalent circle at the

point of reading) and

D_f is the diameter of the float, in inches.

Predictability charts are provided with the flowmeter. That

portion of the chart pertaining to this experiment is reproduced in

Figure 51 . Calibration tables are also sent with the flowmeter

for measuring air or water flow rates. Tables for other gases or

liquids are prepared as follows:

1. Calculate the net weight of the float, F, immersed in the

fluid:

$$F = \frac{W(\rho_f - \rho)}{\rho_f}$$

where ρ = density of the fluid in grams per milliliter at conditions of

flow,

W = weight of the float in grams (1.030), and

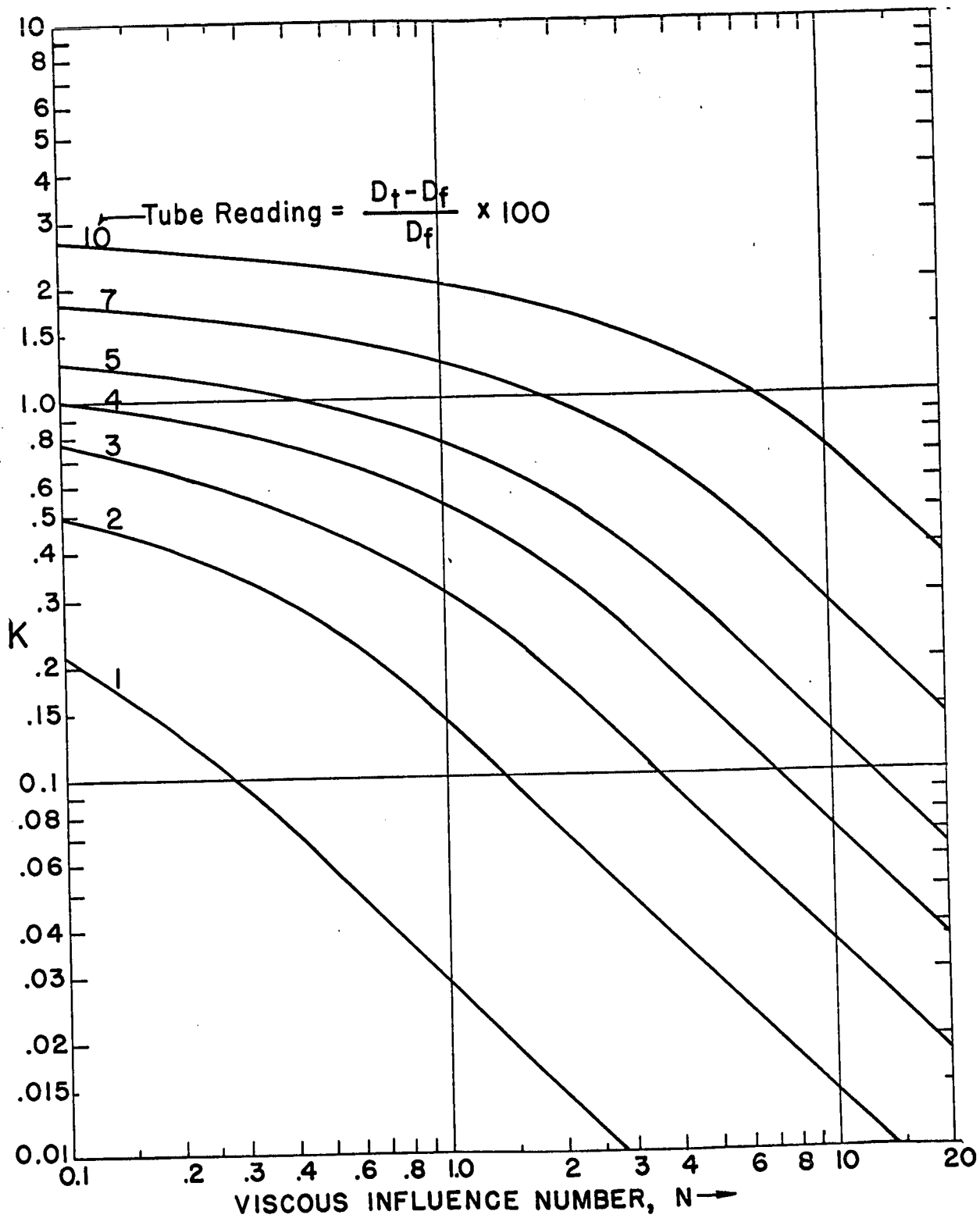ρ_f = density of the float in grams per milliliter, (2.28).

Figure 51. Predictability Chart

136

2. Calculate the viscous influence number, N:

$$N = \frac{\mu}{\sqrt{F\rho}}$$

where μ = viscosity of fluid at conditions of flow in centipoises.

3. Calculate the instrument constant, C:

$$C = \frac{453.6}{\rho_0} D_f \sqrt{F\rho} \qquad (A.3)$$

where ρ_0 = density of fluid at standard conditions (70° F. and 1 atmosphere) in grams per milliliter.

4. Read the flow coefficient, K, from the predictability chart, Figure 51, for each tube reading.

5. Calculate the volume flow at standard conditions for each tube reading in milliliters per minute:

$$V_n = C \times K_n \text{ (for each of n tube readings)} \qquad (A.4)$$

Example. To illustrate this method of calibrating the flowmeter, consider air flowing at 70° F. and 1 atmosphere pressure. Density is 0.0012 grams/milliliter and viscosity is 0.01812 centipoise.

Using equation (A.1):

$$F = 1.030 \; \frac{2.28 - 0.0012}{2.28} = 1.029.$$

Equation (A. 2) yields:

$$N = \frac{0.01812}{\sqrt{1.029 \times 0.0012}} = 0.515.$$

From Figure 51, the values of K for each tube reading corresponding to N = 0.515 are:

$K_2 = 0.249$

$K_3 = 0.449$

$K_4 = 0.69$

$K_5 = 0.95$

Calculate the instrument constant, C, with equation (A. 3):

$$C = \frac{453.6}{0.0012} \times 0.375 \sqrt{1.029 \times 0.0012} = 5090.$$

Multiply the instrument constant, C, by each flow coefficient, K_n to obtain the following calibration table:

TABLE IV

PREDICTABILITY FLOWMETER CALIBRATION TABLE

Tube reading (Center of ball)	Flow rate ml/min	Flow rate, cu in/sec
2	1270	1.291
3	2290	2.327
4	3510	3.567
5	4830	4.908

APPENDIX B

ABSOLUTE CALIBRATION OF FLOWMETERS

An absolute calibration of both flowmeters used for the experimental work was performed to ensure that the flow of nitrogen was measured as accurately as possible. A schematic of the calibration set-up is given:
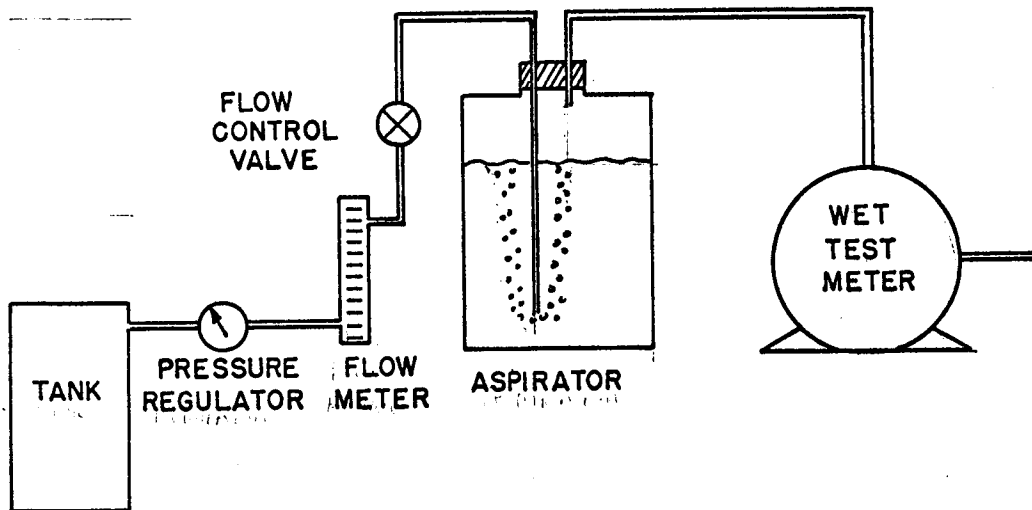

Figure 52. Schematic of Set-Up for Flowmeter Calibration

The wet-test meter measures volume flow at low flow rates. It was calibrated with a one-tenth cubic foot bottle certified exact by the National Bureau of Standards (certificate on file in the Mechanical Engineering Department).

Observation was made of the supply pressure, float reading, and the time required for one-tenth cubic foot of nitrogen to pass

through the wet-test meter. Tests were conducted at various supply pressures to obtain smooth curves throughout the range of float readings observed during the tests conducted with the air bearing. In each case, the volume measured was for _saturated_ nitrogen at atmospheric pressure and room temperature. The volume was corrected to a corresponding volume of dry nitrogen gas at standard temperature and pressure. The results of the calibration are as indicated in Figures 53 and 54.

The following procedure was used to make the correction:

a. The vapor pressure of water at room temperature is subtracted from atmospheric pressure at the time of the test. This gives the true pressure of _dry_ nitrogen which passed through the wet-test meter.

b. The volume passed (172. 8 cubic inches) at room temperature is corrected to the volume at standard temperature and pressure by multiplying 172. 8 by the volume correction factor[38] for the temperature of the gas passing through the meter and the corrected pressure of the _dry_ gas. This gives the volume of dry nitrogen passing through the wet-test meter at standard conditions of temperature and pressure.

The weight flow may now be found by multiplying by the specific weight of nitrogen at S. T. P. (Figure 55).

---

[38]Charles D. Hodgman (ed.), _Handbook of Chemistry and Physics_, (twenty-ninth edition; Cleveland: Chemical Rubber Publishing Company, 1945) p. 2255
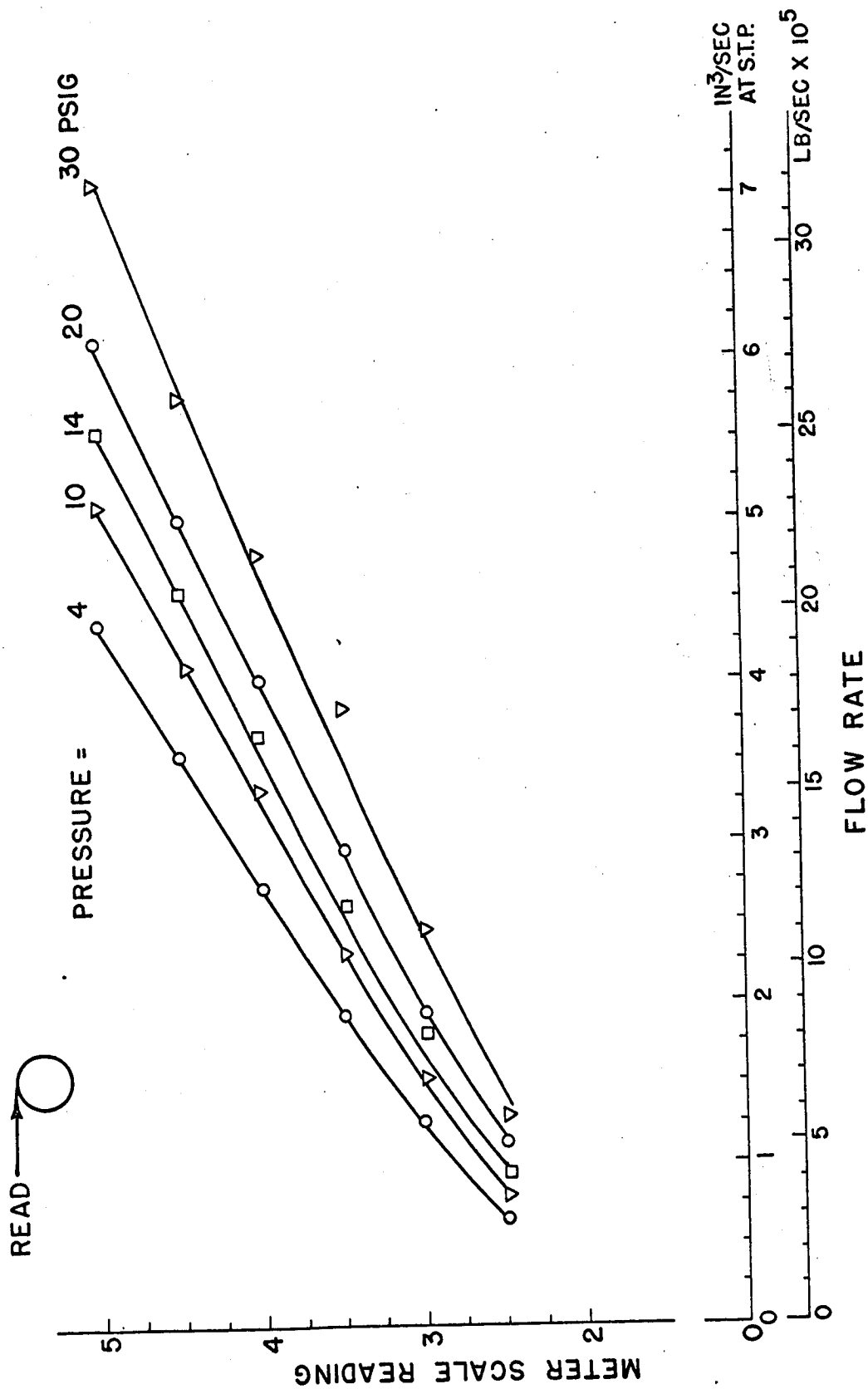
Figure 53. Calibration Curves, Predictability Flowmeter
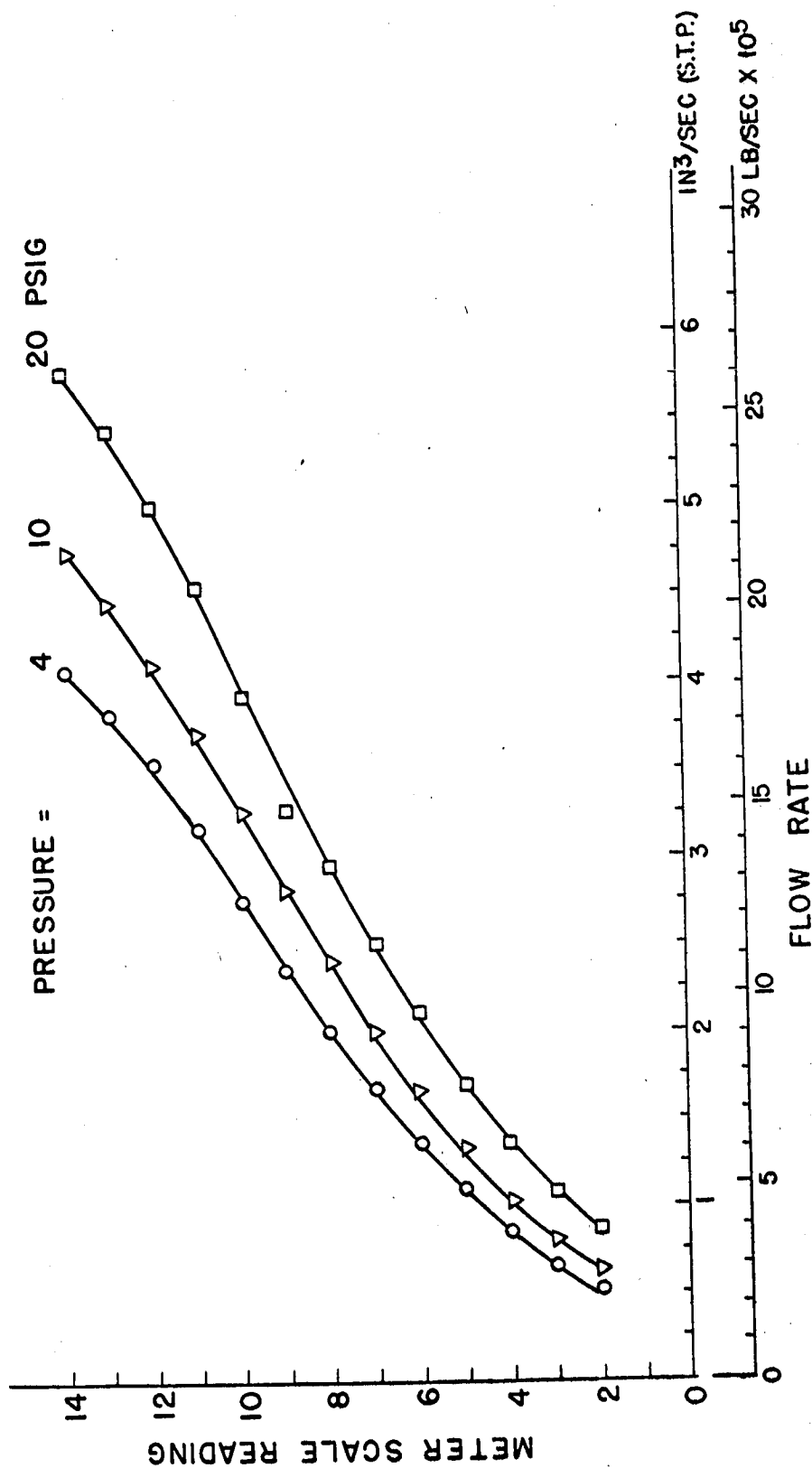
Figure 54. Calibration Curves, Fisher and Porter Rotameter

SPECIFIC WEIGHT OF DRY N_2, LB/IN^3
VS. PRESSURE, PSIG
AT CONSTANT TEMPERATURE, 72° F.

$$\frac{P_1}{\rho_1} = \frac{P_2}{\rho_2} = RT = 351,900$$

PRESSURE, LBS / SQ·IN
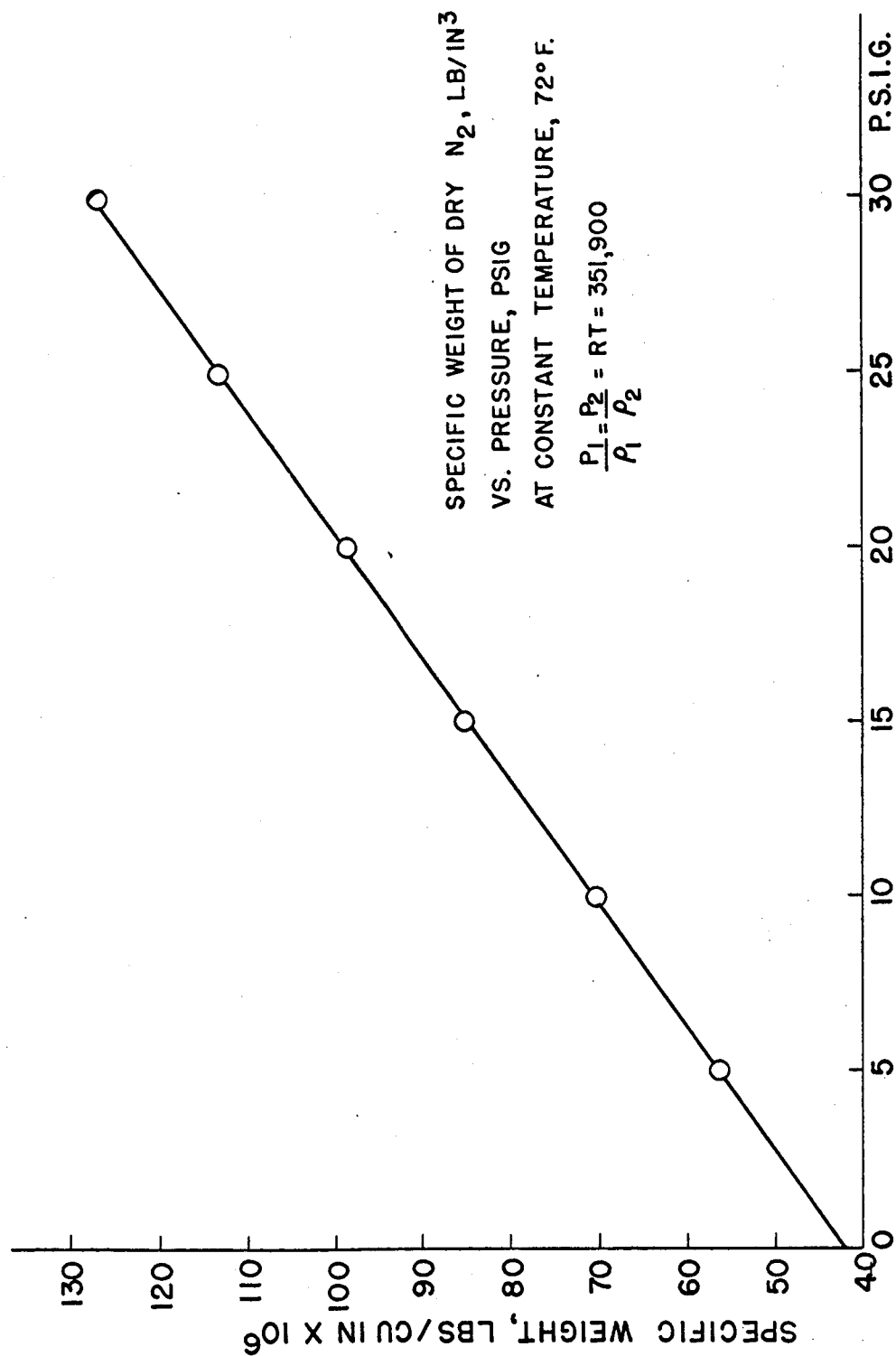
SPECIFIC WEIGHT, LBS/CU IN X 10^6

Figure 55. Specific Weight of Dry Nitrogen vs Pressure,
Temperature Constant, 72° F

APPENDIX C

AIR GAGE

The Sheffield PRECISIONAIRE air gage is designed
primarily for use in precision inspection of assembly-line parts,
but was used effectively in this experiment to measure movements
of the glass bearing under load to five-millionths of an inch.
PRECISIONAIRE instruments are available with magnifications
of 1,000, 2,000, 5,000, 10,000, 20,000, and 40,000 to 1 which
have graduations of 0.0002, .0001, .00005, .00002, .00001, and
.000005 inch respectively. The instrument used has an amplification
of 10,000 to 1; each division represents 20 millionths of an inch
(0.00002"). However, deflections may be estimated to 5
millionths of an inch.

An air supply of 40 to 125 psi is required for operation of
the gage. The supply air passes through a filter supplied with the
instrument (which must be mounted at least 18 inches below the
instrument to effectively trap oil and water) then through an integral
regulator which reduces the pressure to 10 psi for use with the tool-
ing. An AIREJET cartridge was used with the Sheffield universal
tool stand for measurements of gap height in this experiment.

The principle of measurement is that as the volume of air
allowed to escape between the face of the cartridge and the work
surface increases, the kinetic energy of the gas flowing through the
calibrated tube increases and exerts a larger force on the float.

causing it to rise in the tube. The distance it rises is proportional to the amount of air escaping which, in turn, depends on the distance between the face of the cartridge and the surface of the work.

Prior to any measurements, the instrument must be calibrated. Calibration requires master "go" and "no-go" gages for conventional use, but when used as a measuring device rather than for inspection work, gage blocks and a surface plate are necessary. A DoAll granite surface plate with an overall accuracy of 50 millionths of an inch was used for the calibration.

The calibration procedure, which must be performed each time the instrument is set up, follows:

a. Wring together two sets of gage blocks with a total difference in height of 0.0009"--the maximum and minimum readings of the instrument scale.

b. Adjust the gage stand and cartridge over the larger set of blocks until the float (B) is near the bottom pointer (D). Letters refer to Figure 56. The calibration set-up is pictured in Figure 57.

c. Turn the float positioning knob (A) to position the top of the float exactly in line with the bottom pointer.

d. Remove the larger set of gage blocks and insert the smaller set. The float will rise in the tube[39] because a larger amount of air is allowed to escape between the top of the gage block and the

---

[39] The float will fly to the top of the tube when the gage blocks are removed. However, there is a spring-loaded float bumper in the top of the instrument tube to prevent damage to the float when the gaging parts are removed from the gaging position beneath the cartridge.

Ⓐ FLOAT POSITIONING KNOB

Ⓑ FLOAT

Ⓒ TOP POINTER

Ⓓ BOTTOM POINTER

Ⓔ CALIBRATION ADJUSTMENT KNOB

FLOAT BUMPER
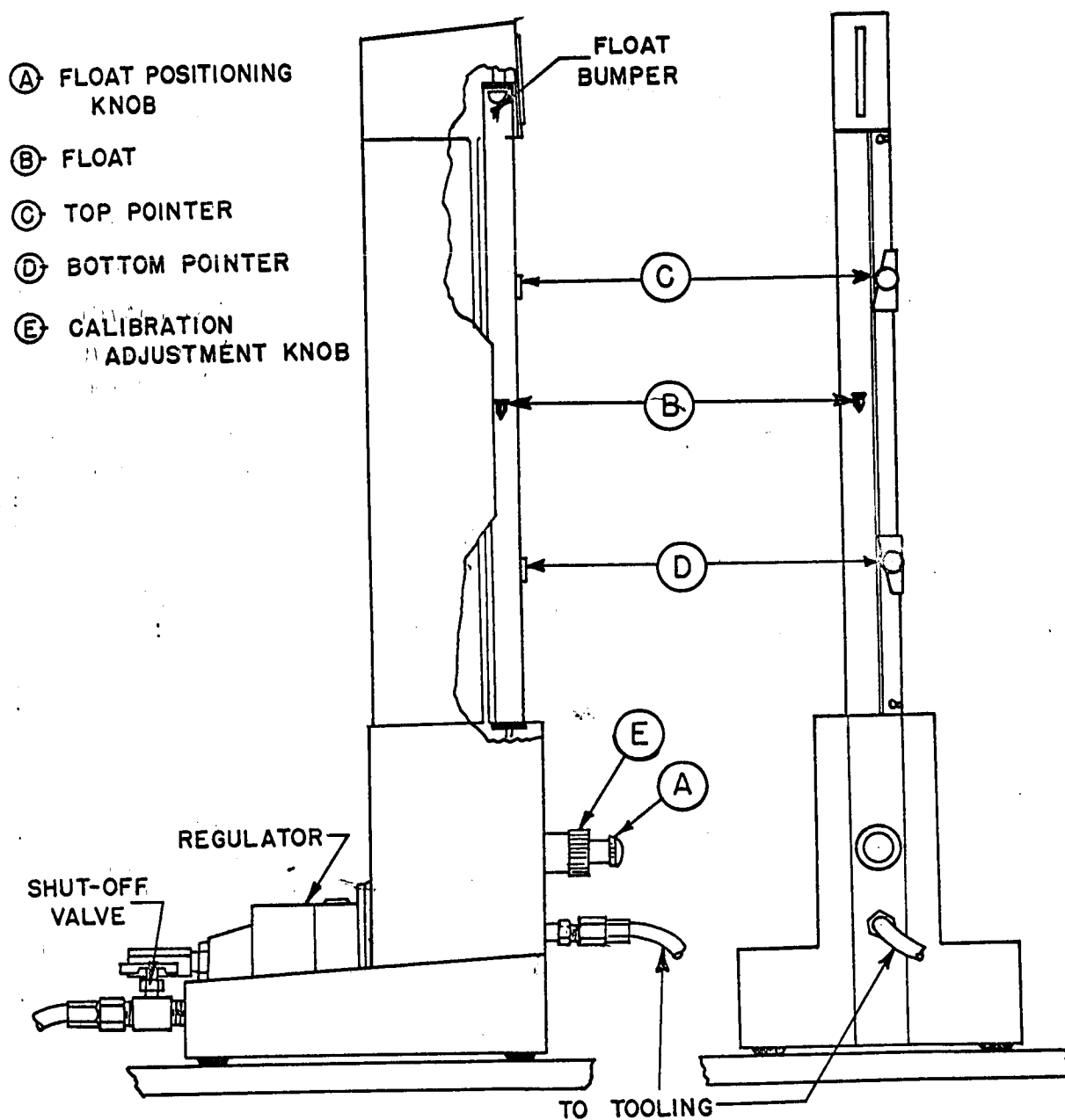
REGULATOR

SHUT-OFF VALVE

TO TOOLING

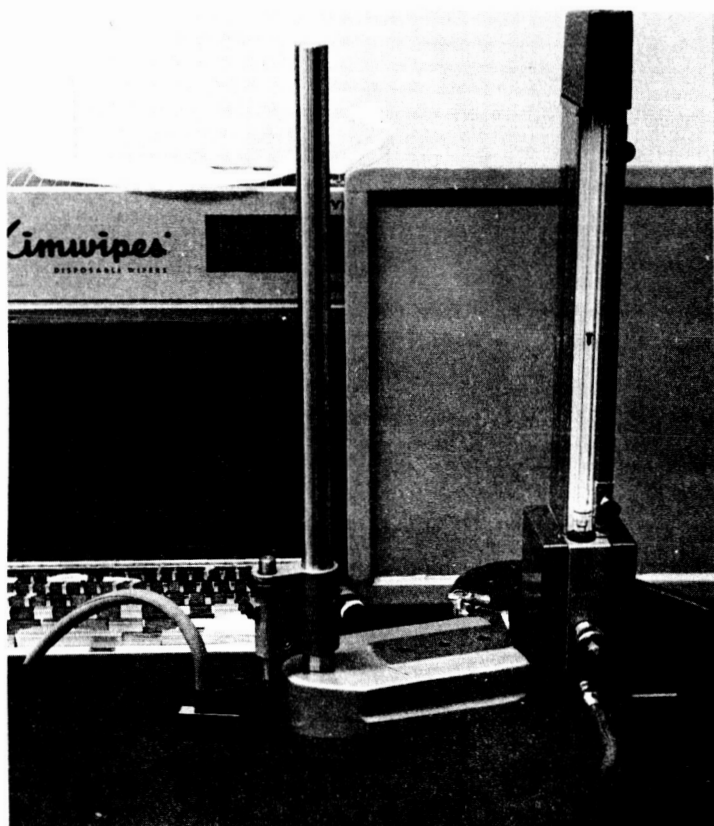Figure 56. Sheffield PRECISIONAIRE Air Gage

Figure 57   Air Gage Calibration

face of the cartridge. The float should be aligned with the top pointer. If so, the instrument is properly calibrated. If not, proceed:

e. (1) Float below pointer. Observe the distance below the upper pointer and turn the calibration adjustment knob (E) until the float is the same distance above the pointer, then position the float in line with the upper pointer with the float positioning knob (A).

(2) Float above pointer. Observe the distance above the upper pointer and turn the calibration adjustment knob (E) until the float is four times that distance below the pointer, then position the float in line with the upper pointer with the float positioning knob (A).

f. Remove the smaller set of gage blocks, and insert the larger set to check the lower float level. If the top of the float is in line with the bottom pointer, the instrument is calibrated. If not, position the float in line with the bottom pointer by using the float positioning knob (A) and repeat steps d, e, and f until the instrument is calibrated.

The float position may be changed with the float positioning knob (A) while the instrument is in use without altering the calibration. The calibration procedure ensures that each numbered division is an exact indication of 0.0001".

The surface to be measured by the AIREJET cartridge must be flat and the cartridge must be perpendicular to the surface. In this experiment, there was a problem in that the adapter supplied with the gage stand was not long enough to extend over the surface.

of the glass bearing. A six inch extension was made to position the cartridge over the glass. A great deal of tedious hand-fitting was required to ensure the gaging cartridge was perpendicular to the surface of the bearing.

Measurements of upward movements of the bearing were made with the float positioned initially at the top of the instrument by turning the float positioning knob (A). The float movement was steady and deflections were easily read to the nearest five millionths of an inch during tests with the air-bearing.

APPENDIX D

VIBRATION METER AND VIBRATION ANALYZER

The General Radio Corporation Type 761-A Vibration Meter and Type 762-B Vibration Analyzer indicate the acceleration, velocity, or displacement of vibrations from 2.5 to 750 cycles per second. Both pieces of equipment are pictured in Figure 58, with the Vibration Meter in the foreground.

Type 761-A vibration meter. A piezo-electric vibration pick-up delivers a voltage proportional to the acceleration of the vibratory motion to the meter. The piezo-electric accelerometer consists of two Rochelle-salt crystals, clamped at three corners and separated by foil strips, drawn in Figure 59. As the plates are deflected by inertial forces, a voltage is generated proportional to the inertial force exerted on the crystal which is proportional to the acceleration. The acceleration voltage is integrated electrically--once to give readings of velocity in inches per second, and once again to give readings of root-mean-square inch displacement of the vibratory motion.

The accelerometer is clamped to the test piece in such a manner that the direction of motion is perpendicular to the plates. The vibration meter was used only as a vibration detecting device in the experimental work and no attempt was made to read absolute values of acceleration, velocity, or displacement.
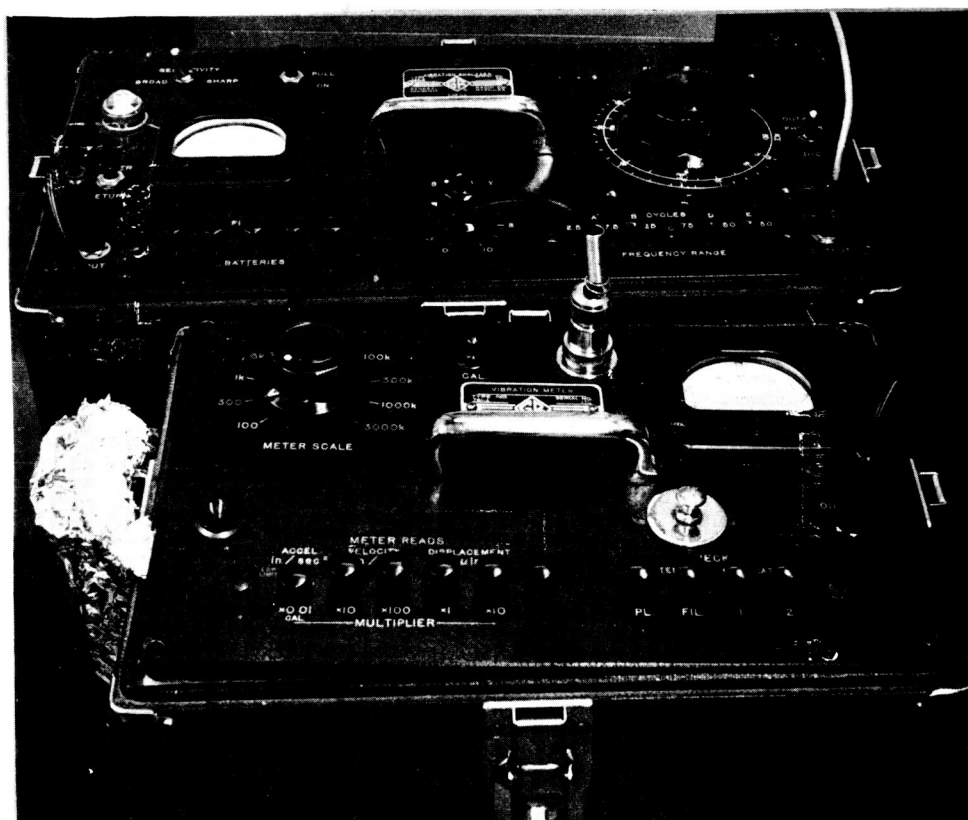
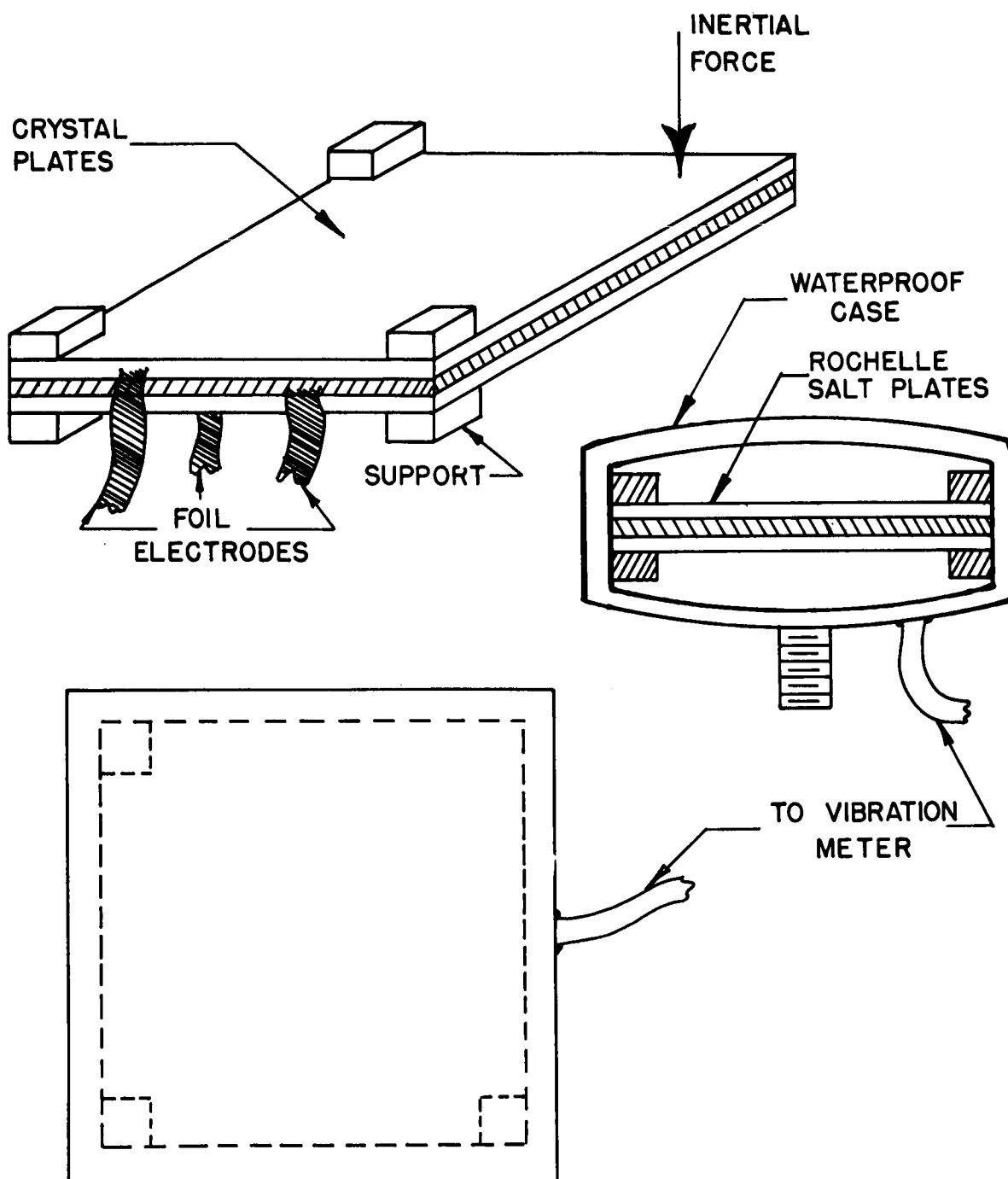Figure 58   Vibration Meter and Vibration Analyzer

Figure 59.   Piezo-Electric Accelerometer Pick-Up[41]

[41]Ayhan Cetiner. "Influence of Elastromeric and Conventional Bearing
    Plates on Beam Vibrations." (MS Thesis, Charlottesville,
    Virginia: University of Virginia, 1963).

Type 762-A Vibration Analyzer.   The vibration meter does not

give information of the frequency of vibrations sensed--only the mag-

nitude of disturbances detected by the accelerometer.   Another

instrument, the vibration analyzer, was used to determine the frequency

of vibrations.   The instrument has five frequency ranges of operation:

2. 5--7. 5, 7. 5--25, 25--75, 75--250, and 250--750 cycles per second.

Selection of the range is made by pushbuttons on the instrument panel.

Tuning within each range is continuous.

Input to the vibration analyzer is from the vibration meter and

a dial on the analyzer indicates the magnitude of the signal at a given

frequency.   An output jack provides a recorder connection to record

the vibration signal at any selected frequency.

The entire frequency spectrum was scanned during the

experimental work of this thesis and recordings made of the vibratory

field present at various selected frequencies.   Signals from the vibration

meter were amplified and recorded by the Offner Type R Dynograph

Recorder.   Results are shown in Figure 43, 44, and 45.

SECTION III

SERVO SYSTEMS

The most difficult and time consuming problem in this part of the work has been the design and construction of the servo motors. All known commerically available motors will cause first order cross coupling terms in at least one coordinate, according to calculations. Motors have been designed theoretically which have only second order cross coupling affects.

A motor experiment tended to support the theoretical predictions for cross coupling. However, definitive data could not be obtained. It was found that an experimental apparatus as complicated as the air bearing would be required for accurate motor testing. Thus, a set of breadboard motors were built.

The breadboard motors made construction possible of one loop of the servo system. This result lent credence to the servo system feasibility. A complete set of control systems are being constructed along with what is anticipated to be a final set of the motors. Final motor data will be taken when system construction is completed.

Complete motor and servo system details will be covered by the next report.

Calibration work has started and equipment has been constructed which is adequate for initial tests of the system.

Leveling the system and keeping it level appears to be a serious problem which had not been anticipated. This problem was defined and initially explored by the Force Measurement Section of the Instrument Research Division of NASA at Langley Field. Preliminary studies have started on an active leveling system. This work will not be completed until the dimensions of the problem are determined from actual operational data. For example, low frequency components in the local vibrational field due to such factors as tides must be delineated by the force balance system itself.

1